# AN EXPERIMENTAL AND NUMERICAL INVESTIGATION OF THE CUTTING FORCES IN DRY MILLING MACHINING PROCESS

A Thesis

by

BRIGHT YVES WILFRIED WADJA

Submitted to the Office of Graduate and Professional Studies of
Texas A&M University
in partial fulfillment of the requirements for the degree of

MASTER OF SCIENCE

| | |
|---|---|
| Chair of Committee, | Jyhwen Wang |
| Committee Members, | Gwo-Ping Fang |
| | Hong Liang |
| Head of Department, | Andreas A. Polycarpou |

May 2014

Major Subject: Mechanical Engineering

## ABSTRACT

The aim in this thesis is the investigation of the cutting forces during a dry milling machining process. An experimental design was developed and the cutting forces were measured based on the cutting input parameters. The cutting forces' signatures are in good agreement with the metal cutting mechanics where effects of the tool run out and vibrations are observed.

A parametric study has been conducted and the results show that the magnitude of the cutting forces at a constant depth of cut increases with a high feed rate and a low spindle speed. These results suggest that the cutting forces depend on the chip load at a constant depth of cut. Also, the increase of the depth of cut generates higher force magnitude due to the volume of material removed.

A three-dimensional Finite Element Analysis (FEA) was conducted using commercial FEA software ABAQUS to predict the cutting forces in a dry milling cutting process. Different cutting input parameters were chosen to predict the cutting forces. The findings show that the predicted cutting forces depend also on the chip load. Later, a close fit has been found from the comparison of the measured and predicted cutting forces. Thus, the FEA model is valid and accurate.

The surface roughness (Ra) was also studied based on different cutting input parameters and CNC machine quality. The results from the investigation show that the surface roughness depends on the chip load and the machine condition. This leads to conclude that the surface roughness can be predicted based on the cutting forces' signatures.

## ACKNOWLEDGEMENTS

I would like to thank Dr. Jyhwen Wang for his guidance and assistance throughout my education life at Texas A&M University. Dr. Jyhwen Wang gave me the opportunity to have a research experience from my undergraduate study and advised me well until the completion of my Master Degree. I am grateful, Dr. Gwo-Ping Fang, for lending me his load cell sensor to complete my research and gave me a position as teacher assistant. I would like to thank Adams Farmer for teaching me how to operate various machines and Dr. Hung Nguyen for allowing me to use the HAAS CNC machine. Also, I would like to thank Dr. Hong Liang and her graduate students for helping me characterize the surface profile of my specimens. Thanks a lot Cheng-Kang Yang for teaching me how to use ABAQUS and for his advice concerning the graduate courses I should take to tackle my research objective.

Finally, thanks to my parents and my wife for their encouragement and financial support.

## TABLE OF CONTENTS

Page

## LIST OF FIGURES

Page

## LIST OF TABLES

Page

# 1. INTRODUCTION: PROCESS MONITORING AND CUTTING FORCES IN MILLING MACHINING

Milling machining, which is one of the metal cutting processes, was first introduced after the industrial revolution. From then, development and innovation led to a cutting process that became fully automated with the creation of Control Numerical Code machines (CNC). CNC machines involve a cutting tool rotating at high speed that follows a programmed tool path during the cutting process. The desired shape of the part is built with CAM softwares such as FEATURECAM where the Numerical Code (NC) is generated. Once the NC code is generated, the code is inputted into the CNC machine and the cutting process follows the programmed path as illustrated in Figure 1 where slots feature have created.

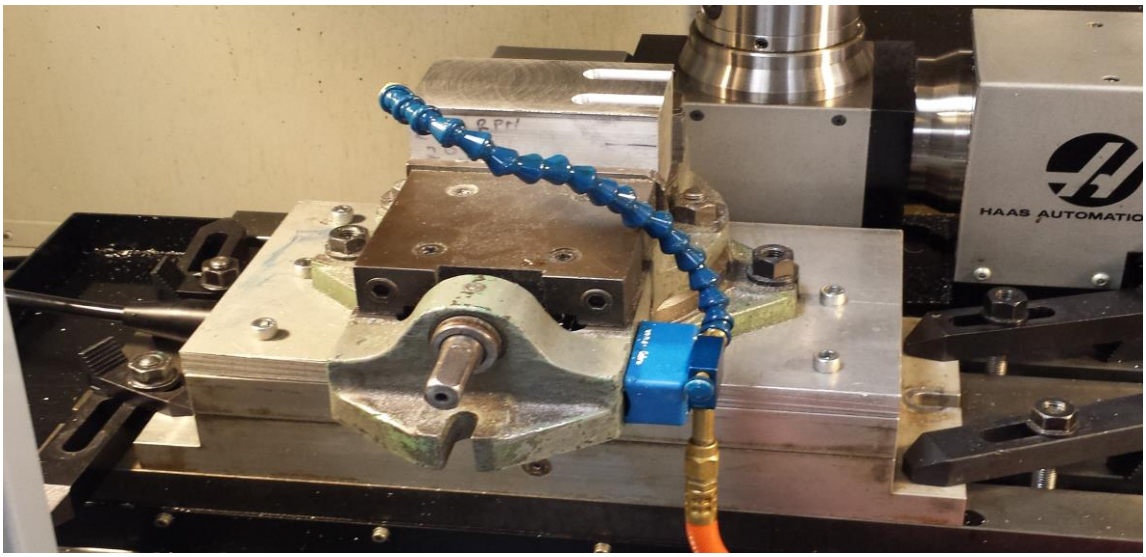


**Figure 1: HAAS CNC machine with work piece mounted on a dynamometer**

The milling cutting process is widely used in manufacturing industries. The need of accuracy to meet the geometry tolerance imposed by customers or designers has been a challenge for manufacturers. Therefore, monitoring the cutting process to overcome the high demand with a short production cycle and maintaining the quality of the parts has become indispensable.

Process monitoring consists of retrieving different variables during the cutting process and describe the cutting or machine condition based on the information gathered. The measurement process can be divided into two categories as described by Liang, Hecker and Landers (2004). The first category is the direct measurement. In this category, the process diagnostics is obtained directly from the measured signal. The other category is the indirect measurement where the process diagnostic is obtained after processing the signal or analyzing the part. Among these techniques, the cutting forces' signature can be used to identify machining characteristics such as part surface texture, tool condition, tool run out and part dimension accuracy where the variables used are typically the cutting input parameters such as the feed rate, the depth of cut, and the spindle speed.

The focus in this thesis is to investigate the effect of cutting input parameters during a dry milling machining process and correlate the cutting forces' signatures to detect part irregularities.

The first phase of this research will consist of study the effect of the feed rate, the spindle speed, and the depth of cut during the cutting process. To do so, an experimental design will be conducted where different spindle speed, feed rate, and depth of cut will

be specified. Then, the cutting forces will be measured according to the specifications set in the experimental design.

The milling machining process will consist of cutting a slot from a work piece made of Aluminum 6061 T6 with a two teeth High Speed Steel end mill tool. The slot feature will be cut following the NC code that describes the tool path motion. The work piece will be mounted on the top of a dynamometer which is a load cell sensor that outputs voltage signal. The outputted voltage signal from the dynamometer will be amplified and then converted from an analog to digital signal. More details description of the equipment essential for measuring the cutting forces will be discussed in section 3. The experiments will be conducted and the results will be presented in section 4.

The second phase will consist of building a Finite Element Analysis model representing the milling cutting process. The commercial software ABAQUS will be used to run the simulation. Before then, a three-dimensional model of the cutting tool will be modeled using the CAD commercial software SOLIDWORKS 2012 and the resulting tool model will be inputted into the FEA software to run the simulation. Once the simulated cutting forces are obtained, the data will be compared to the experimental cutting forces to verify the accuracy of the FEA model

The last phase will consist of measuring the average surface roughness Ra using a ZYGO white light interferometer on each specimen cut during the experiments. The measured Ra values will be compared based on the feed rate, the spindle speed, and the depth of cut. And then, a correlation between the cutting forces and the surface roughness will be established.

# 2. LITERATURE REVIEW

Previous works and researches that have been conducted during the past years involving the estimation of the cutting forces by the means of experimental results, analytical model, numerical simulation, and the effect of cutting forces on the surface finish of the part will be reviewed in this section.

## 2.1 Process monitoring: history and development

Process monitoring consists of measuring different variables that are involved in the production of a specific part. Monitoring the cutting process has been used to increase the productivity as well as the reliability of the finished part in term of quality. Indeed, variables such as force, power, and vibration signal can be used to diagnose the accuracy of a particular process. A review done by Liang, Hecker and Landers (2004) in the ongoing researches throughout the past thirty years shows the discovery of accurate findings in research labs. However, the implementation in industry is still limited due to limitation of accurate sensors and a standard process to monitor these variables.

## 2.2 Cutting forces measurement and prediction

An early model of the prediction of the cutting forces has been established by Merchant (1945) where the single point edge tool cuts the work piece to form a continuous chip and creates a new surface which is in plane to the original surface.

The cutting forces are estimated by analyzing the shear plane deformation using the cutting tool geometries such as the rake angle and the shear plane angle. The shear plane angle is computed from the relative velocity of the tool with the work piece and the chip formed. The Merchant's model is suitable to estimate the cutting forces for the case of a turning process where a continuous chip is assumed to be formed with a constant shear strain.

Devor and Kline (1983) studied the effect of the tool run out on the cutting forces in milling machining. The tool run out is defined as an offset of the tool center from the CNC tool holder which results a change in the tool teeth cut radius with respect to the axis of rotation. Indeed, teeth on the offset side of the tool will have a larger cutting radius than the other teeth on the opposite side. The tool run out leads to an uneven cutting or non-uniform chip load. An explicit form of the cutting forces has been modeled where the equations stated that the cutting forces are proportional to some cutting forces' coefficients and the chip load including the shift of the cutting radius produced by the tool run out. The chip load is defined as the chip thickness formed by each teeth of the tool during the cutting process. A simplify model of the chip load is described by Equation 1:

$$\text{Chip Load} = \frac{\text{Feed Rate}}{\text{Spindle Speed} \times \text{Number of Teeth}} \tag{1}$$

The cutting forces' coefficients are estimated by averaging and curve fitting the measured cutting forces in the X and Y principal direction from a set of experiments

where different feeds and spindle speeds are used. The comparison between the predicted and measured cutting forces is presented in Figure 2.

| | *X* Force | | | | *Y* Force | | | |
|---|---|---|---|---|---|---|---|---|
| | % Spindle | | % Tooth | | % Spindle | | % Tooth | |
| Test | *M* | *P* | *M* | *P* | *M* | *P* | *M* | *P* |
| 1 | 96 | 92 | 4 | 4 | 92 | 90 | 5 | 7 |
| 2 | 83 | 76 | 16 | 22 | 69 | 55 | 26 | 41 |
| 3 | 91 | 89 | 7 | 5 | 84 | 88 | 10 | 7 |
| 4 | 63 | 70 | 27 | 25 | 52 | 59 | 34 | 33 |
| 5 | 95 | 98 | 2 | 1 | 88 | 98 | 4 | 1 |
| 6 | 58 | 67 | 29 | 19 | 52 | 62 | 33 | 23 |
| 7 | 36 | 35 | 52 | 55 | 22 | 25 | 65 | 63 |
| 8 | 58 | 70 | 30 | 18 | 49 | 71 | 40 | 23 |
| 9 | 36 | 42 | 58 | 53 | 15 | 25 | 79 | 71 |

*M* = measured force signal. *P* = predicted force signal.

**Figure 2: Summary of average predicted and measured cutting forces with average percentage of change between peaks force due to the tool run out effect, Devor and Kline ( 1983).**

Based on the results obtain in Figure 2, the predicted and measured cutting forces are compared and an error percentage of 5 to 15 % is observed. A change in the peaks values of the cutting forces is also observed which is due to non-uniform chip load among the tool teeth.

A similar work in predicting the milling cutting forces has been conducted by Budak, Altintas and Armarego (1996) where the cutting forces' coefficients are estimated from the orthogonal cutting experiments using the shear strain, stress, friction coefficient, tool design parameters, and cutting variable inputs. Results from the

empirical model illustrated in Figure 3 have a close fit with the calibrated milling cutting forces.

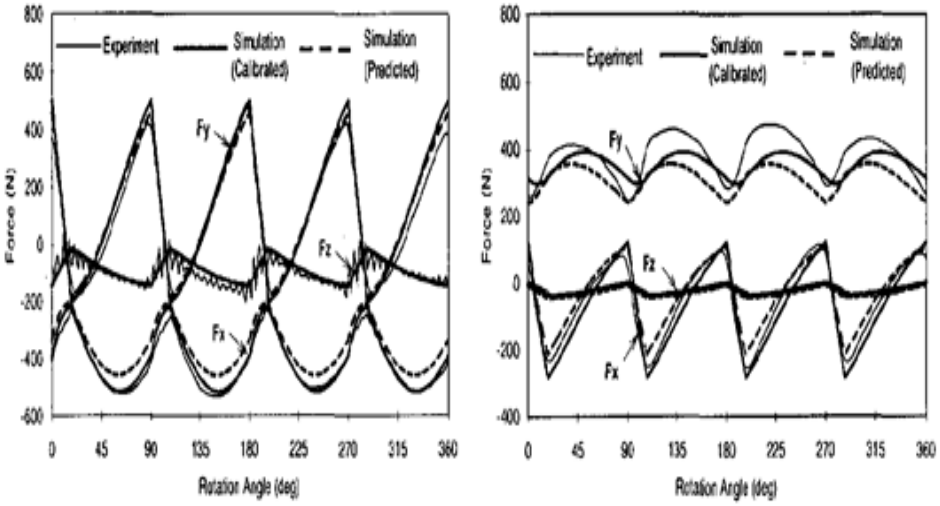


**Figure 3: Comparison between measured and predicted milling cutting forces, Budak, Altintas and Armarego (1996).**

Ko, Yun, Cho and Ehmann (2002) developed a new method to determine the cutting forces' coefficients which was used to compute the cutting forces in a milling process. Contrary to early approaches, the cutting forces' coefficients were dependent on the cutting condition and calibration of these coefficients was needed when the cutting condition was changed. The new approach consisted of computing the instantaneous cutting forces' coefficients at the stage where the tool first entrance into the work piece including the offset of cutting radius and angle which describe the tool run out. Then, the established equations of the cutting forces will depend on the chip load and the coefficients determined from a set of experimental data. Figure 4 shows the comparison

between the predicted and measured cutting forces. The results obtained present a good match with the measured cutting forces. The percentage of error from the predicted and measured cutting forces is estimated to be 2 to 8 %.

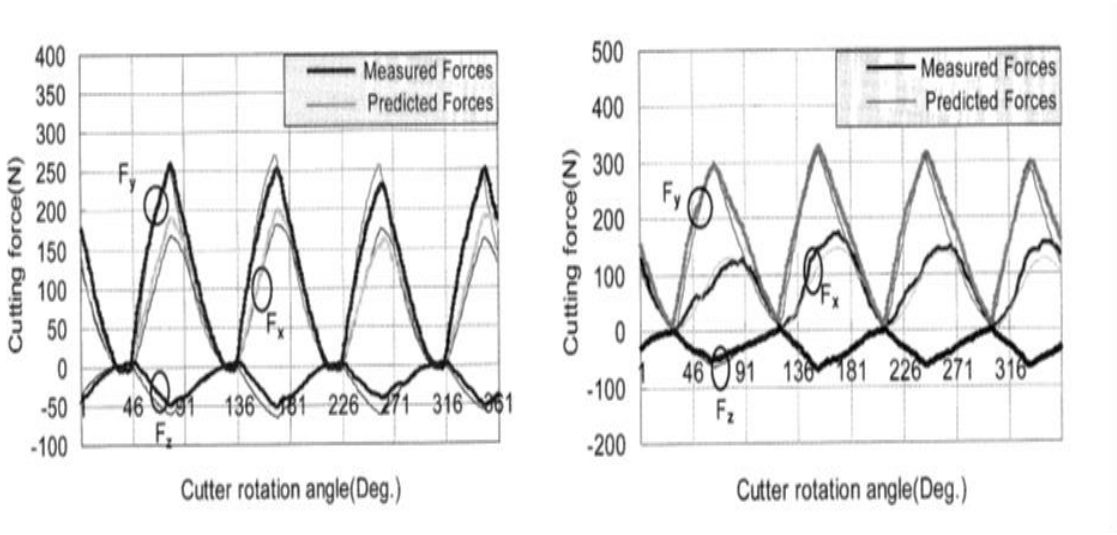


**Figure 4: Comparison of measured and predicated cutting forces, Ko, Yun, Cho and Ehmann (2002).**

Contrary to the previous researches conducted in estimating the cutting forces' coefficients in a milling cutting process, Adetoro and Wen (2009) used an Arbitrary Lagrangian Eulerian FEA Formulation to estimate the average cutting forces' coefficients. Their model consists of a simulation of an orthogonal cutting.

The cutting forces are obtained from the orthogonal cutting simulation results and the least square's method is used to extract the cutting forces' coefficients. Once the cutting forces' coefficients are obtained, there are inputted into the empirical model. The empirical model describes the cutting forces in the X and Y directions which are

proportional to the cutting coefficients and the chip load without including the effect of the tool run out. The predicted cutting forces in the X and Y directions are then compared to the experimental cutting forces measured by Ko, Yun, Cho and Ehmann (2002) and presented in Figure 5.

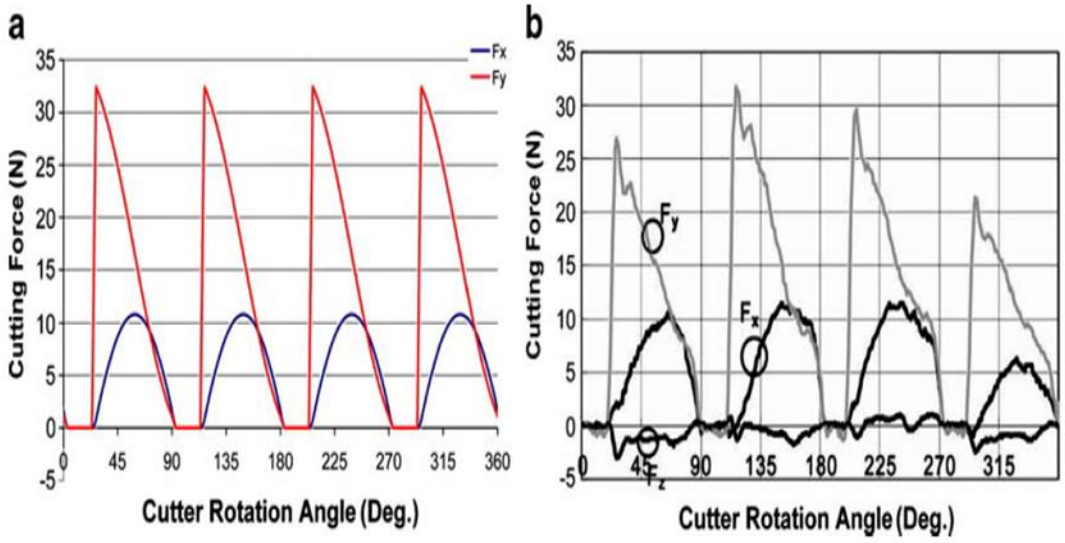


**Figure 5: a. Predicted cutting forces, Adetoro and Wen (2009). and b. Measured cutting forces, Ko, Yun, Cho and Ehmann (2002).**

A different approach was used by Rivière-Lorphèvre and Filippi (2009) to model the effect of the cutter radial run out in estimating the cutting forces. The tool path based on the kinematics of the tool motion was used to estimate the tool offset. The cutting forces' coefficients were computed using the methodology described by Devor and Kline (1983). The predicted cutting forces without taking the new model of the tool run out were plotted against the measured cutting forces in Figure 6 and the predicted cutting

forces with the exact model of the tool run out against the measured cutting in Figure 7. From Figure 6, a variation in the peaks values can be observed from the measured cutting forces whereas the peaks values of the predicted cutting forces are constant. This variation is mainly due to the uneven cutting which results a change in the chip load.

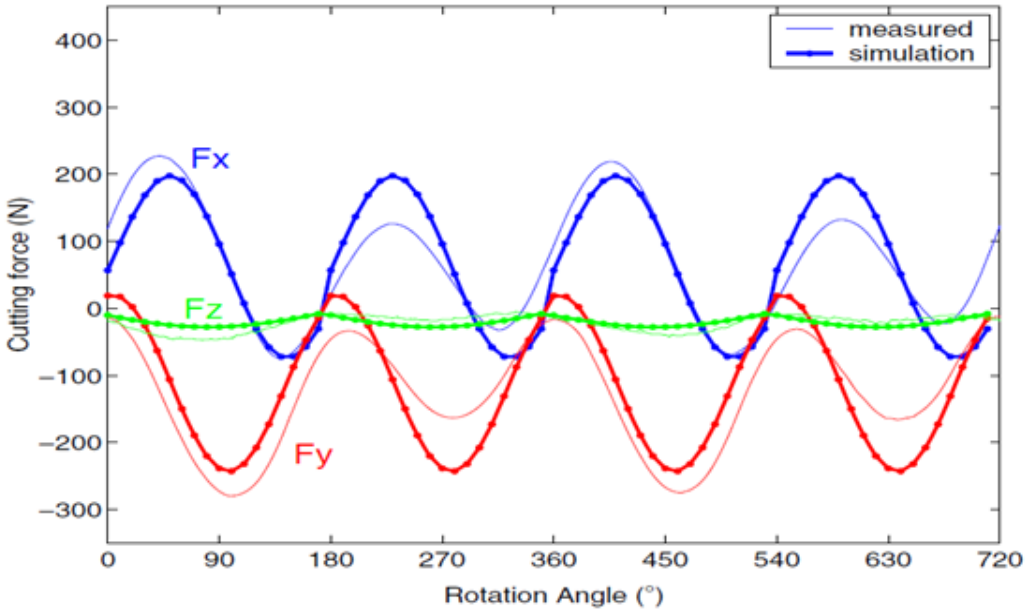


**Figure 6: Measured vs. predicted cutting forces without the tool run out, Rivière-Lorphèvre and Filippi (2009).**

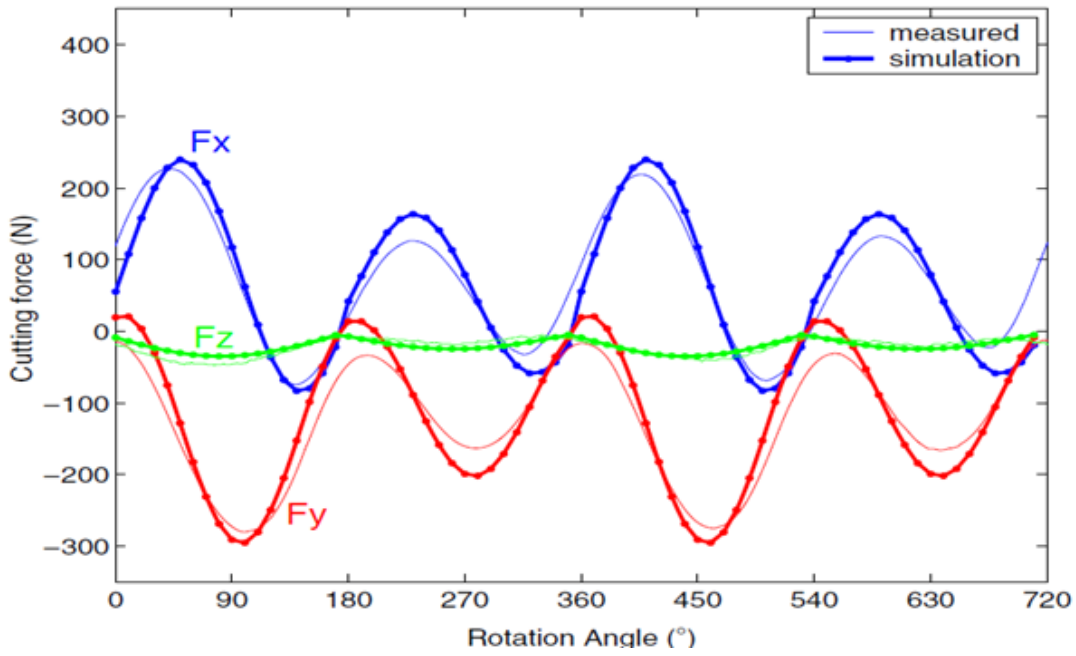


**Figure 7: Measured vs. predicted cutting forces with the tool run out, Rivière-Lorphèvre and Filippi (2009).**

### 2.3 Finite element analysis for milling cutting forces prediction

Another approach to predict the cutting forces during a milling process involves constructing a Finite Element Analysis model. Indeed, cutting variables and material properties can be easily inputted into the FEA model. The analysis is done using commercial softwares where built in functions can be used to construct the model and compute the cutting forces.

The first FEA model describing the milling cutting process was done by Özel and Altan (2000) using the commercial software DEFORM 2D. The main objective of developing this analysis was to predict the chip flow, the cutting forces, temperature and stress distribution around the tool teeth using two teeth flat uncoated carbide end mill

tool with no helix angle in dry milling condition. To do so, a slot profile was designed to be cut from P-20 steel. Testing data describing the work piece was used to develop the material flow stress as well as the friction coefficient and temperature evolution. These data were used in the FEA model to compute the cutting forces. A comparison of the average measured cutting forces with the FEA cutting forces was done and presented in Figure 8.

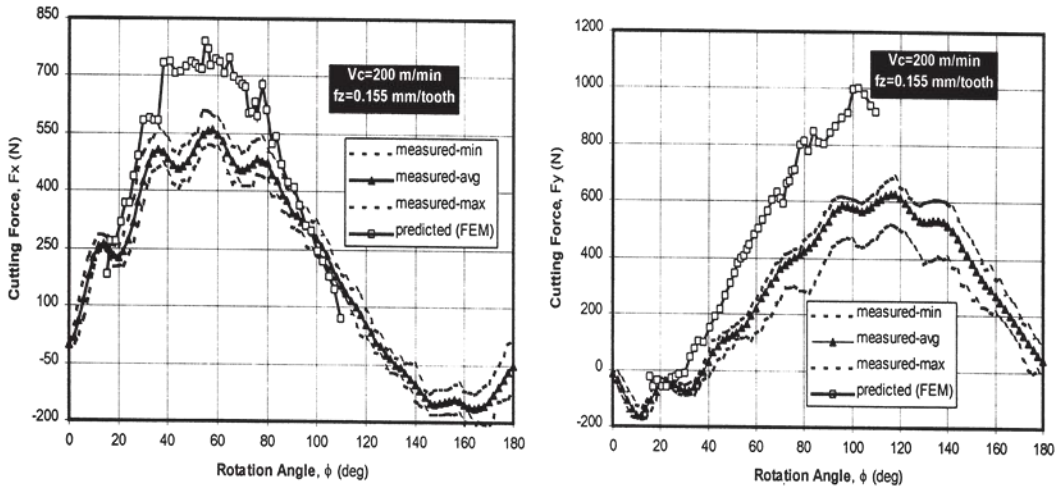


**Figure 8: Cutting forces comparison, Özel and Altan (2000).**

The plots from Figure 8 show that the FEA cutting forces peaks values are higher than the measured cutting forces. According to the authors, the variation is due to the FEA remeshing technique used to calculate the stress from the tool-chip contact.

A three-dimensional orthogonal cutting simulation was performed by Llanos, Villar, Urresti and Arrazola (2009) using the commercial software ABAQUS explicit. The Arbitrary Lagrangian Eulerian formulation was used to simulate the chip formation

of AISI 4140 steel .The tool was assumed to be rigid and the flow stress of the work piece was model using the Johnson Cook's plasticity equation where the stress depends on the strain rate and temperature evolution. Results from the simulation show a significant difference between the measured and simulated cutting forces.

The most recent FEA simulation describing the three-dimensional milling cutting process was developed by Maurel-Pantel, Fontaine, Thibaud and Gelin (2012). Their work consists of a shoulder cutting simulation (90 degree cut) using the commercial FEA software LS DYNA. Since the cutting of the work piece is assumed to be dependent on the strain rate and the temperature, the Johnson Cook's plasticity model is used to describe the flow stress of the 304 L steel used as the work piece material. The failure model is based on the strain at fracture which was assumed to be constant. The model assumes that the elements failed and chips are formed once the computed fracture strain of each element reaches the specified fracture strain.

The end mill tool design consists of the actual measured dimensions of the real tool used in the cutting process. The tool is assumed to be rigid and a constant coefficient of friction is used to describe the tool and work piece contact based on the Coulomb's friction law. In order to verify the cutting forces computed from the FEA results, the cutting forces have been measured experimentally and then plotted against the predicted cutting forces from the FEA. The results from the cutting forces comparison show a 35 % difference in the transverse force (X direction), 5% difference in the feed force (Y direction) and a 5 % in the Z direction if the absolute value of the

measured cutting forces is used. The plots describing the comparison between the measured and computed cutting forces are shown in Figure 9.

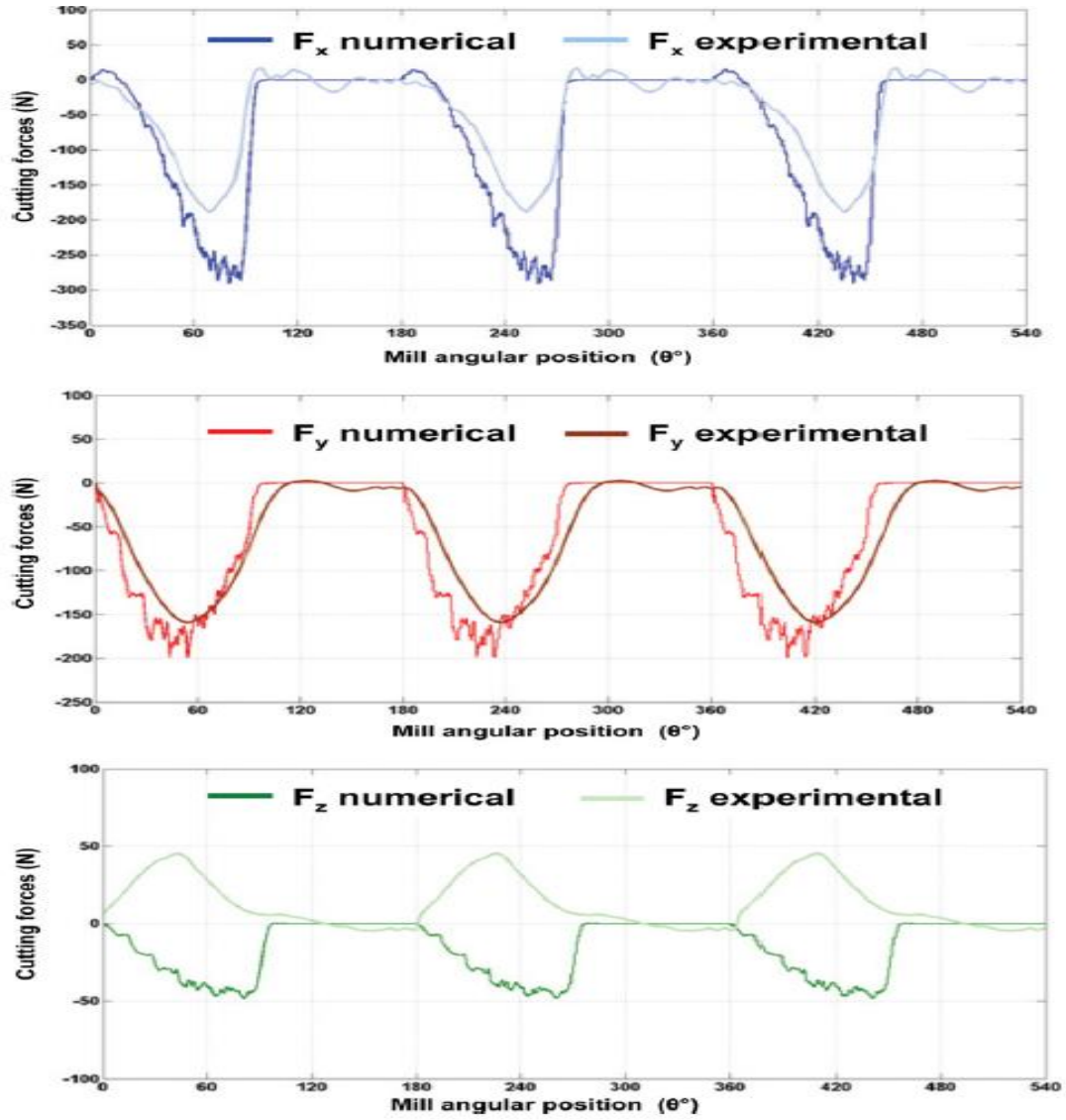


**Figure 9: FEA vs. measured cutting forces, Maurel-Pantel, Fontaine, Thibaud and Gelin (2012).**

## 2.4 Surface finish in machining process

The surface finish is a factor very important in a machining process. Indeed, many factors such as the cutting input parameters can influence the resulting surface finish of a work piece. According to Benardos and Vosniakos (2003) in their review about predicting the surface roughness in machining, there are four different approaches used over the past years to describe the surface profile. Based on the scope of this research, approach based on mechanical machining theory, machining variables input parameters with design experiment will be reviewed in this section.

Early prediction of the average surface roughness was done by Knight and Boothroyd (1988) for the case of a turning process where the average surface roughness $R_a$ depend on the feed per tooth or chip load $f$ and the corner radius of the tool $r_\varepsilon$.

$$R_a = \frac{0.0321 f^2}{r_\varepsilon} \tag{2}$$

But divergence in comparing the measured $R_a$ from Equation 2 was found according to review done by Benardos and Vosniakos (2003).

Grzesik (1996) used the Brammertz's formula and included the undeformed chip thickness $h_{\min}$ which is based on the feed rate per unit revolution to estimate the surface roughness as shown in Equation 3.

$$R_{zt} = \frac{f^2}{8r_\varepsilon} + \frac{h_{\min}}{2}\left(1 + \frac{r_\varepsilon h_{\min}}{2}\right) \tag{3}$$

A turning cutting process is then done and the measured surface profile is compared to the one predicted from Equation 3 as shown in Figure 10.

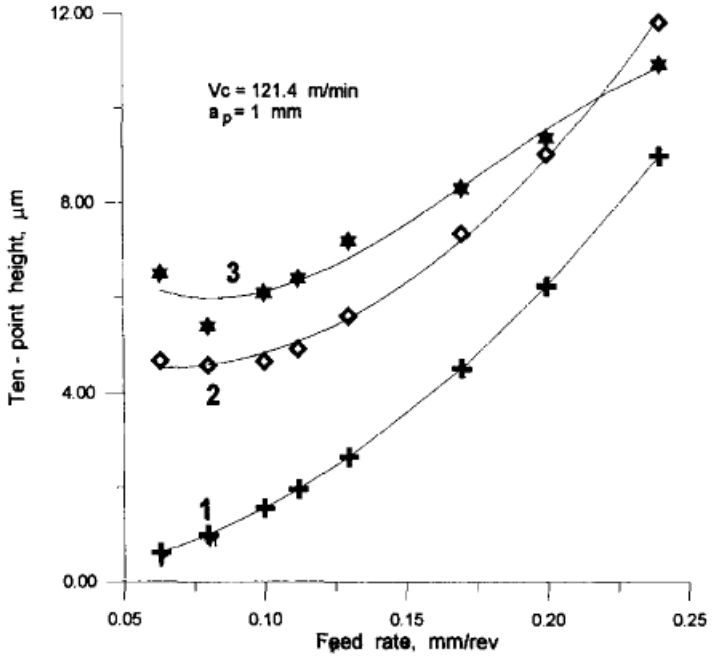


**Figure 10: Comparison between experimental and predicted surface roughness, Grzesik (1996).**

Lin and Chang (1998) studied the effect of vibration in predicting the surface roughness of machined parts. Indeed, a surface topography model based on a numerical code was established to predict the surface finish of part during a turning process. The simulation model is based on the difference of the height to the reference surface of the part which involves the feed rate, the nose radius of the tool, and the amplitude of vibration measured during a turning cutting process. The vibration amplitude was measured with an accelerometer mounted on the tail stock of work piece. The measured surface topography in the axial direction from the experimental turning test is then

compared with topography simulation model with the cutting input parameters and the vibration amplitude recorded from the accelerometer as shown in Figure 11.

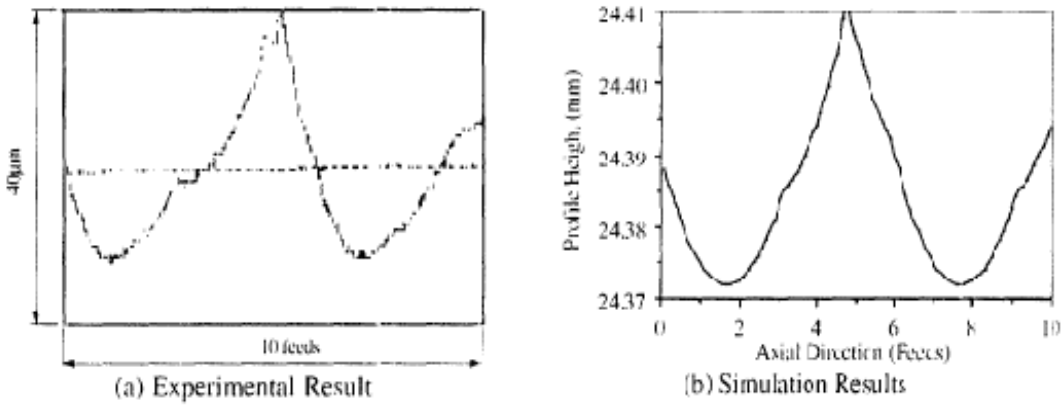


**Figure 11: Comparison between experimental and simulation of the surface profile Lin and Chang (1998).**

The comparison between the experimental and simulation results shows a 15% discrepancy. The authors argue that the discrepancy is due to the fact that the vibrations along the other directions were not taken into account in the simulation model. Therefore, they concluded that the surface roughness depends also on the vibration frequency which is the ratio of the vibration amplitude and the spindle speed rotation. Results in investigating the vibration frequency show that the vibrations in the radial direction have more significant influence on the surface roughness than the vibration in the tangential and axial direction.

Lee, Kang, Jeong and Kim (2001) established a method to predict the surface profile and roughness in high speed end milling. The authors argue that the surface

profile can be predicted using vibration signal's patterns from the milling process. But first, the author established an algorithm that describes the flutes of the end mill tool position based on the feed rate per revolution and the tool engagement angle. The vibration patterns are then measured from the acceleration signal and the amplitude frequency of the vibration is then added to the simulation algorithm. Experiments are conducted and the simulated surface roughness is compared to the results obtained in the experiments. Based on the comparison, the authors argue that the results from the simulation cannot accurately describe the surface roughness. This fact is due to the non-inclusion of chip formation and tool wear. Figure 12 shows the comparison between simulation and experimental surface profile.

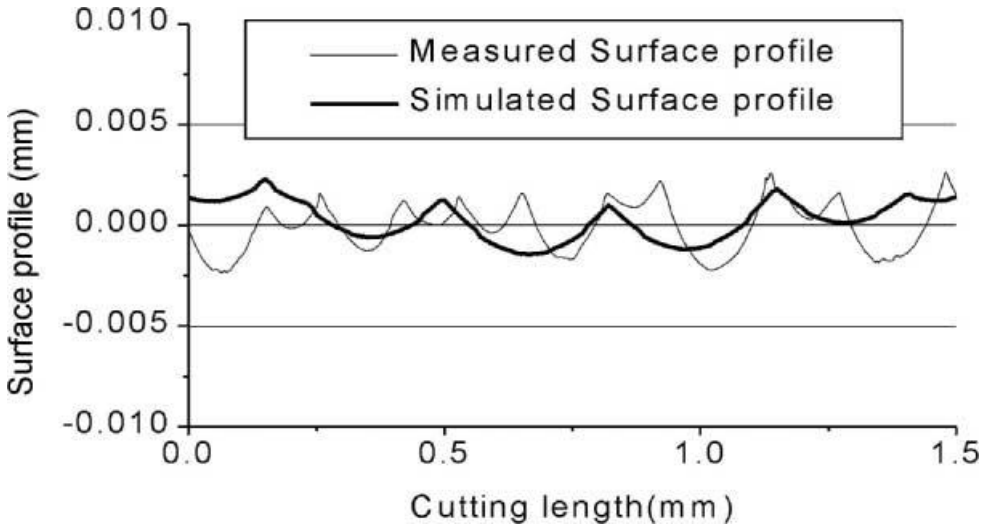


**Figure 12: Measured and simulated surface profile, Lee, Kang, Jeong, Lee and Kim (2001).**

Kuttolamadom, Hamzehlouia and Mears (2010) studied the effect of the feed rate during the milling cutting process. An experimental design is set where six slots are cut with different cutting input parameters during an up milling process (tool rotation direction against the table feed direction). The surface roughness of the part is measured in the inner center line surface of the slot with a Zygo white light interferometer.

The surface roughness is then plotted against the feed rate at different spindle speeds as shown in Figure 13.

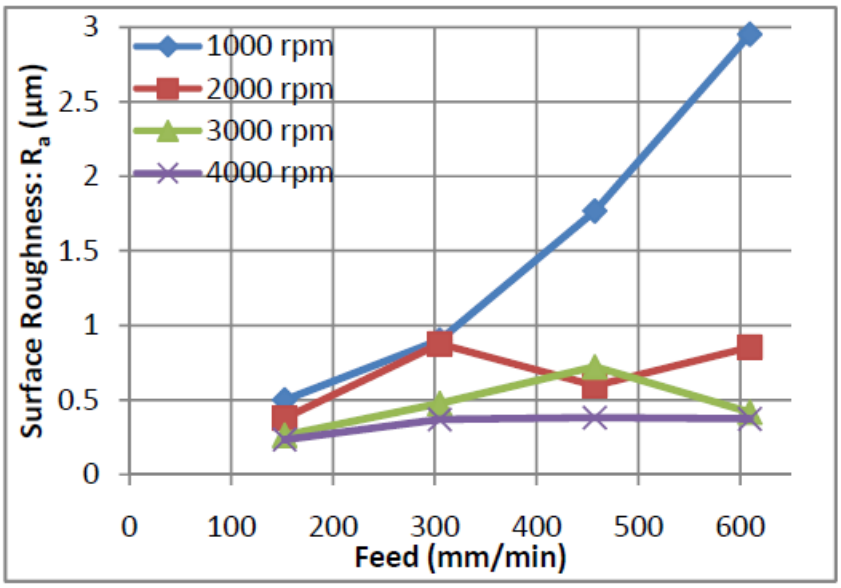


**Figure 13: Surface roughness vs. feed rates of milling part at different cutting speeds, Kuttolamadom, Hamzehlouia and Mears (2010).**

Results from Figure 13 show in general, the surface roughness increases as the feed rate value increases and a lower surface roughness value is observed at higher spindle speed.

## 2.5 Scope of present research

Although the cutting forces in milling machining process can be predicted from either empirical or simulation models, there are still issues that need to be addressed. Based on the literature review presented in this section, issues that can be highlighted are:

Empirical equations to predict the cutting forces during the cutting process are mostly based on estimating the cutting forces' coefficients which require time consuming experiments. Even though previous results present a good match with the experimental measured cutting forces value, the cutting forces' coefficients will be invalid if the work piece material is changed.

Numerical method as well as Finite Element Analysis models in predicting the cutting forces in machining processes are mostly reduced to a two-dimensional model which best fit the case of an orthogonal cutting. The only three-dimensional model, which best represents the milling cutting process, was done for case of a 90 degree cut. The comparison of the predicted and measured cutting forces shows a high percentage of difference.

The surface profile of the machining part was estimating based on the amount of vibration during the cutting process. Good predictions of the surface profile were established (15 % error) but again are limited to the case of a turning cutting processes.

The present work focused on developing better understanding of the cutting forces patterns during a dry milling process and on creating an efficient way to simulate the cutting forces.

Having an efficient way of predicting the cutting forces will be beneficial to the tool and part manufacturers where the cutting forces will be used to design more efficient tool and increase the part productivity.

Even though experiments can be used to determine the cutting forces during a milling cutting process, the cost and time associated with running experiments can be significant. Therefore, a numerical simulation could be used to predict the cutting forces.

Moreover, since the cutting forces' signature contains all the cutting parameters as well as machining characteristics, imperfections from machining part can be identified at the early stage of the machining process which will save a lot of time for quality control.

# 3. EXPERIMENTAL SET-UP

This section will describe the method followed to conduct the experiments. A detail description of the equipment used to measure the cutting forces during the milling process will be presented.

## 3.1 Introduction

To be able to measure the cutting forces, an experiment set up was built. The main instrument used consists of a strain gage multicomponent dynamometer which is mounted on the cutting table. The low magnitude analog output voltage from the dynamometer is sent to an amplifier. The amplified voltage signals are then converted from analog to digital signals and transferred to the data acquisition software. The data gathered from the data acquisition software are then exported to Microsoft Excel where proper scale factors are used to convert the outputted voltages to forces.

The commercial software FEATURECAM will be used to generate the Numerical Code for the slot feature that will be cut from the work piece using a HAAS CNC machine. The Numerical Code will contain the selected cutting input parameters that will be used during the milling process.

## 3.2 Cutting tool and work piece material

To conduct the experiments, a two teeth end mill cutter as shown in Figures 14 and 15 will be used to create the slot feature into the work piece. Choosing a two teeth

cutter to cut the specimen was adequate in the sense that each tooth will cut the material within a half revolution and the cutting forces' signature will be easy to interpret. The detail specifications of the tools are listed in Table 1.

**Table 1: End mill tool specification**

| Niagara Square End Mill | |
|---|---|
| Mill Diameter (Inch) | 0.625 |
| Helix Angle | 30 Degree |
| Rake Angle | 10 Degree |
| Number of Flutes | 2 |
| Material | High Speed Steel |
| Coating | None and TiN |
| Flute Type | Spiral |
| Cutting Direction | Right Hand |
| Center Cutting | Yes |

**Figure 14: Uncoated end mill Niagara tool**

**Figure 15: TiN coated end mill Niagara tool**

The work piece material used in the experiment will be the Aluminum 6061-T6. It is one of the most used structural materials in machining processes due to its low cost and machinability. Further details about the material's mechanical properties will be illustrated in section 5.

### 3.3 Data acquisition components

The main components used to measure the cutting forces during the milling process are the dynamometer, an amplifier, the analog-digital signal converter, and the data acquisition software.

#### *3.3.1 Dynamometer*

The Dynamometer used in this experiment is a AMTI MC818. The table mounted dynamometer measured the impulse generated during the cutting process using the strain gage inside its core. The dynamometer has 4 channels outputs composed of three orthogonal forces channels $F_x, F_y, F_z$ and a moment about the X direction. The impulses analog voltages from the cutting process are outputted to the amplifier.

#### *3.3.2 Amplifier*

In order to magnify the output signals from the dynamometer, which are in order of microvolts/volt-unit load, an amplifier is required. Indeed, a compatible amplifier matching the specifications of the strain gage load sensor is a Missile Command Amplifier (MCA 4 3636) as shown in Figure 16. The gain, which is the scale of magnification of the signal, was set to 2000 for the channel in the X, Y direction and 4000 for the channel in the Z direction. Different gain values are used because the

voltages outputted in the X and Y direction are higher than in Z direction and the maximum bridge excitation of the amplifier is set to a value of +/- 10 volts. Based on preliminary cutting forces' measurement, the outputted voltages in the X and Y direction exceeded the voltage limit when a gain is set to 4000.


**Figure 16: AMTI Missile Command Amplifier**

A critically damped low pass filter with a switch giving the user to choose a cut off frequency of 10.5 Hz or 1050 Hz is built in the amplifier. The main purpose of the filter is to remove unwanted noise from the output signal. Since the cutting process requires a dynamic measurement, the cut off frequency of 1050 Hz was chosen according to the amplifier user's manual. Also, the outputted signal magnitude will not be attenuate since the maximum spindle speed of 3000 rpm (revolutions per minute) of

the cutting tool with a cutting frequency of 100 Hz per teeth does not exceed the cut off frequency of 1050 Hz.

Before measuring the cutting forces, the system requires a warm up of 30 minutes. After the system warms up, a system balance is needed to ensure that the voltage reading at the initial stage is close to zero volts. Each channel on the top cover of the amplifier has a LED pair which indicates the voltage output reading sign (positive or negative). A proper balance will make the LED light to turn off and can be done by turning the potentiometer with a screw driver in either clockwise or counter clockwise direction until the LED light disappears. More details about set in up the system can be found in the AMTI user guide.

### *3.3.3 Analog-digital signal converter*

The analog to digital signal converter used to measure the cutting forces has a purpose of converting the analog output signal coming from the amplifier to a digital signal where the signal is sent to the data acquisition software. The converter used is NI USB – 6008 made by National Instrument (NI).

A total of 16 available channels can be found on each side of the converter where connections can be made from the amplifier to the converter. A differential method connection will be done since the output connectors of the amplifier consists of positive and negative voltage. Therefore, each positive connector will be assigned to a specific channel label on the analog side of the converter and the negative connector will be on the ground channel as specified in NI user's guide. The positive connector from the X, Y, and Z direction was connected respectively to channel AI2, AI5, AI5 and negative

connection to the channel AI3, AI6, AI9. The NI converter and wiring is shown in Figure 17.

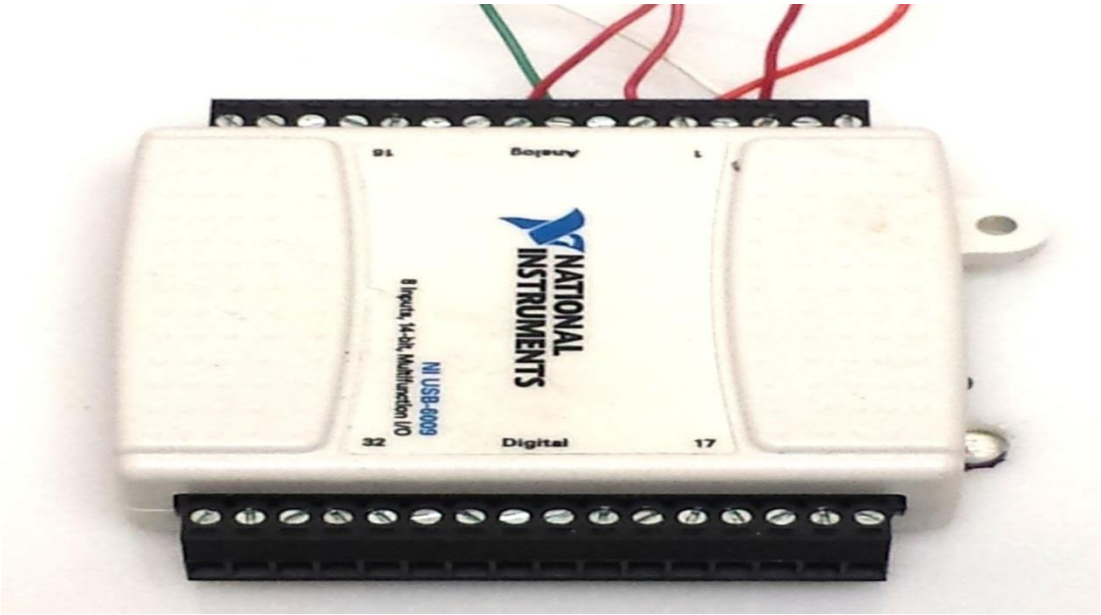


**Figure 17: NI analog to digital converter**

### *3.3.4 Data acquisition software*

After being converted from analog to digital, the voltage signal is sent via a Universal Serial Bus to the installed software Lab View Signal Express. The voltage signal is then recorded during the cutting process with a sampling rate based on the cutting speed. Indeed, the voltage is outputted with a time step corresponding to one degree of the cutting revolution. Post data processing is done using Microsoft excel where the voltages is converted to forces based on the scale factor obtained during the system calibration.

# 4. MILLING MACHINING EXPERIMENTS

In this section, dry milling cutting experiments will be conducted and the cutting forces will be measured. The experiments will be conducted according to the experimental design where cutting input parameters will be specified.

## 4.1 Introduction

Milling experiments are conducted to measure the cutting forces. A table mounted dynamometer with a fixed Cartesian coordinate system is set on the cutting table where the work piece is clamped on its surface. The cutting direction is set in the sense that the feed cutting direction correspond to the X axis of the fixed Cartesian coordinates system of the dynamometer. The transverse clockwise direction is set to the Y axis, and the normal to the top surface of the work piece is set to the Z direction as shown in Figure 18.

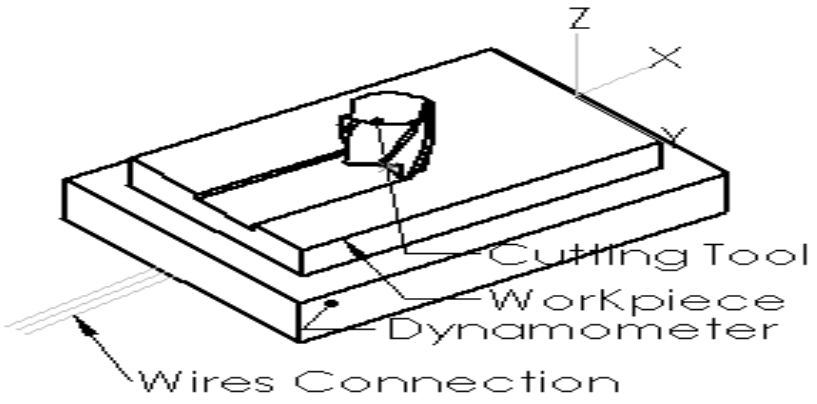


**Figure 18: Schematic of dynamometer with work piece and cutter**

A slot feature designed with FEATURECAM will be cut based on the experimental design described in Table 2.

**Table 2: Experimental design of milling cutting process**

| Experiment | Spindle speed (revolutions/min) | Feed (mm/min) | Depth (mm) |
|---|---|---|---|
| 1 | 2500 | 508 | 2.54 |
| 2 | 2500 | 635 | 2.54 |
| 3 | 2500 | 762 | 2.54 |
| 4 | 2750 | 508 | 2.54 |
| 5 | 2750 | 635 | 3.175 |
| 6 | 2750 | 635 | 2.54 |
| 7 | 2750 | 762 | 2.54 |
| 8 | 3000 | 508 | 2.54 |
| 9 | 3000 | 635 | 2.54 |
| 11 | 3000 | 762 | 2.54 |
| 10 | 2500 | 508 | 3.175 |
| 12 | 2750 | 635 | 5.08 |

The experimental design described in Table 2 consists of a modified half fraction factorial design where the cutting input variables such as the spindle speed, the feed rate, and the depth of cut will be compared based on the cutting forces measured during the milling process. The half fraction factorial design has been chosen to minimize the number of experiments and be able to study the effect of the cutting inputs parameters on the cutting forces. The reference cutting input parameters is described in Experiment 1 where the later experiments have an increase of 25 % based on the half fraction factorial design experiment method.

### 4.2 Cutting forces measurement from Experiment 1

The cutting forces are measured based on the cutting input parameters described in Table 2 for Experiment 1. Two different end mills with their respective detailed specifications listed in Table 1 will be used to describe the cutting forces during a dry milling process. The only difference between the tools is that one tool is coated with a Titanium Nitride material and the other is uncoated.

#### *4.2.1 Uncoated tool*

The forces' trend consists of an uncoated two teeth cutting tool where the cutting forces in the X, Y, Z directions are plotted against the cutting revolution in Figure 19.

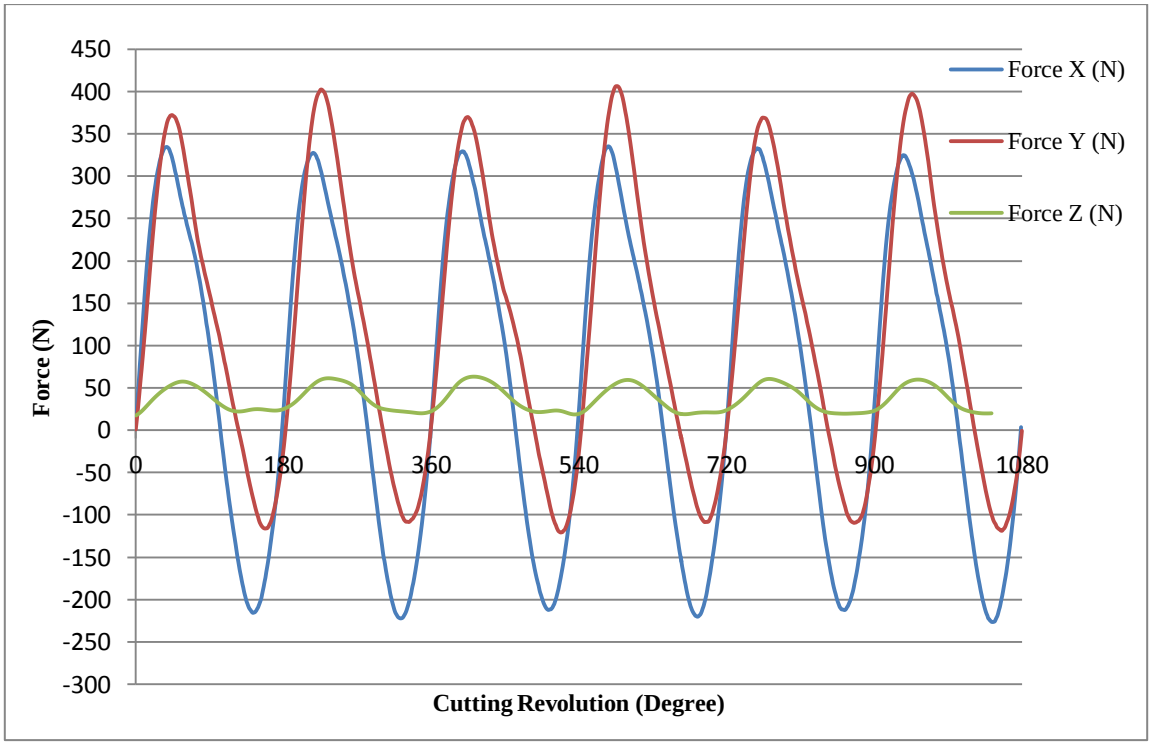


**Figure 19: Cutting forces from Experiment 1 with uncoated tool**

The first observation is that the cutting forces' patterns behave as a sinusoidal wave. These patterns describe the mechanic of cutting which is mainly due to the combination of the spindle speed and the feed rate.

The wave pattern repeats itself every 180 degrees where every half revolution represents the material being cut by one tooth of the tool.

The negative forces magnitude that can be observed in the X and Y direction is due to the tool teeth cutting position based on the fixed reference frame of the dynamometer's coordinate system. When the tool rotates and the teeth motion is aligned in the positive direction of the load cell sensor reference frame, the outputted forces are positive. When the teeth motion is in the negative direction, the outputted forces are negative.

The cutting forces in the Z direction are always positive because of the tool design and the reference coordinate system of the dynamometer pointed outward from its top surface. Based on the tool specifications, the tool has a center cut profile which allows the material to be also cut from its center. Indeed, when the tool teeth are not engaged during the cutting process (every 180 degrees), the dynamometer still sensing a force due to the contact of the center of the tool and the work piece which makes the cutting forces to never drop to zero.

The difference of the peaks values in the X and Y forces outputted for one tooth cutting cycle is due to the phenomena of up and down milling. In up milling, where the cutting rotation is in opposite direction of the feed direction, the outputted forces are

higher. However, in down milling, the cutting rotation is in the same direction as the feed direction which results in a lower magnitude of the cutting forces.

Another observation is the change in the magnitude of the peaks values of the cutting forces in the X and Y direction. The change in the peaks values from the cutting forces in the X direction is about 7 N and 30 N in the Y direction. Under normal circumstances, the cutting forces' peaks values should be the same every half revolution of the tool. The change in the peaks values is mainly due to the effect of the tool run out. The tool run out as described by Rivière-Lorphèvre and Filippi (2009) creates an uneven cutting where the chip load is not constant. In the present experiment, the measured value of the tool run out is about 14 micrometer.

### *4.2.2 Titanium Nitride Coated tool*

A Titanium Nitride Coated tool with similar tool design has the uncoated tool was used to perform the slot milling using the cutting input parameters specified in Experiment 1. The cutting forces were measured in the similar process as before and the forces were plotted in Figure 20.

The first observation that can be made is the high disturbance of the forces in the X and Y direction. The non-uniform forces' pattern suggested an uneven cutting motion among the cutting teeth. Again this phenomena is due to the tool run out which was measured to be 21 micrometer relatively larger than the tool run out measured with the uncoated tool.

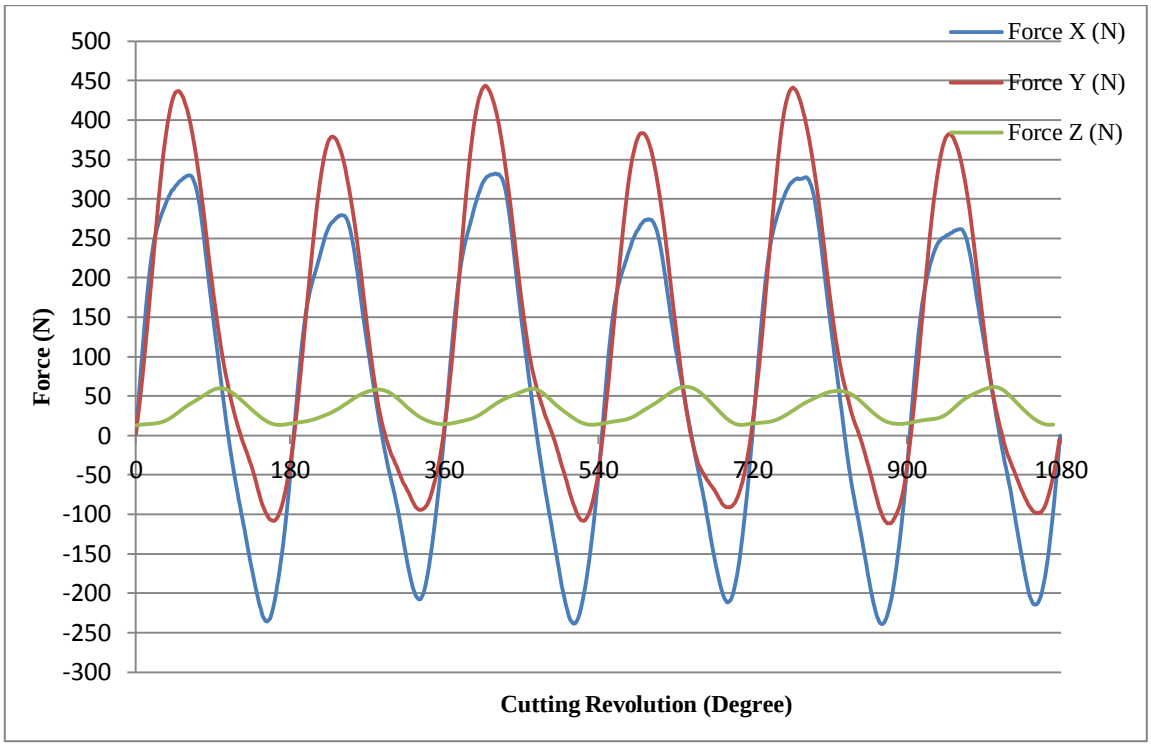


**Figure 20: Cutting forces from Experiment 1 with Titanium Nitride Coated tool**

Except the non-uniform forces' pattern due to the excessive run out, the profile of the cutting forces has same characteristic as the profile of the forces measured with the uncoated tool. One difference might be the magnitude of the forces' peaks between the coated and the uncoated tool. Due to the high disturbance from the coated tool, a fair comparison between the magnitudes of the forces' peaks from the two plots above cannot be done.

### 4.3 Parametric study of the cutting forces

After the interpretation of the pattern of the cutting forces, the next step is to study the effect of the cutting input parameters on the cutting forces. Indeed, the three

cutting input variables listed in the experimental design table, which are the feed rate, the spindle speed, and the depth of cut, will be analyzed to find their influence on the cutting forces. The uncoated tool will be chosen to run these experiments since a low variation in the peaks values of the cutting forces was observed contrary to the Titanium Nitride coated tool.

### *4.3.1 Effect of the feed rate*

To study the effect of the feed rate on the cutting forces, the measured forces values from Experiments 1, 2, 3 will be plotted and analyzed with a constant spindle speed of 2500 rpm and depth of cut of 2.54 mm. Similarly, the feed effect will be study at a spindle speed of the 3000 rpm from experiments 8, 9, 11 with a constant depth of cut of 2.54 mm.

#### *4.3.1.1 2500 revolutions per minute spindle speed*

The cutting forces in the X, Y, and Z direction based on three different feed rates with cutting speed of 2500 RPM are presented in Figures 21, 22, 23 respectively.

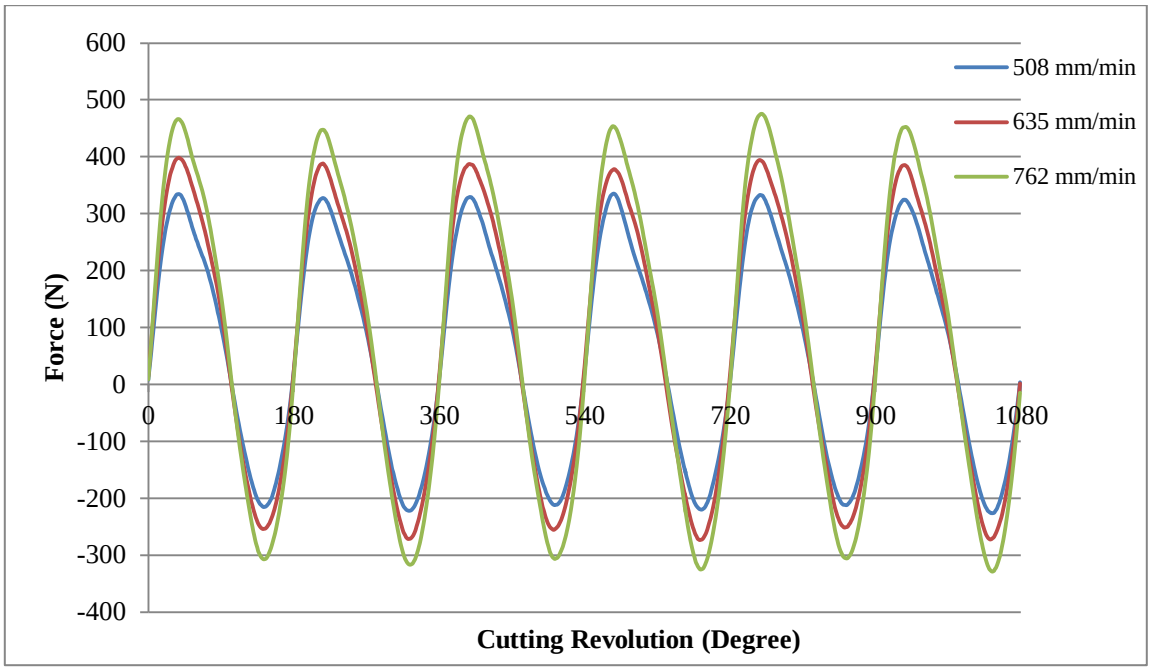


**Figure 21: Effect of the feed rate on the cutting forces in the X direction at 2500 RPM**

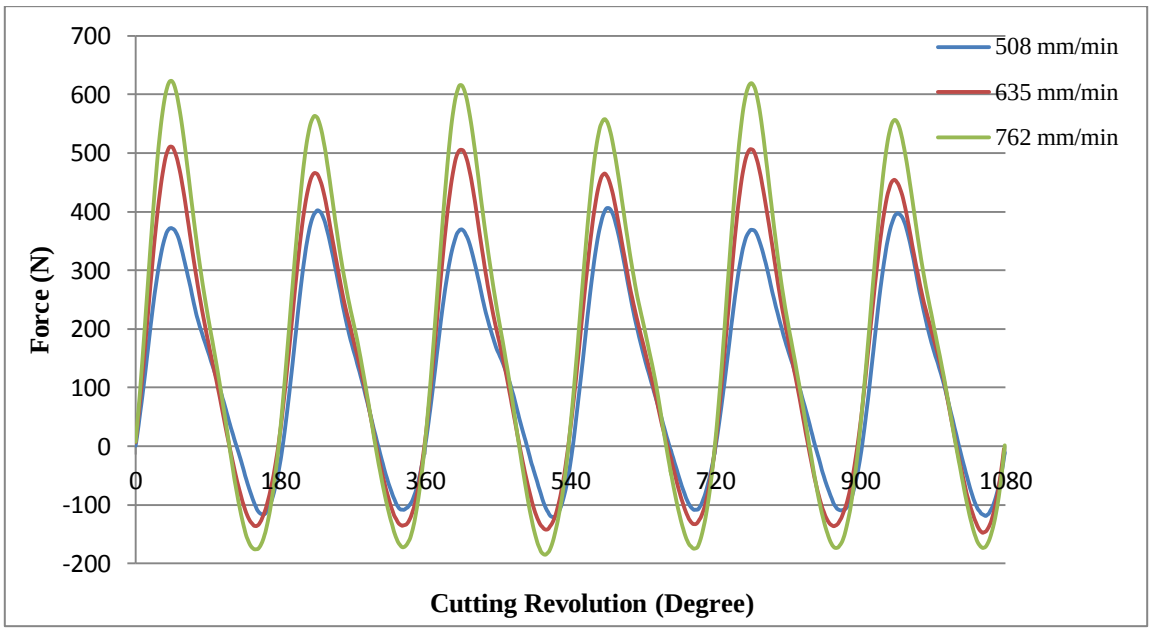


**Figure 22: Effect of the feed rate on the cutting forces in the Y direction at 2500 RPM**

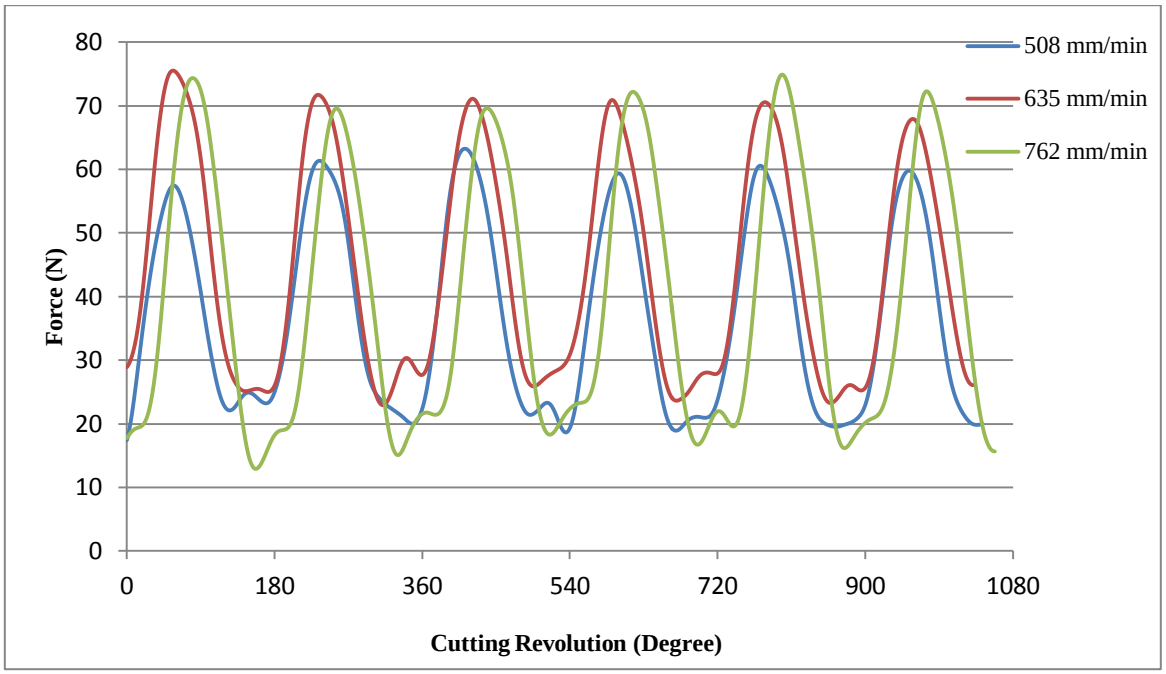


**Figure 23: Effect of the feed rate on the cutting forces in the Z direction at 2500 RPM**

An increase of the cutting forces from Figures 21, 22, 23 can be observed in general as the feed rate increases except in the Z direction where small perturbation can be seen when the feed rate value is set at 635 mm/min and 762 mm/min. This perturbation is due to the chips formed during cutting process that are trapped under the tool. Indeed, as the tool moves in the feed direction at higher speed, the magnitude of the vibration increases which creates more fluctuations in the measured cutting forces.

The increase of the cutting forces as the feed rate increase is due to the chip load as described in Equation 1. It is based on the amount of material that each tooth will remove during the cutting process. When the feed rate increases, the amount of the

material that is needed to be removed increases, therefore more forces are required to cut the material.

*4.3.1.2 3000 revolutions per minute spindle speed*

The cutting forces in the X, Y, and Z direction based on three different feed rates with a cutting speed of 3000 RPM are presented in Figures 25, 26, 27 respectively.

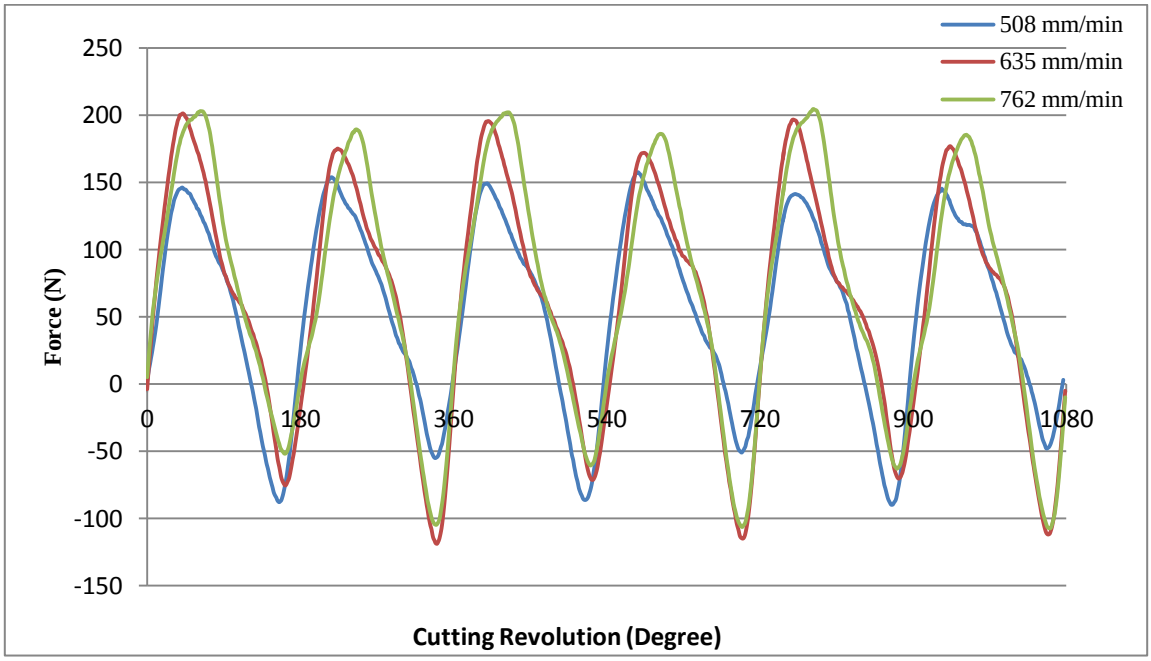


**Figure 24: Effect of the feed rate on the cutting forces in the X direction at 3000 RPM**

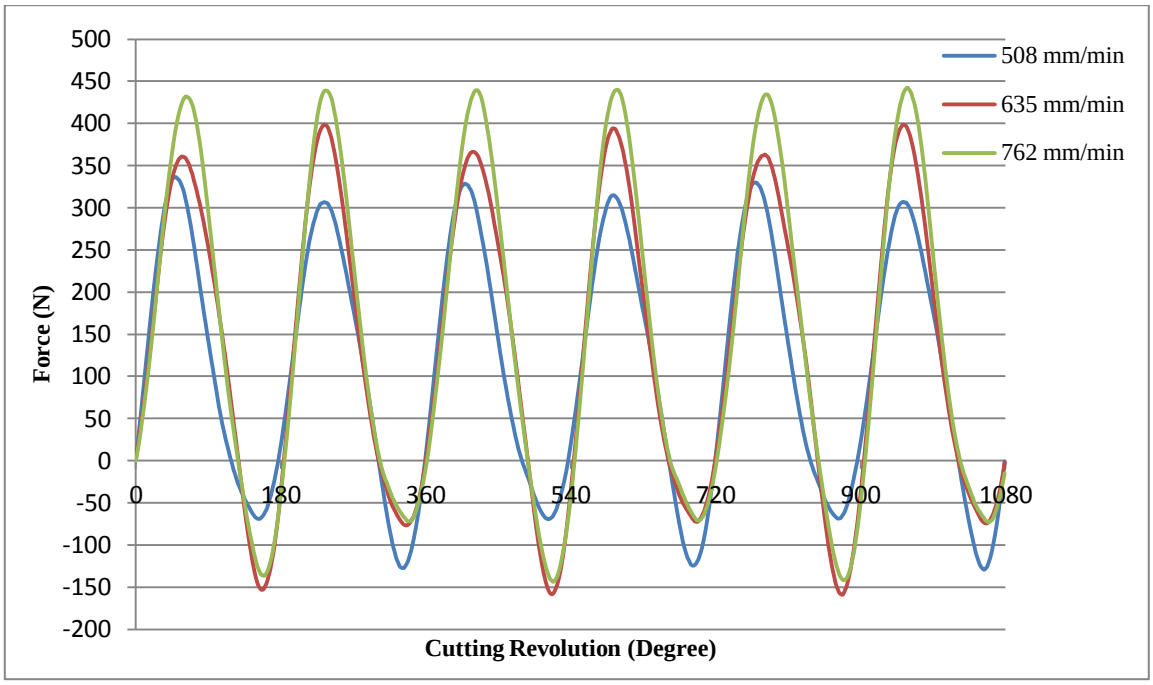


**Figure 25: Effect of the feed rate on the cutting forces in the Y direction at 3000 RPM**

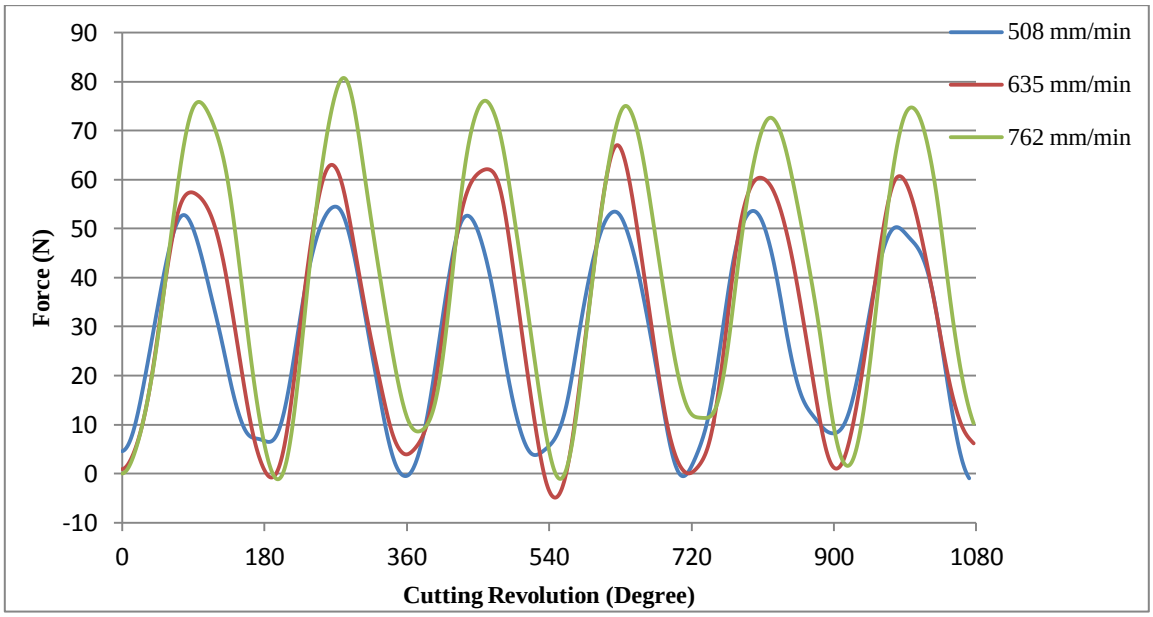


**Figure 26: Effect of the feed rate on the cutting forces in the Z direction at 3000 RPM**

Based on the plots presented in Figures 25, 26 and 27 the cutting forces increase as the feed rate increases.

Also, the non-uniformity mostly in the lower peaks values of the cutting forces can be observed. This behavior is due to the effect of spindle speed and the tool run out. At higher spindle speed, the effect of the tool run out has a more significant effect on the pattern of the cutting forces.

### *4.3.2 Effect of the spindle speed*

To study the effect of the spindle speed on the cutting forces, the measured forces from Experiments 1, 4, 8 will be plotted and analyzed with a constant feed rate of 508 mm/min and depth of cut of 254 mm. Similarly, the spindle speed effect will be studied at a constant feed rate of 762 mm/min from experiments 3, 7, 11 with a depth of cut of 2.54 mm.

#### *4.3.2.1 508 mm/min per minute feed rate*

The cutting forces in the X, Y, and Z direction based on three different spindle speeds with a feed rate of 508 mm/min are presented in Figures 27, 28, 29 respectively.

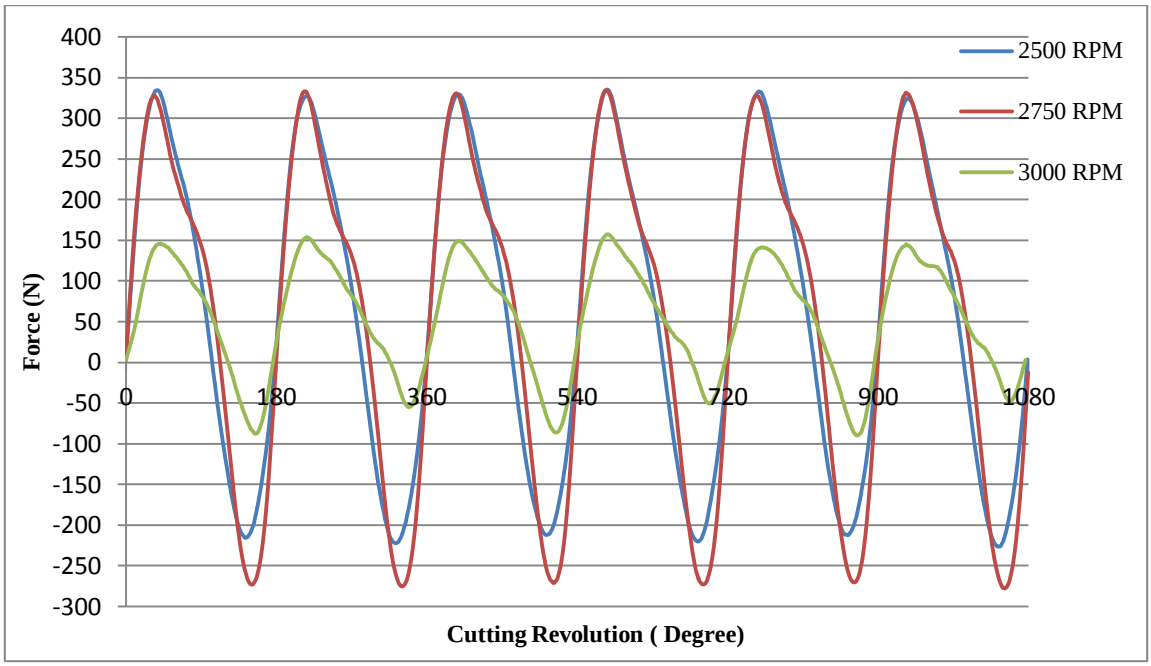


**Figure 27: Effect of the spindle speed on the cutting forces in the X direction at 508 mm/min**

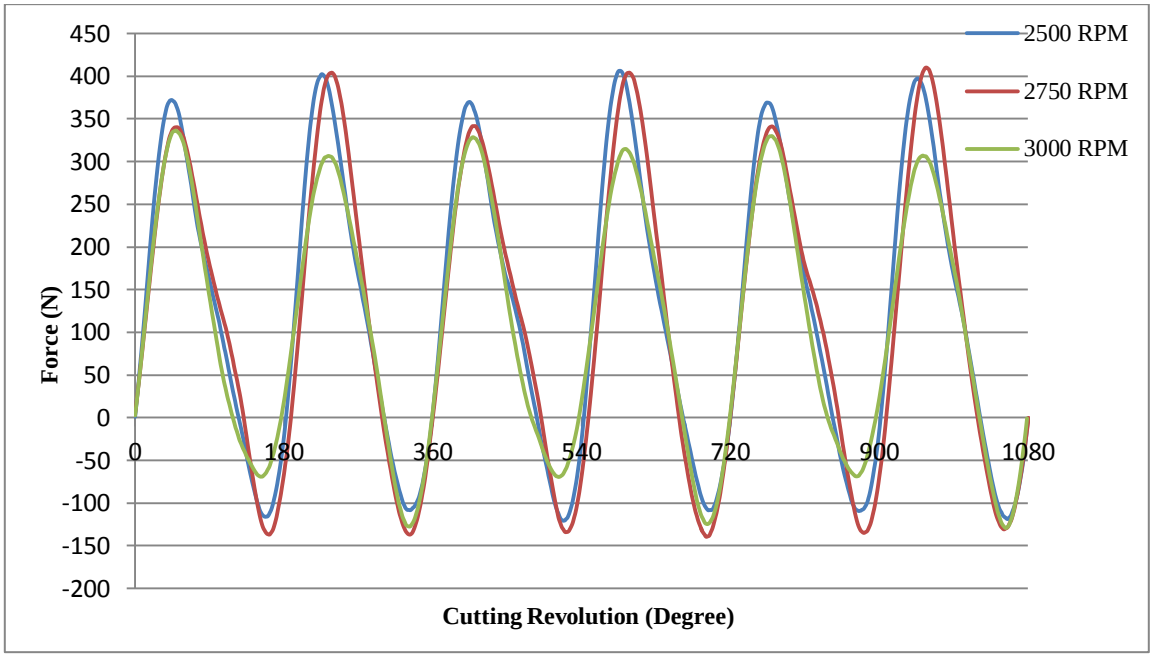


**Figure 28: Effect of the spindle speed on the cutting forces in the Y direction at 508 mm/min**

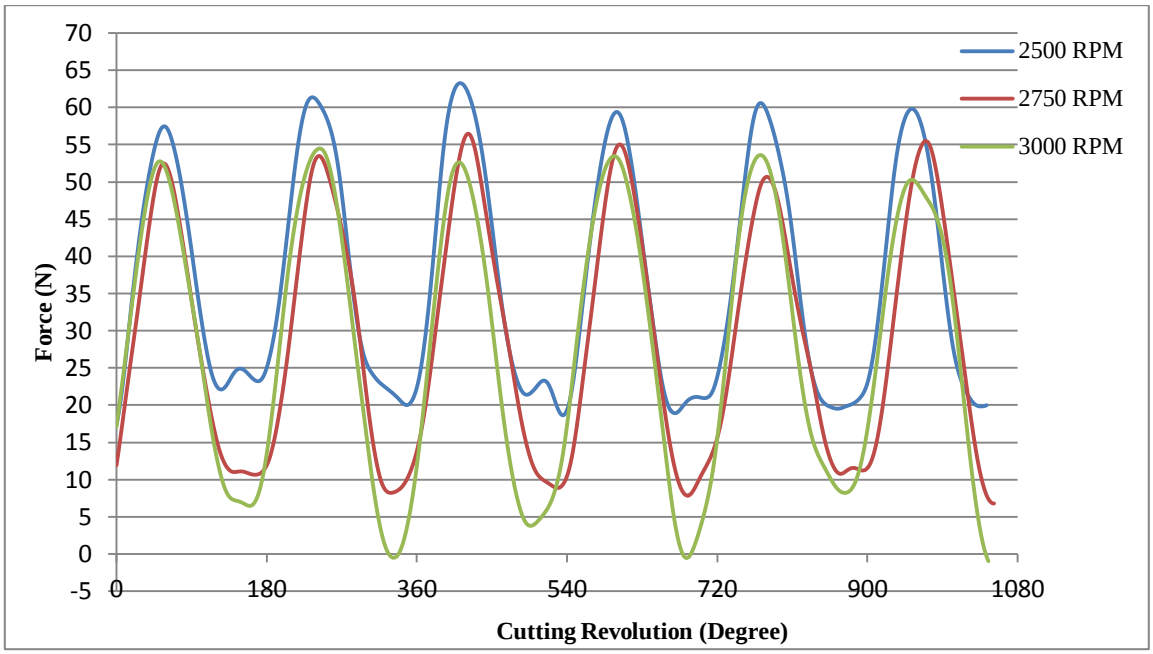


**Figure 29: Effect of the spindle speed on the cutting forces in the Z direction at 508 mm/min**

Based on the plots from Figures 27, 28 there is slight variation of the cutting forces magnitude when the spindle speed is at 2500 RPM and 2750 RPM, except for the lower peaks values where the forces at 2750 RPM have higher magnitude that the forces at 2500 PM.

Comparing the forces in the X, Y and Z direction at 3000 RPM with the other at 2500 RPM and 2750 RPM, a relatively low force magnitude is observed. Again, the low force magnitude at 3000 RPM is justified by the chip load as described in Equation 1. When the spindle speed increases at a constant feed rate, the chip load decreases, therefore lower forces are required to cut the material.

*4.3.2.2 762 mm/min per minute feed rate*

The cutting forces in the X, Y, and Z direction based on three different spindle speeds with a feed rate of 762 mm/min are presented in Figures 30, 31, 32 respectively.

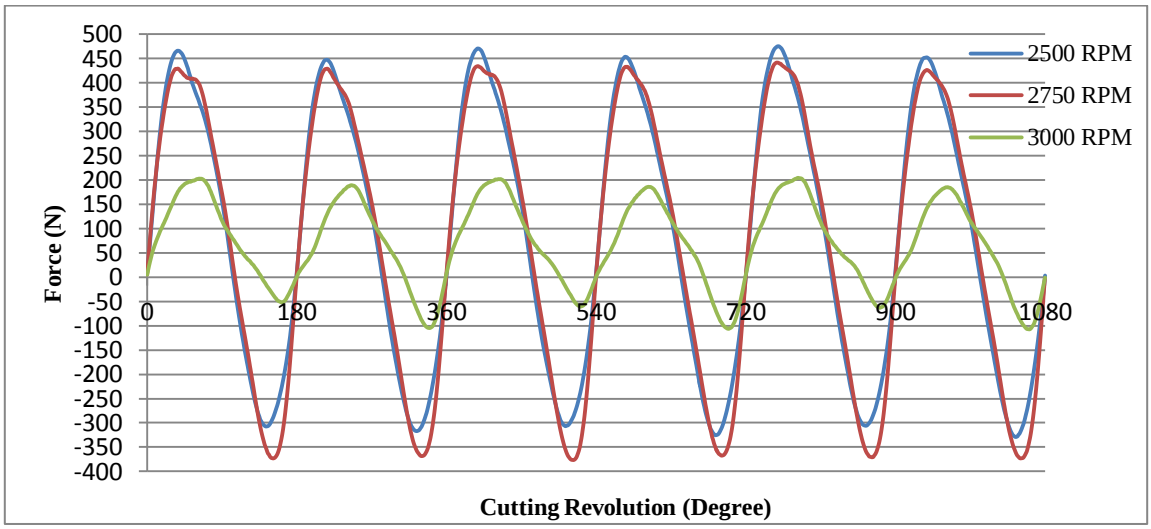


**Figure 30: Effect of the spindle speed on the cutting forces in the X direction at 762 mm/min**

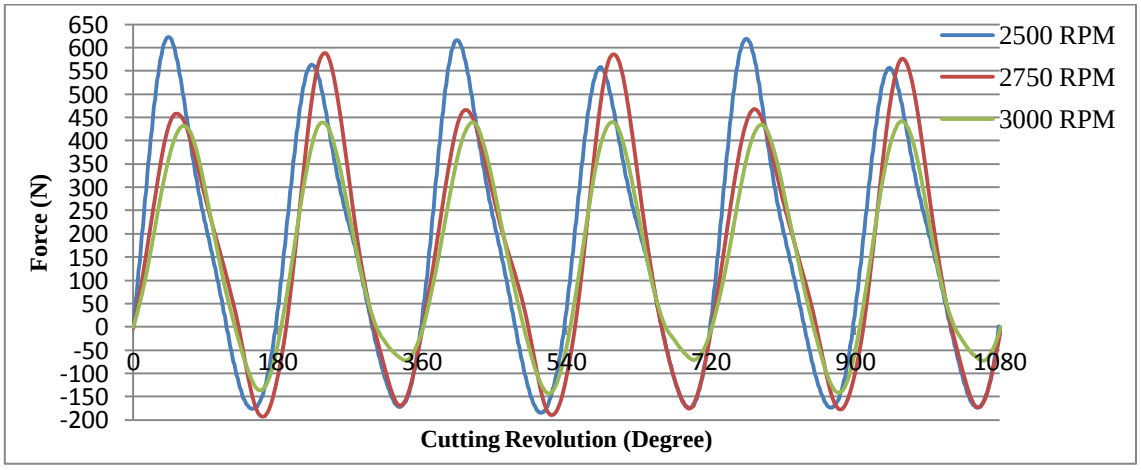


**Figure 31: Effect of the spindle speed on the cutting forces in the Y direction at 762 mm/min**

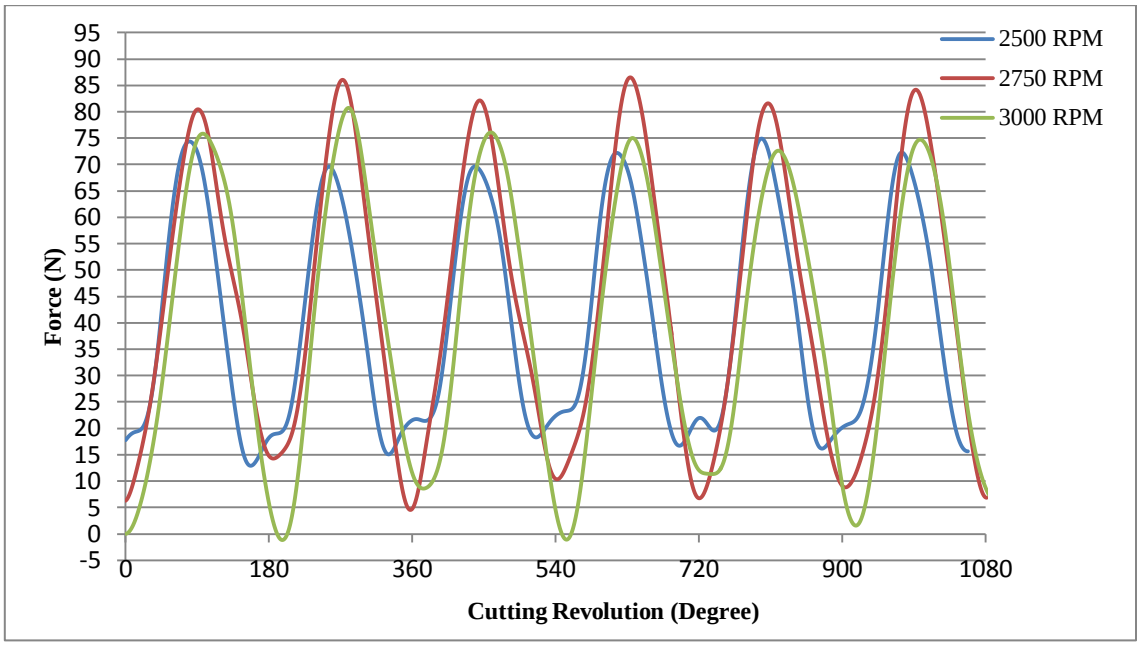


**Figure 32: Effect of the spindle speed on the cutting forces in the Z direction at 762 mm/min**

From the Figures 30 to 32, a slight variation of the cutting forces in the X direction can be observed at 2500 RPM and 2750 RPM except the low peaks values where the cutting forces are higher at 2750 RPM.

In the Y direction, a significant variation of the peaks values of the forces magnitude can be observed. This is due to the tool run out as explained in the previous analysis. The magnitude of the cutting forces at 2500 RPM is higher than the forces at 2750 RPM.

At 3000 RPM, a low magnitude of the cutting forces is observed compared to the other cutting speeds. Again, as the spindle speed increases, lower forces are required to cut the material.

### *4.3.3 Effect of the depth of cut*

The depth of cut plays an important role in machining. Cutting at higher depth can decrease the machining time and increase the productivity. To study the effect of the depth of cut on the cutting forces, the measured forces from experiments 5, 6, 12 will be plotted and analyzed with a constant feed rate of 635 mm/min and a spindle speed of 2750 RPM. The cutting forces in the X, Y, Z direction is presented in Figures 33, 34, 35 respectively.

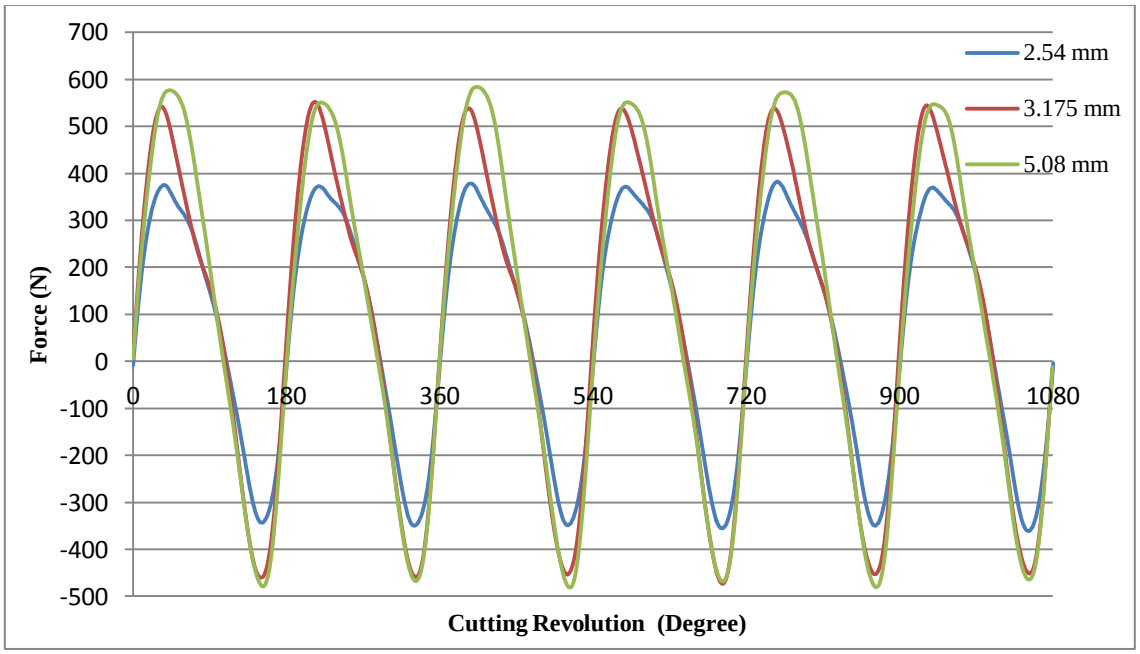


**Figure 33: Effect of the depth of cut on the cutting forces in the X direction**

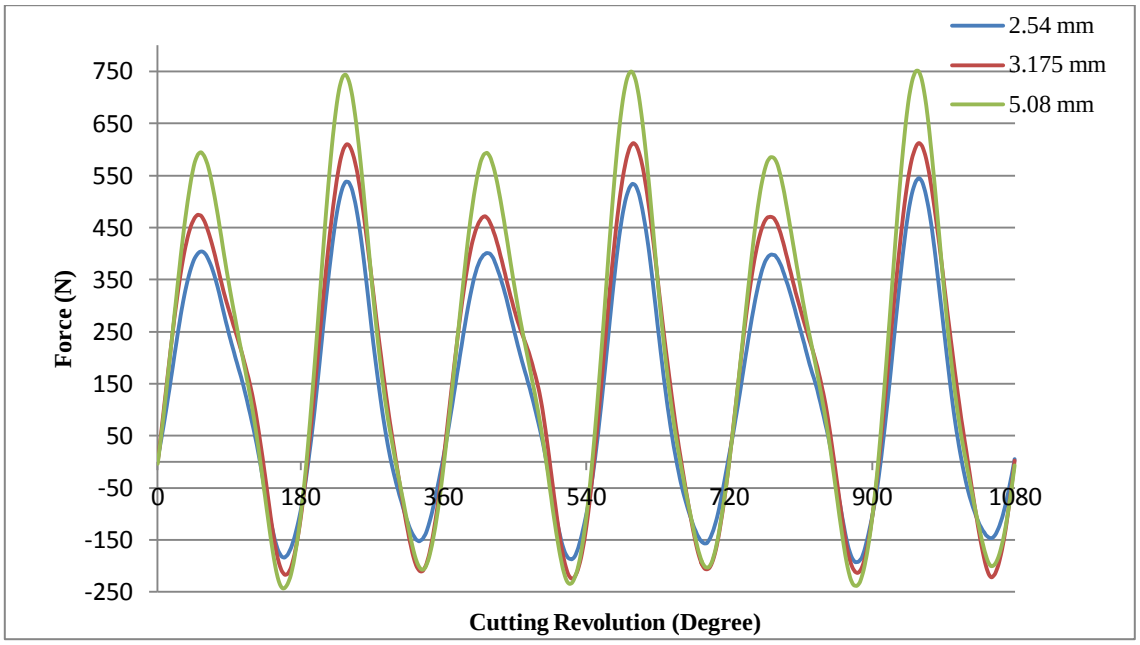


**Figure 34: Effect of the depth of cut on the cutting forces in the Y direction**

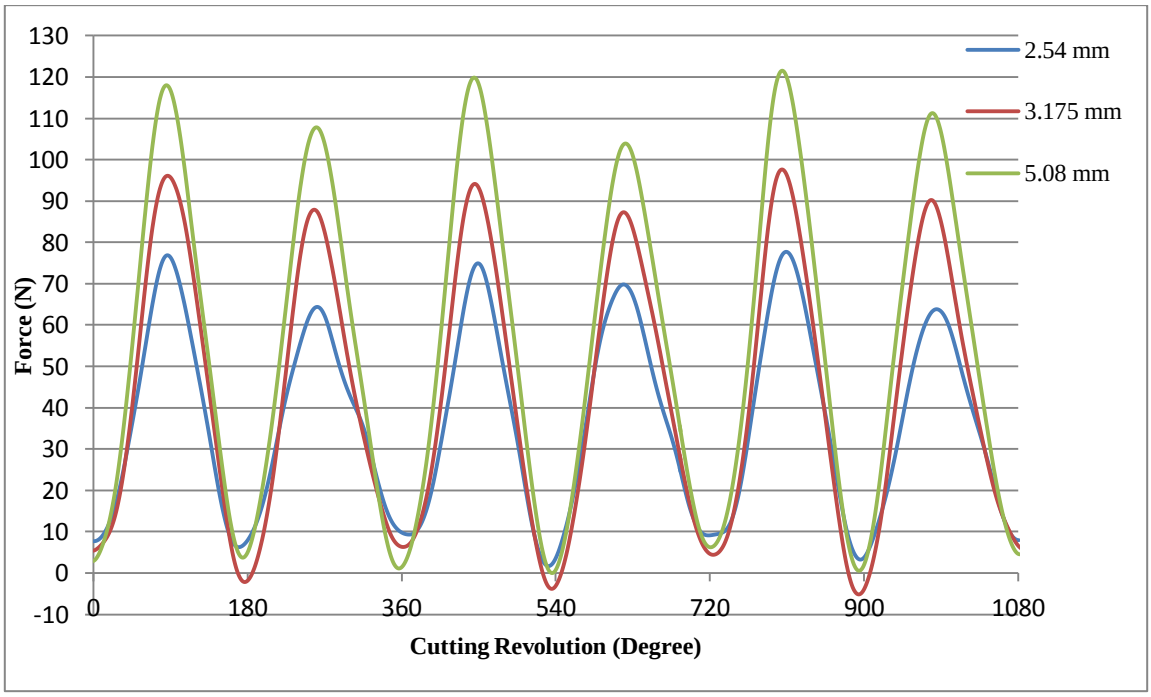


**Figure 35: Effect of the depth of cut on the cutting forces in the Z direction**

Based on the plots in Figure 33, the cutting forces in the X direction increase as the depth of cut increases except when the cut depth is set at 3.175 mm and 5.08 mm where a small change of 32 N is observed.

In Figure 34, the cutting forces in the Y direction increase to 67 N and 129 N respectively from a cut depth of 2.54 mm to 3.175 mm and 3.175 mm to 5.08 mm.

In Figure 35, the cutting forces in the Z directions also increase to 20 N and 24 N respectively from a cut depth of 2.54 mm to 3.175 mm and 3.175 mm to 5.08 mm. The change in the peaks values of the cutting forces in Figures 36 and 37 is also due to the effect of the tool run out which create a non-even cutting among the tool teeth. In general, as the depth of cut increases, the magnitude of the cutting forces also increases. This fact is due to the amount of material cut during the milling process since the volume of material removed increases when deeper cuts are done.

### *4.3.4 Cutting forces and work piece step up*

To investigate the effect of the part initial set up on the machine table, the work piece was intentionally clamped with a ramp angle approximately of 2 degree. Indeed, the tool will cut the work piece at a higher depth of cut which will be reduced as the tool move in the feed direction. The cutting forces in the X, Y and Z direction were measured at 2500 RPM, 508 mm/min and the plots are presented in Figures 36, 37 and 38.

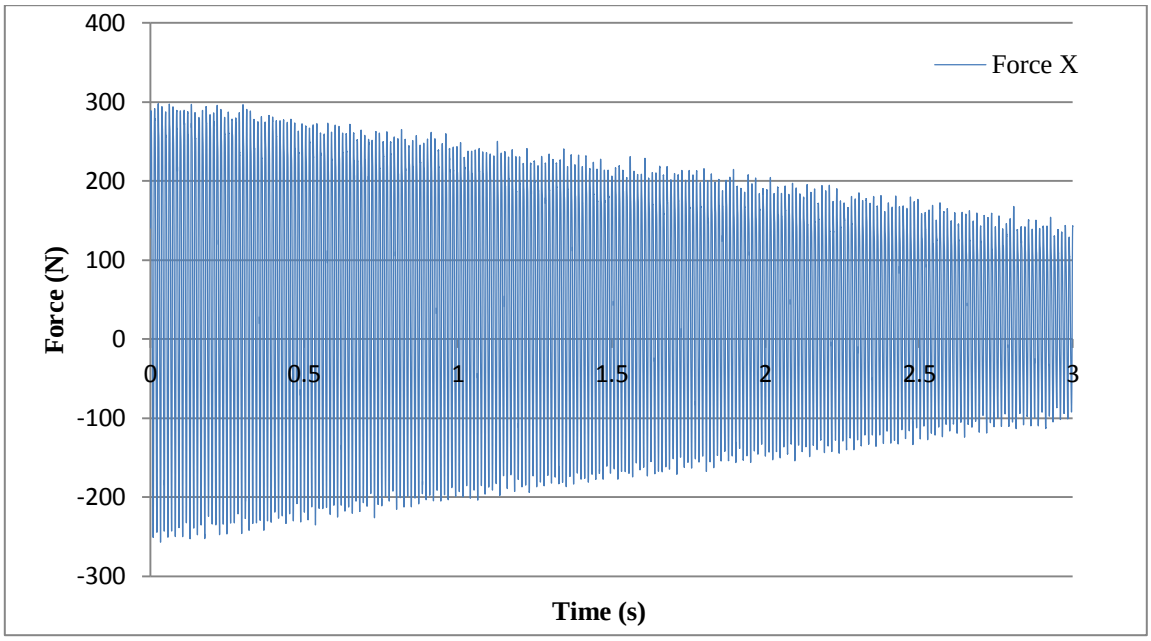


**Figure 36: Cutting forces in the X direction with a ramp of 2 degree**

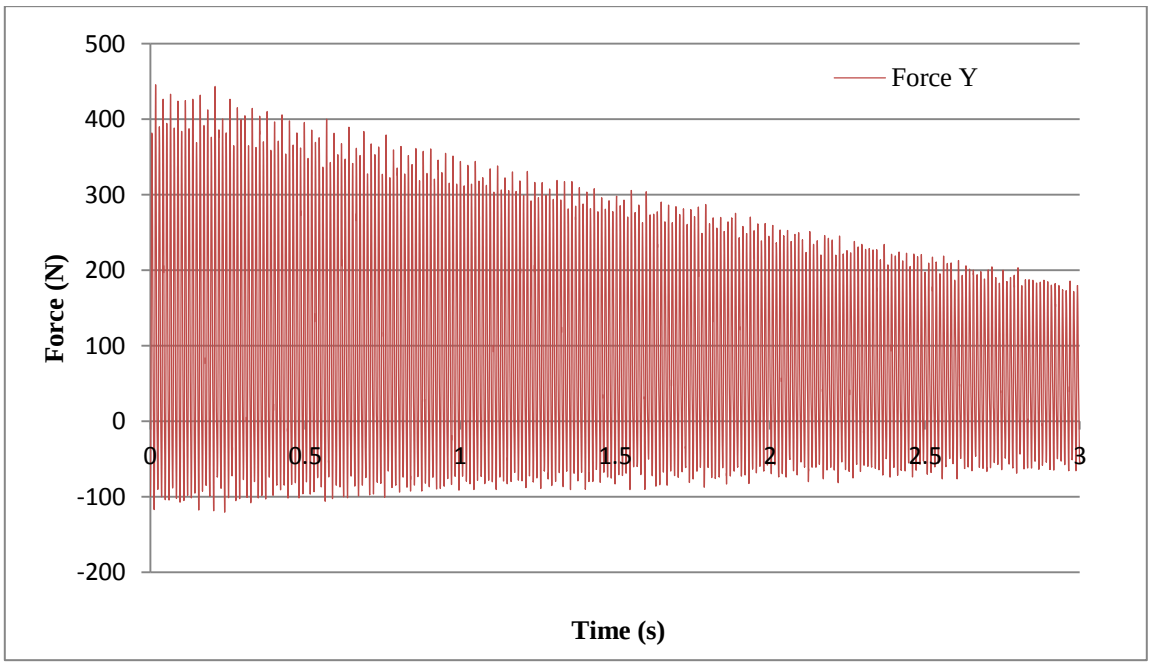


**Figure 37: Cutting forces in the Y direction with a ramp of 2 degree**

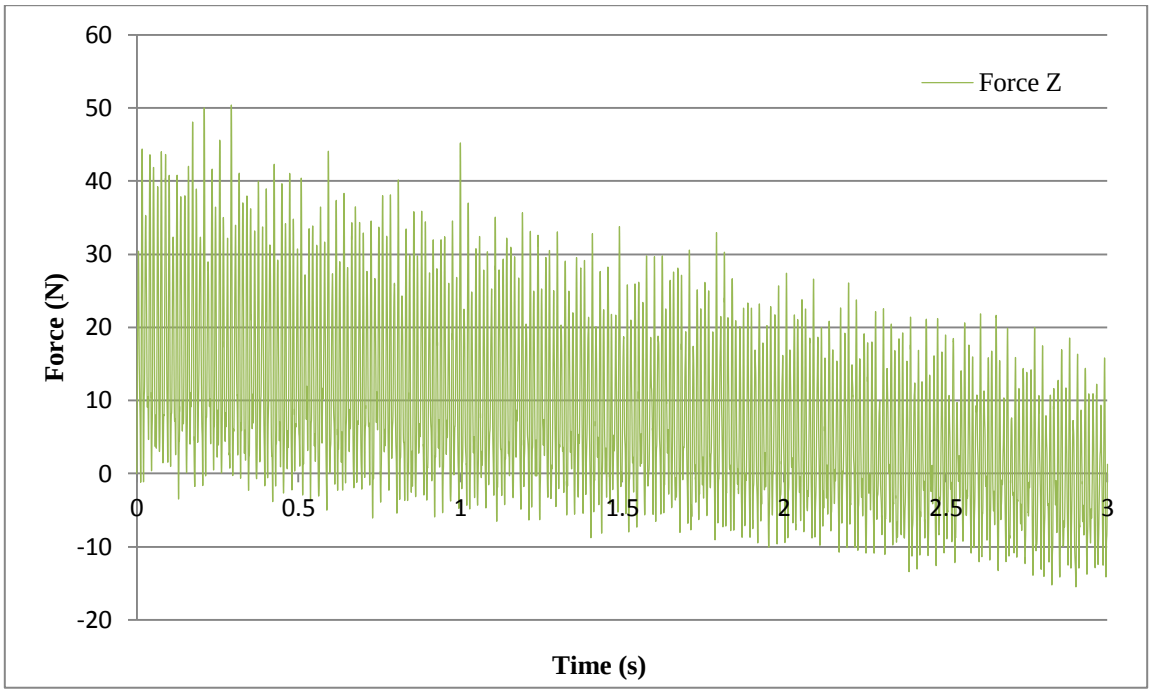


**Figure 38: Cutting forces in the Z direction with a ramp of 2 degree**

From Figures 36 to 38, the magnitude of the cutting forces decreases as the tool moves in the feed direction. The decrease of the cutting forces' magnitude is due to amount of material removed as the tool moves linearly into the work piece. As shown in the previous section, as the depth of the cut decreases, the cutting forces' magnitude decreases also. These results show that the work piece misalignment with the cutting table can be observed using the cutting forces' signature.

### *4.3.5 Cutting forces and CNC machine condition*

The milling cutting process was done using a different CNC machine. An old CNC machine was used to cut the specimen following the exact machining parameters, tool, and work piece material which was done using the HAAS CNC machine.

Preliminary inspection about the condition of the old CNC machine shows that the Quill as highlighted in Figure 39, which is part of CNC machine where the tool holder is inserted, had some mechanical problems. The inspection shows that the bearing inside have been damaged which created an eccentricity between the tool holder and the spindle gear rotation axis. The problem of eccentricity leads to the significant tool run out and vibration during the cutting process.

**Figure 39: Old CNC machine**

The cutting forces were measured using the same experiment set up at a spindle speed of 2500 RPM, a feed rate of 508 mm/min and a depth of cut of 2.54 mm. Figures 40, 41, 42 show the measured cutting forces in X, Y, and Z direction respectively.

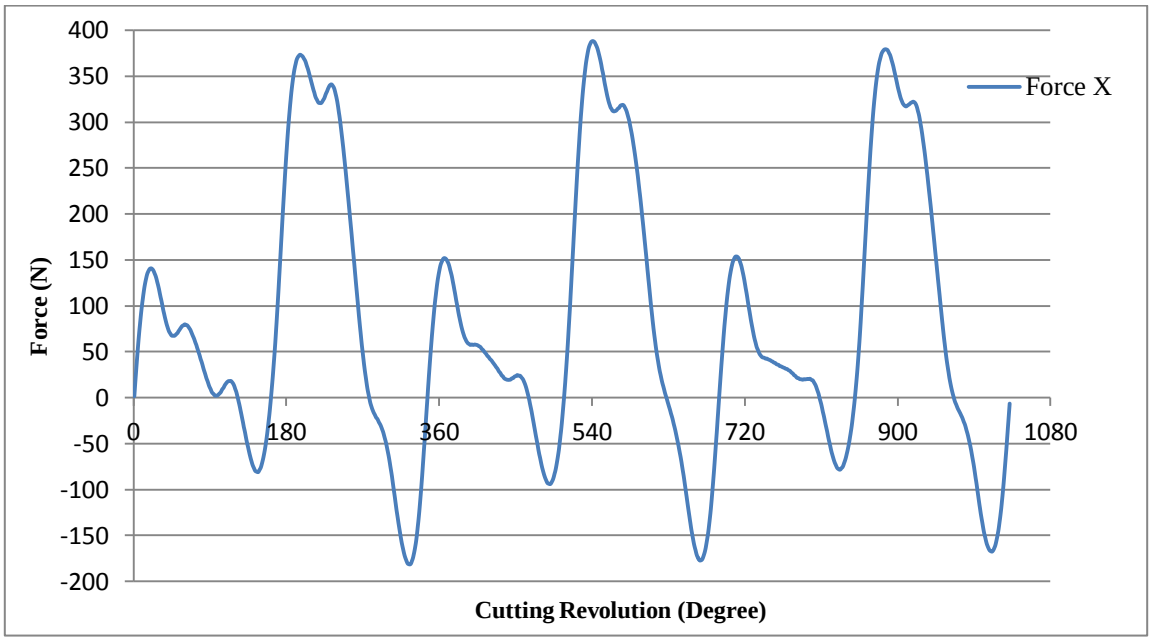


**Figure 40: Cutting forces in the X direction at 2500 RPM, 508 mm/min, and 2.54 mm with an old CNC machine**

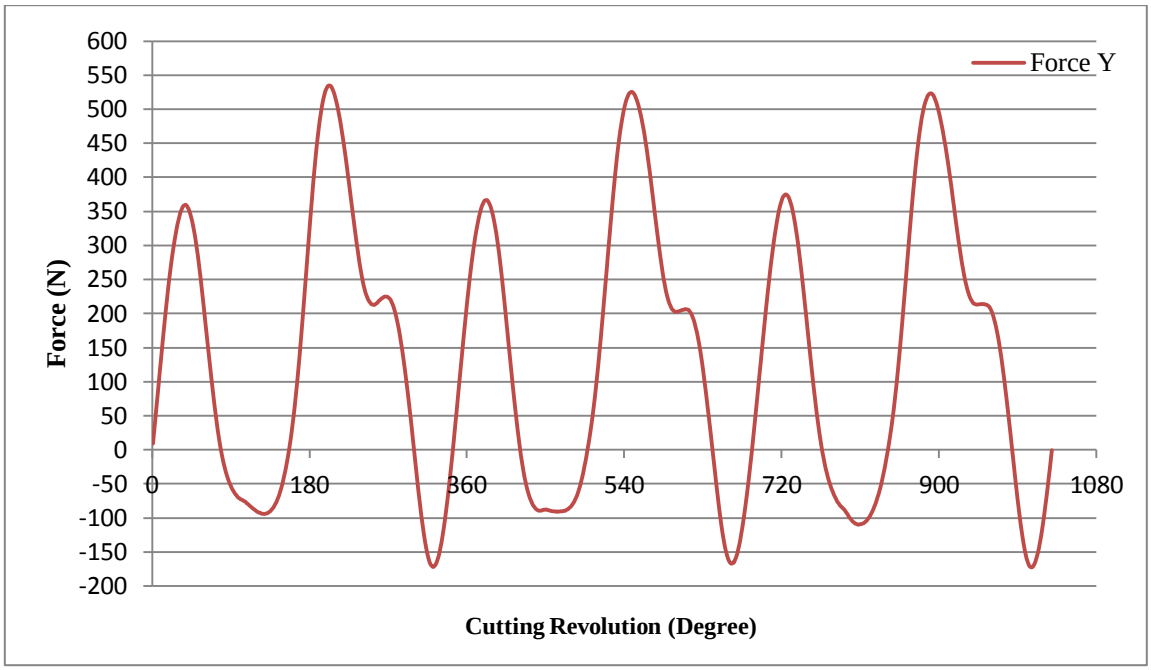


**Figure 41: Cutting forces in the Y direction at 2500 RPM, 508 mm/min, and 2.54 mm with an old CNC machine**

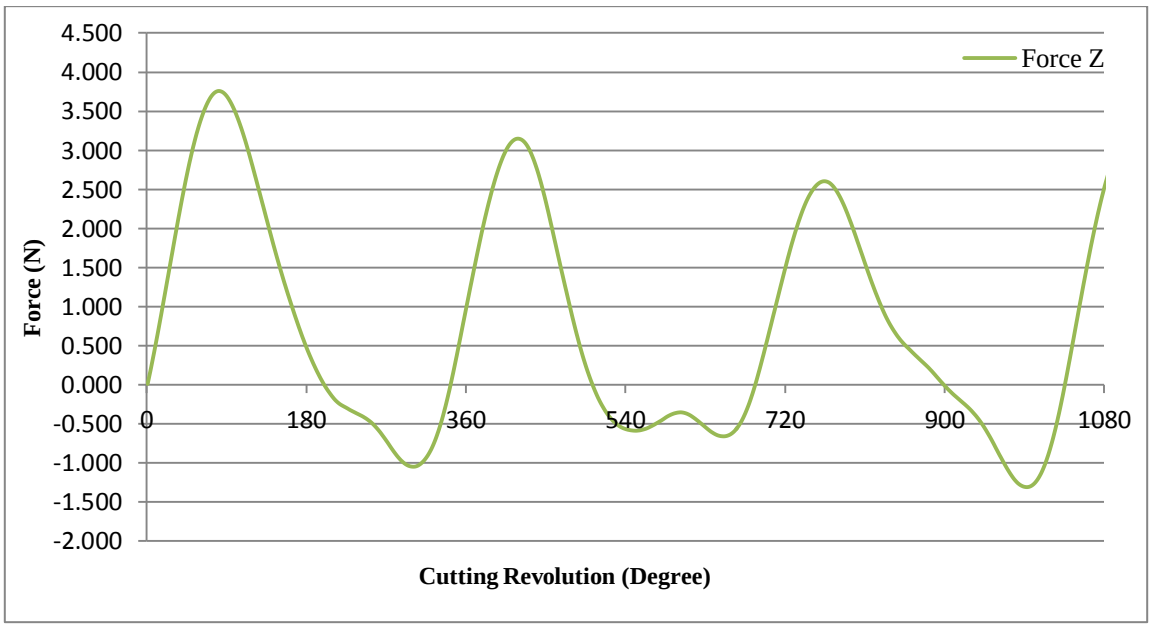


**Figure 42: Cutting forces in the Z direction at 2500 RPM, 508 mm/min, and 2.54 mm with an old CNC machine**

The measured cutting forces in the X direction from Figure 40 shows a significant deviation from the peaks values of about 229 N whereas a change in the peaks values of the force of 7 N is observed when the HAAS CNC machine was used to cut the specimen.

The deviation in the peaks values is also observed in Figure 41 from the cutting forces in Y direction. The deviation in the magnitude of the force is about 175 N whereas a change in the peaks values of the force 30 N is observed when the HAAS CNC machine was used.

The significant difference in the magnitude of the peaks forces in the X and Y direction from the measured forces using the old CNC machine is due to the excessive tool run out. The tool run out creates an uneven chip load among the tooth.

The magnitude of the cutting forces in the Z direction is relatively low compared to the measured forces in the Z direction using the HAAS CNC machine in Figure 19. The low cutting forces' magnitude in the Z direction is due to the excessive vibration that could be heard during the cutting process due to the damaged bearing from the old CNC Quill. The vibration also caused the steps feature observed in the forces pattern measured in the X and Y direction within one cutting revolution. The cutting revolution, which should be every 180 degree per tooth, is observed to be 160 degree. This means that even though the input spindle speed of 2500 RPM was prescribed to cut the slot, the actual spindle speed during the cutting process was reduced approximately to 2223 RPM. The actual spindle speed was calculated based on the time recorded during the cutting process.

### 4.4 Results from the parametric study

Different cutting input parameters were used and the cutting forces were measured. The first investigation that has been conducted was to study the effect of the feed rate on the cutting forces. Based on the results obtained, the cutting forces in all directions increase as the feed rate increases. The increase of the cutting forces is due to the chip load which increases as the feed rate increases. Therefore, higher forces are needed to cut the material.

The second investigation that has been conducted was to study the effect of the spindle speed on the cutting forces. Based on the results obtained, the cutting forces in all directions generally decrease as the spindle speed increases except at 2750 RPM where the cutting forces did not change much. Again the decrease of the cutting forces is due to the effect of the spindle speed on the chip load. At higher cutting speed, the chip load decreases which leads to low cutting forces.

The third investigation that has been conducted was to study the effect of the depth of the cut on the cutting forces. Based on the results obtained, the cutting forces increase as the depth of the cut increases. Indeed, as the depth of the cut increases, more material need to be removed; therefore the magnitude of the cutting forces increases.

The last investigation was to evaluate the effect of the machine condition on the measured cutting forces. The cutting process was done using a poor condition CNC machine and the measured cutting forces were compared to the cutting forces measured with the calibrated CNC machine. The measured cutting forces from the poor CNC machine present some interesting features such as high deviation from peak to peak

forces' magnitude which confirmed the excessive tool run out. Also, excessive vibrations result steps pattern observed in the forces trend and a low force magnitude in the Z direction.

# 5. FINITE ELEMENT MODEL SIMULATING THE DRY MILLING CUTTING PROCESS

In this section, an approach and a method to develop the cutting simulation will be described. Indeed, a parametric study will be done to show the effect of the cutting input parameters on the predicted forces. Thus, the predicted cutting forces will be compared to the measured cutting forces to show the accuracy of the FEA model.

## 5.1 Introduction

The milling cutting process simulation consists of a tool rotating at a high speed and the work piece which moves linearly against the tool. This simulation is very complex in the sense that it involves a tool that cut a material and large deformations are generated which create a nonlinear dynamic problem. The two adequate simulation methods, which are available in the commercial ABAQUS 6.12 FEA software that can be used to simulate the cutting process, are ABAQUS Implicit and Explicit.

The implicit method used an implicit time integration which is mostly adequate for dynamics or quasi static problems. The implicit method gives very accurate solution but the computational time is costly for large dynamics problem since the stiffness matrix needs to be rebuilt every time increment. However, the explicit method gives fast and accurate results as long as small time increments are used. The stiffness matrix is updated based on previous step time increments, the material properties, and the geometrical changes.

The explicit method will also reduce the computational time which is one main factor when running an FEA simulation.

### 5.2 Tool and work piece three-dimensional model

Due to the geometric complexity of the end mill tool, the cutting section of the tool was drawn using the CAD software SOLIDWORKS 2012. The provided dimensions (Table 1) specified by the tool manufacturer were not enough to create the three-dimensional profile of the tool. The missing dimensions were manually measured using the DINO LITE Digital Microscope. A step file was then generated once the completed profile was created and then imported into ABAQUS. The tool was assumed to be discrete rigid even though wears and heat transfer between the work piece and the tool interaction in a real time cutting environment are present. The discrete rigid assumption will save a lot of computational time since the mesh generated from the tool will not take part of the computation. However, the work piece was modeled using the part module of ABAQUS because of its simplicity. The work piece was model as a three-dimensional deformable body, since chips are expected to be formed during the cutting process. A semi-circle precut describing 180 degree rotation of tool was done to the work piece to save the computational time.

## 5.3 Material properties and failure model

### *5.3.1 Cutting tool*

Since the cutting tool was assumed to be a rigid body, no material properties were assigned to it. However, a reference point, which was set at its center mass, was inserted. Putting the reference point at its center of mass will allow the cutting forces to be outputted. The inertia properties were directly calculated from the FEA software based on the geometry of the tool.

### *5.3.2 Work piece*

The Aluminum 6061 T6 was used as work piece material. Since the cutting is a dynamic process based on large deformation with strain rate and temperature dependence, the Johnson Cook's plasticity model for isotropic material were used to model the flow stress as described in Equation 4, ABAQUS (2012).

$$\bar{\sigma} = \left[A + B\left(\bar{\varepsilon}^{pl}\right)^{n}\right]\left[1 + C\ln\left(\frac{\dot{\bar{\varepsilon}}^{pl}}{\dot{\varepsilon}}\right)\right]\left[1 - \left(\frac{T - T_r}{T_m - T_r}\right)^{m}\right] \tag{4}$$

The first bracket describes the material strain hardening, the second bracket describes the strain rates effect and the last bracket describes the temperature softening effect. The constant A, B, n are related to the strain hardening, C is related to the strain rate, m is related to the temperature softening. The term $\bar{\varepsilon}^{pl}$ is the plastic strain, $\dot{\bar{\varepsilon}}^{pl}$ the equivalent plastic strain rate, $\dot{\varepsilon}$ the reference strain rate, $T_r$ the reference temperature, $T_m$ the melting temperature, and $T$ the computed temperature. The cutting process is

assumed to be adiabatic, thus the change of the temperature is based on the density $\rho$ and the specific heat $C_p$ of the material.

Since the work piece material is classified as a ductile material, the ductile damage criterion is used to define the failure of the material which in this case describes the chips generation during the cutting process. The damage or failure of the elements, which is based on the plastic strain, occurs when the value of damage parameter $W_D$ is equal to 1 and elements are deleted. The ductile damage failure criterion is described in Equation 5, ABAQUS (2012).

$$W_D = \int \frac{d\bar{\varepsilon}^{pl}}{\bar{\varepsilon}_D{}^{pl}\left(\eta, \dot{\bar{\varepsilon}}^{pl}\right)} \tag{5}$$

The term $\bar{\varepsilon}_D{}^{pl}$ is the equivalent plastic strain when the damage occurs and it depends on the stress triaxiality $\eta$ and the equivalent plastic strain rate. The stress triaxiality is defined as the ratio of the pressure stress and the equivalent Von Mises stress.

To compute the equivalent plastic strain when the damage occurs, the Johnson Cook's damage criterion is used as described in Equation 6, ABAQUS( 2012).

$$\bar{\varepsilon}_D{}^{pl} = \left[d_1 + d_2 \exp\left(-d_3\eta\right)\right]\left[1 + d_4 \ln\left(\frac{\dot{\bar{\varepsilon}}^{pl}}{\dot{\varepsilon}}\right)\right]\left[1 + d_5\left(\frac{T - T_r}{T_m - T_r}\right)\right] \tag{6}$$

The terms $d_1$, $d_2$, $d_3$, $d_4$, $d_5$ represent the failure coefficients. Once the damage occurs, the energy release rate is assumed to be zero.

The Aluminum 6061 T6 material parameters from experimental data are presented in tables 3, 4 and 5.

**Table 3: Aluminum 6061 T6 general mechanical properties, Zhu, Mobasher, Rajan and Peralta (2011).**

| *Material* | *Elastic modulus (GPA)* | $\rho$ *(kg/m$^3$)* | *Poison Ratio* | $C_p$ (J/kg-K) | $\dot{\varepsilon}$ (1/s) |
|---|---|---|---|---|---|
| Al 6061 T6 | 69 | 2700 | 0.33 | 896 | 1.0 |

**Table 4: Aluminum 6061 T6 Johnson Cook Plasticity, Zhu, Mobasher, Rajan and Peralta (2011).**

| *Material* | *A (MPA)* | *B (*MPA） | *n* | *c* | *m* |
|---|---|---|---|---|---|
| Al 6061 T6 | 282 | 484 | 0.396 | 0.082 | 1.34 |

**Table 5: Aluminum 6061 T6 Johnson Cook effective plastic strain, Lesuer (1999).**

| *Material* | $d_1$ | $d_2$ | $d_3$ | $d_4$ | $d_5$ |
|---|---|---|---|---|---|
| Al 6061 T6 | -0.77 | 1.45 | -0.47 | 0 | 1.6 |

The sign of the parameter $d_3$ used to compute the effective plastic strain was changed to a positive sign as recommended from the ABAQUS (2012) user's manual. The reference and melting temperature used in the simulation are respectively 293 K and 925 K.

### 5.4 Element type and mesh

A variety of element types are available in ABAQUS explicit. The choice of element is based on the type of analysis that is conducted and the outputted variables that are requested. Selecting the wrong element type will lead to a wrong analysis, thus erroneous results.

### *5.4.1 Cutting tool element and mesh*

The cutting tool was imported from SOLIWORDS and was modeled as a discrete rigid part. The option of discrete rigid was attributed to cutting tool due to its complicated geometry and the assumption that the tool will not deform during the contact interaction with the work piece. As a rigid body, all nodes from the tool will be similar. To be able to output the reaction forces that will represent the measured cutting forces, a reference node was inserted at its center of mass. Since the tool has a rigid definition with complicated geometry shape, the rigid element type R3D3 was selected. The R3D3 element type stands for a rigid triangular element with 3 nodes. The cutting tool was meshed with 44 968 elements where the mesh density was increased in the part of the tool where complicated geometry features were present. The meshed tool is presented in Figure 43.

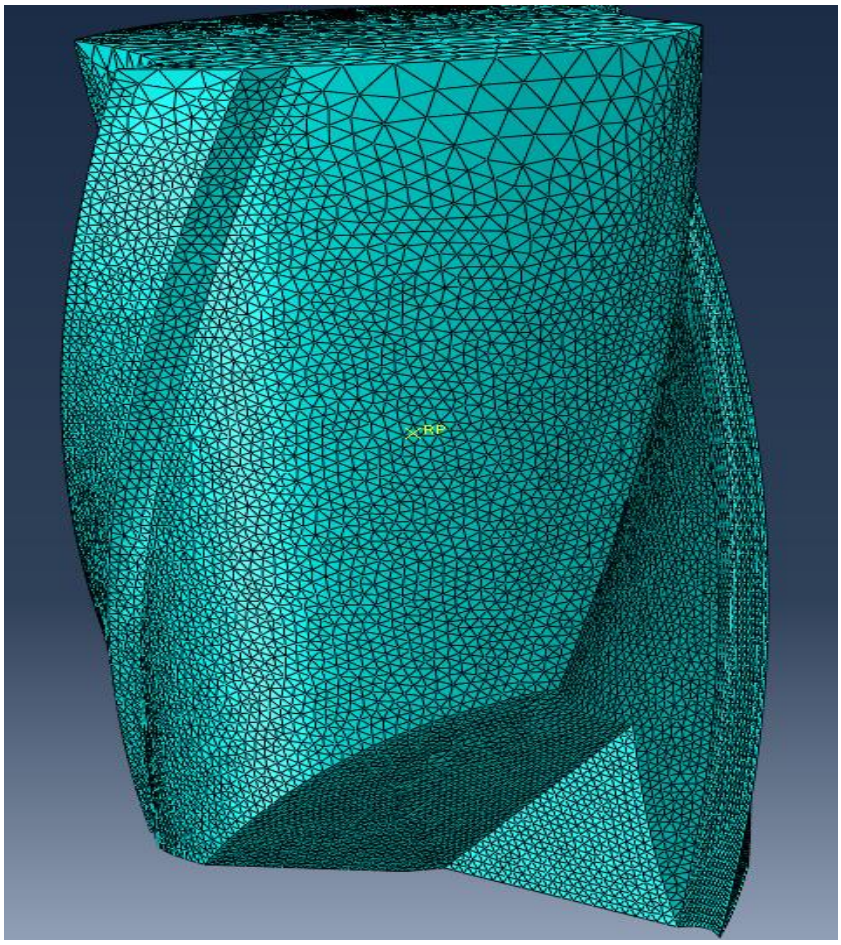


**Figure 43: Meshed cutting tool**

### *5.4.2 Work piece element and mesh*

The work piece has been modeled as a deformable body. Based on the geometry and type of analysis that is conducted, three-dimensional stress of eight nodes hexahedron elements with reduced integration and hourglass control C3D8R were used to mesh the work piece. Three-dimensional stress elements were used because the outputs requested are the reaction forces in the three principal directions. The reduced

integration point option was used so that the integration can be done at a single node. Since the cutting process is a high rate dynamics process, C3D8R elements were the recommended choice based on effectiveness and computational efficiency.

Also, since the failure criterion is based on element deletion, the mesh size at the contact area of the work piece is very important. Indeed, the mesh size at the contact zone should be based on the chip load for chip to be formed during the cutting process. According to the experimental design, the minimum chip load occurs when the cutting speed is set to 3000 RPM and the feed rate to 508 mm/min. At these cutting inputs, the chip load value is 85 $\mu m$. The contact zone of the work piece was meshed with elements of an equivalent length of 20 $\mu m$ where the chip load is about 4.25 times the element size. The other areas where contact does not occur where meshed with low density element to save some computational time. Finally, the work piece was meshed with a total of 479 184 elements. The meshed work piece is illustrated in Figure 44 and 45.

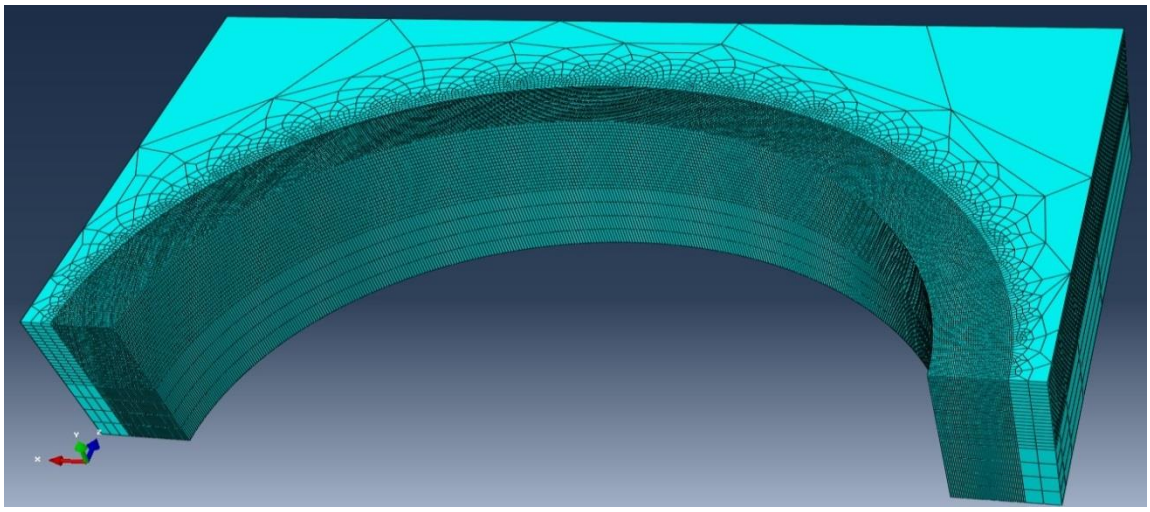

**Figure 44: Meshed work piece**

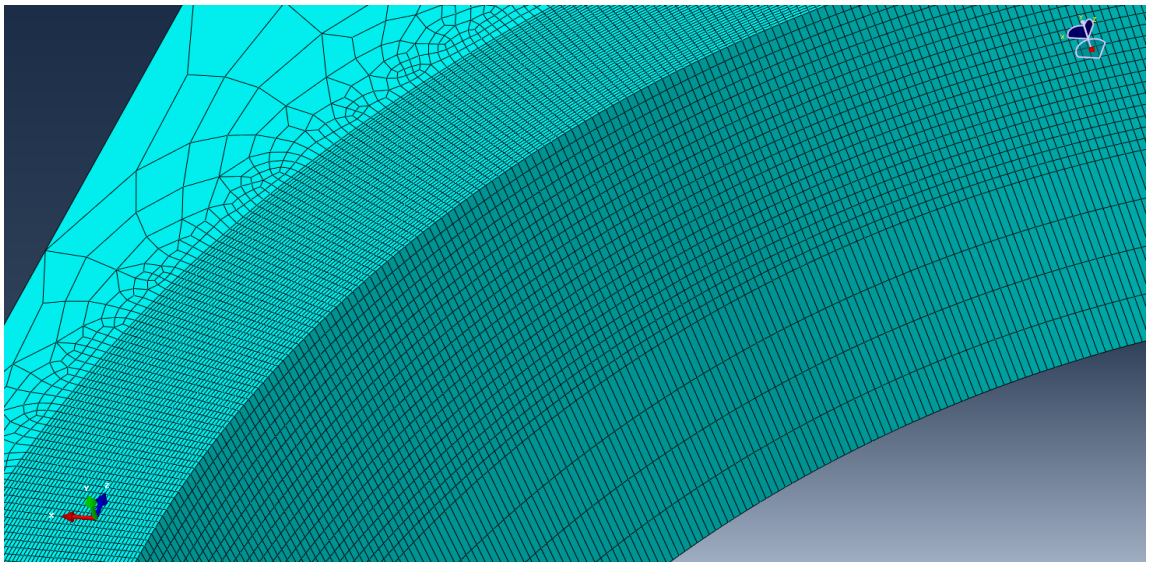

**Figure 45: Contact zone meshes of the work piece**

### 5.5 Contact and interaction

The general contact algorithm was used to model the interaction between the tool and work piece. Selected surface pair option was used to define the contact area between the tool and work piece. An element based surface was used to defined the contact area of the tool and node based surface was used to define the contact area of the work piece. A node based surface was used to define the contact area of the work piece because of the chip formation. When the chips are formed, interior elements from the work piece need to be removed and new surface need to be generated. The last step consists of modifying the input file by creating a new surface generation and adds a key word "INTERIOR" to the node based surface.

A study conducted by Tao (2002) shows that the coefficient of friction during the tool and work piece contact is not constant and depends on the temperature generated

during the cutting process. However, a user defined friction model is not supported when the general contact algorithm is used in ABAQUS 2012. Therefore, the basic Coulomb's friction model was used as friction model. The Coulomb's friction model is defined in Equation 6 from the ABAQUS ( 2012) user's manual.

$$\tau_{crit} = \mu p \tag{6}$$

The equation above states that two bodies in contact can start sliding when the critical shear stress $\tau_{crit}$ exceeds the maximum allowed shear stress. The critical shear stress is defined by the product of the friction coefficient $\mu$ and the pressure stress $p$. A fixed friction of 0.9735 was used during the simulation based on the results provided by Tao (2002) when studying the effect of temperature on the friction coefficient on Aluminum 6061 T6.

The boundary condition was modeled based on the actual experiment. The tool was allowed to rotate in the clockwise direction with a magnitude defined by the spindle speed at its center of mass. The work piece was constrained to move in the feed direction at a velocity defined by the feed rate. An initial temperature similar to the reference temperature used in the Johnson Cook's equations was applied to the work piece. The Figures 46 and 47 show the chip formation from the simulation results.

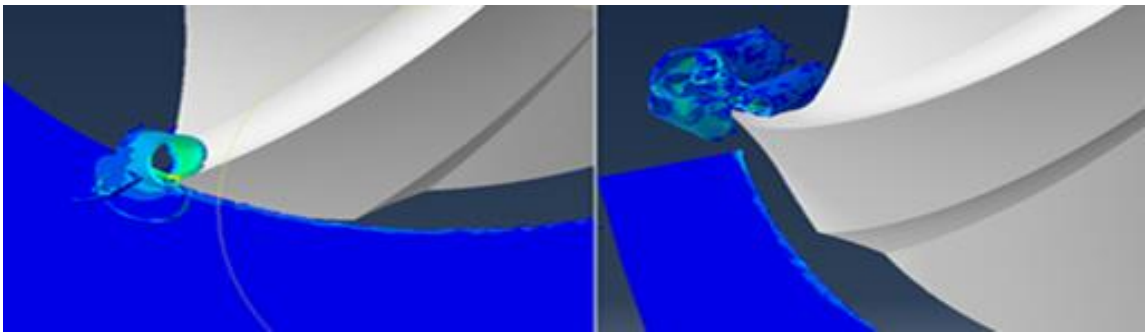

**Figure 46: Chip formation FEA cutting simulation without mesh**

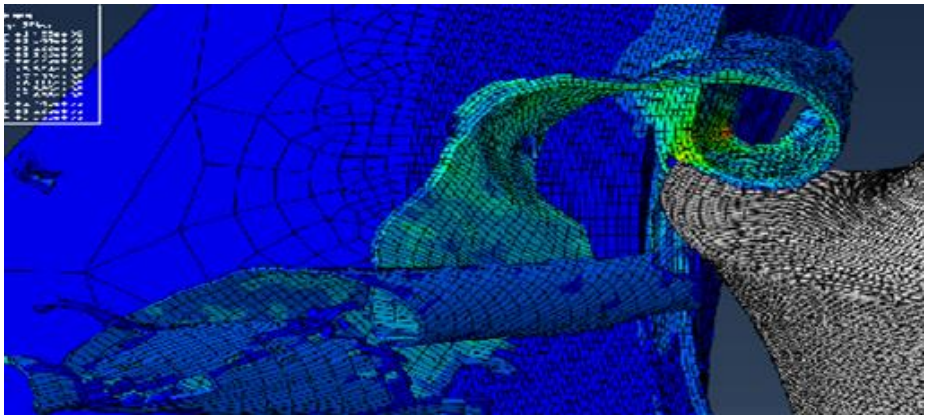

**Figure 47: Chip formation FEA cutting simulation with mesh**

## 5.6 Simulation and results

### *5.6.1 Mass scaling effect*

Due to the large size of the model, a fixed mass scaling was used to speed up the computation. The use of mass scaling will increase the density of each element and the time step. Based on the user's manual, the desired output with and without mass scaling option should be monitored. A fixed mass scale of 500 was used in the simulation. To see the effect of the scale factor, the outputted forces for the initial cut with and without the scale factor were compared in Figures 48, 49, 50 at 2500 RPM, 508 mm/min, and 2.54 mm the depth of cut.

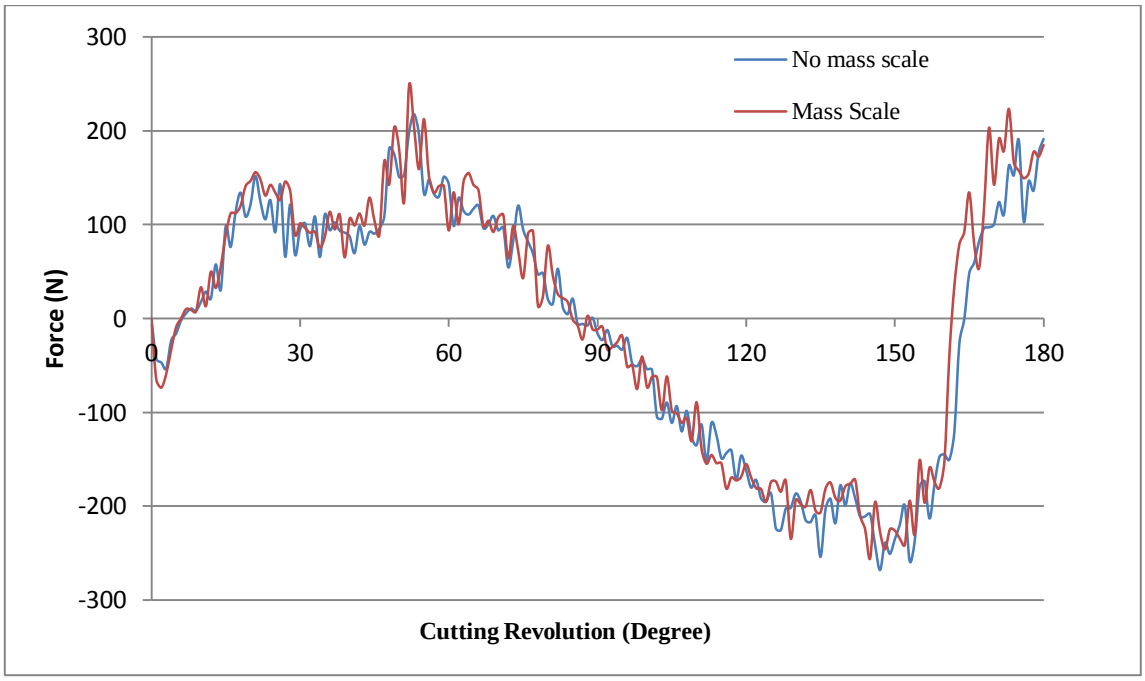


**Figure 48: Effect of the mass scaling in the X direction**

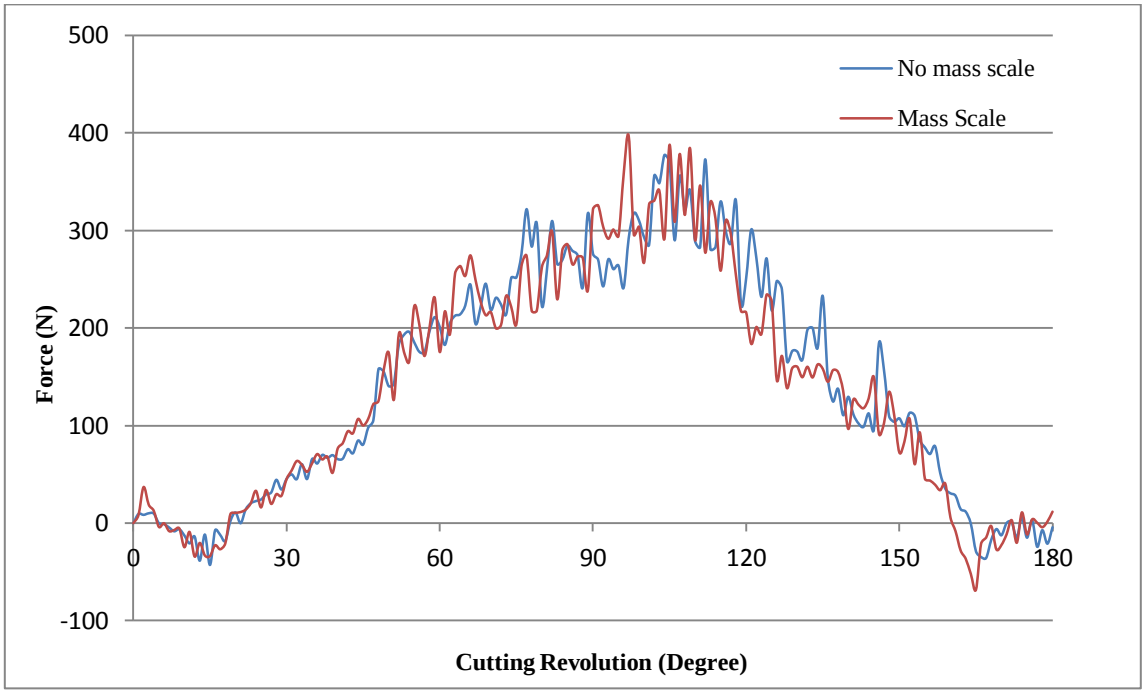


**Figure 49: Effect of the mass scaling in the Y direction**

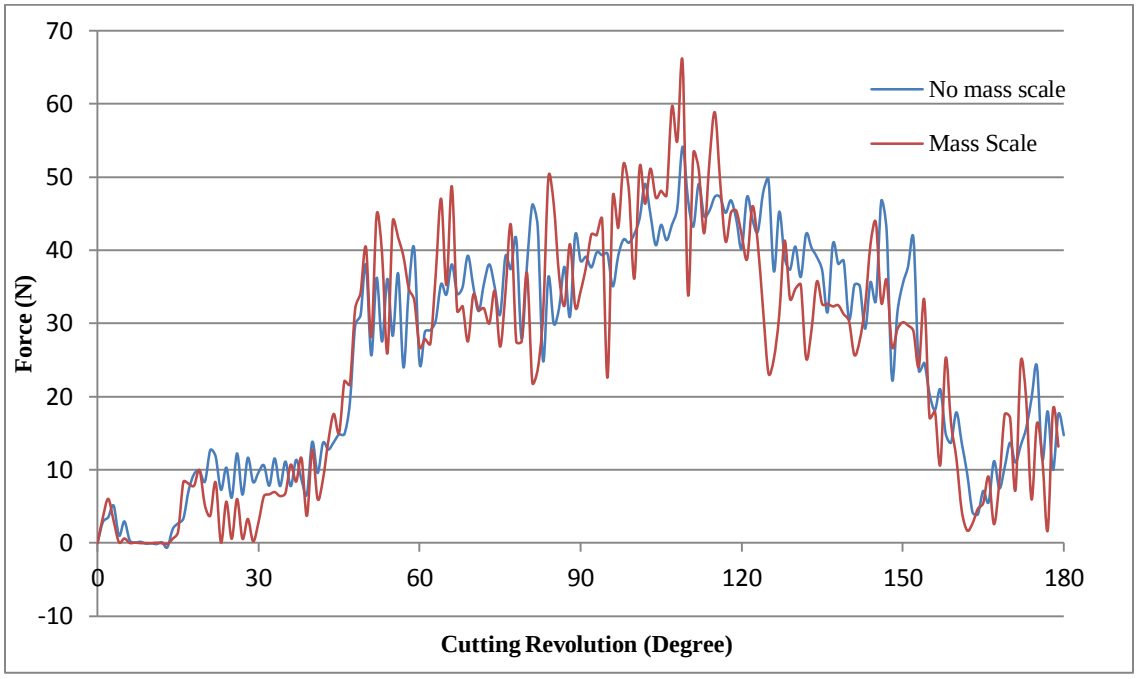


**Figure 50: Effect of the mass scaling in the Z direction**

Based on the data presented in Figures 48, 49, 50 the change in the forces value by using a fixed mass scale factor of 500 is minimal but a noisy signal is observed. Therefore, a fixed mass scale factor will be used in the analysis. Also, the computational time is reduced by a factor of 5 when using the scale factor of 500.

### *5.6.2 Effect of the feed rate on the cutting forces*

To study the effect of the feed rate, the simulated cutting forces data will be compared at a constant speed of 2500 RPM and a depth of cut 2.54 mm. The simulated forces in the X, Y, and Z direction will be plotted respectively in Figures 51, 52, 53.

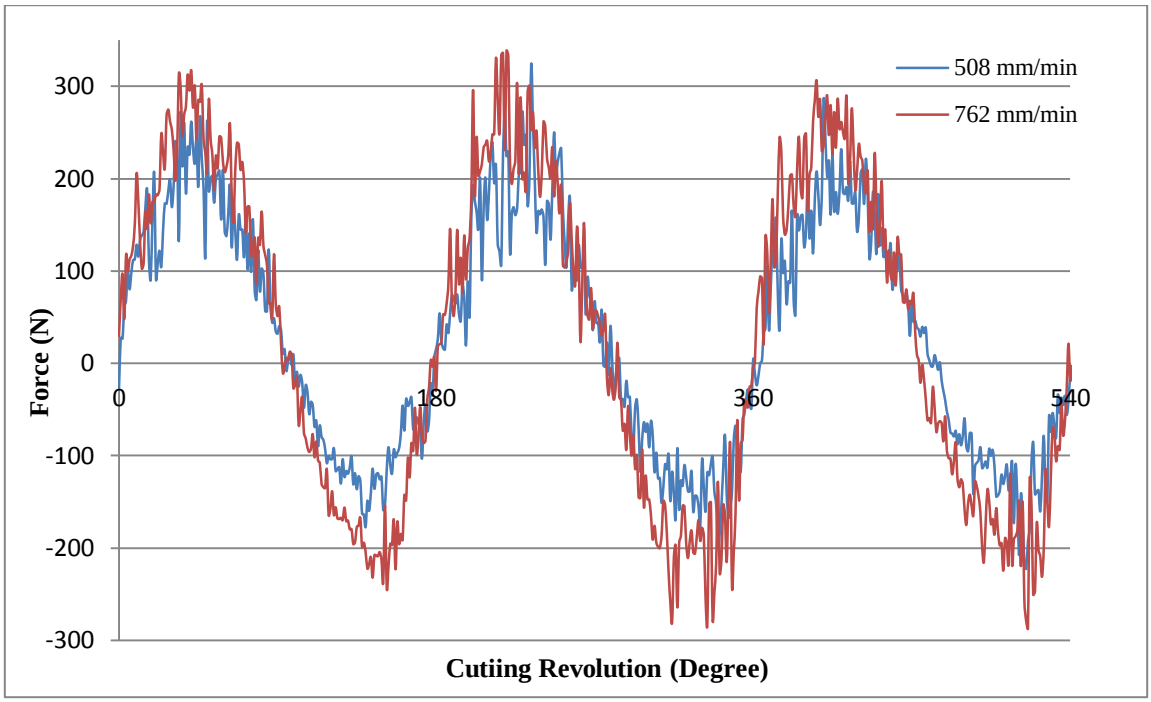


**Figure 51: Feed rate effect on FEA forces in the X direction**

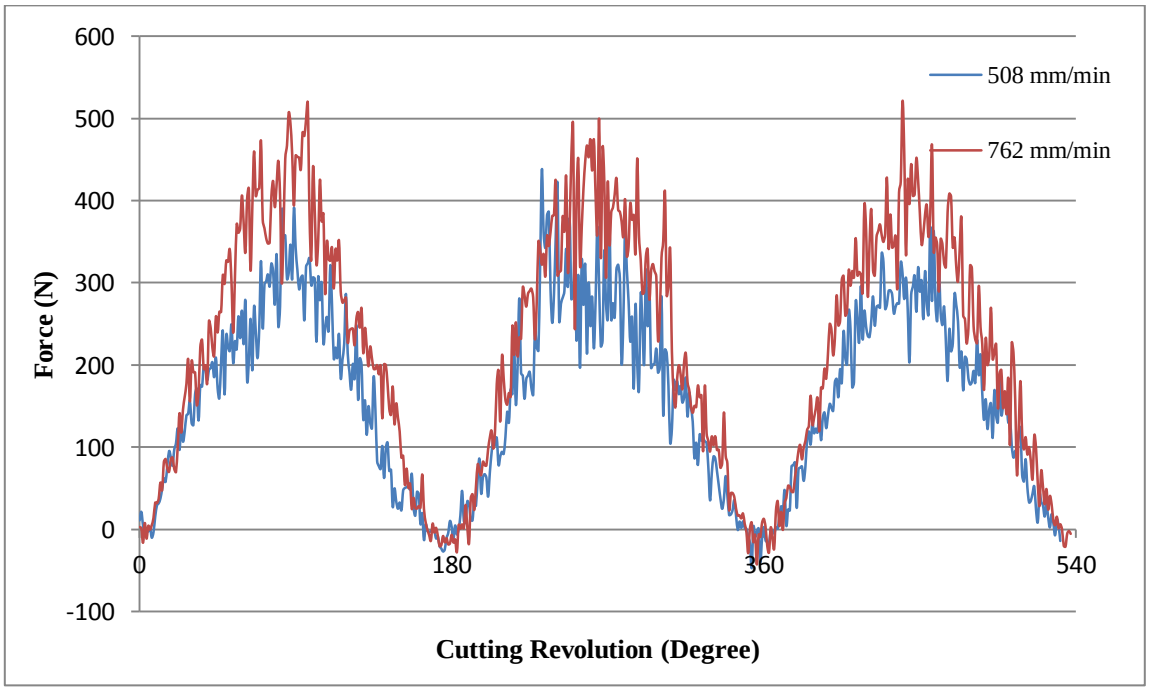


**Figure 52: Feed rate effect on FEA forces in the Y direction**

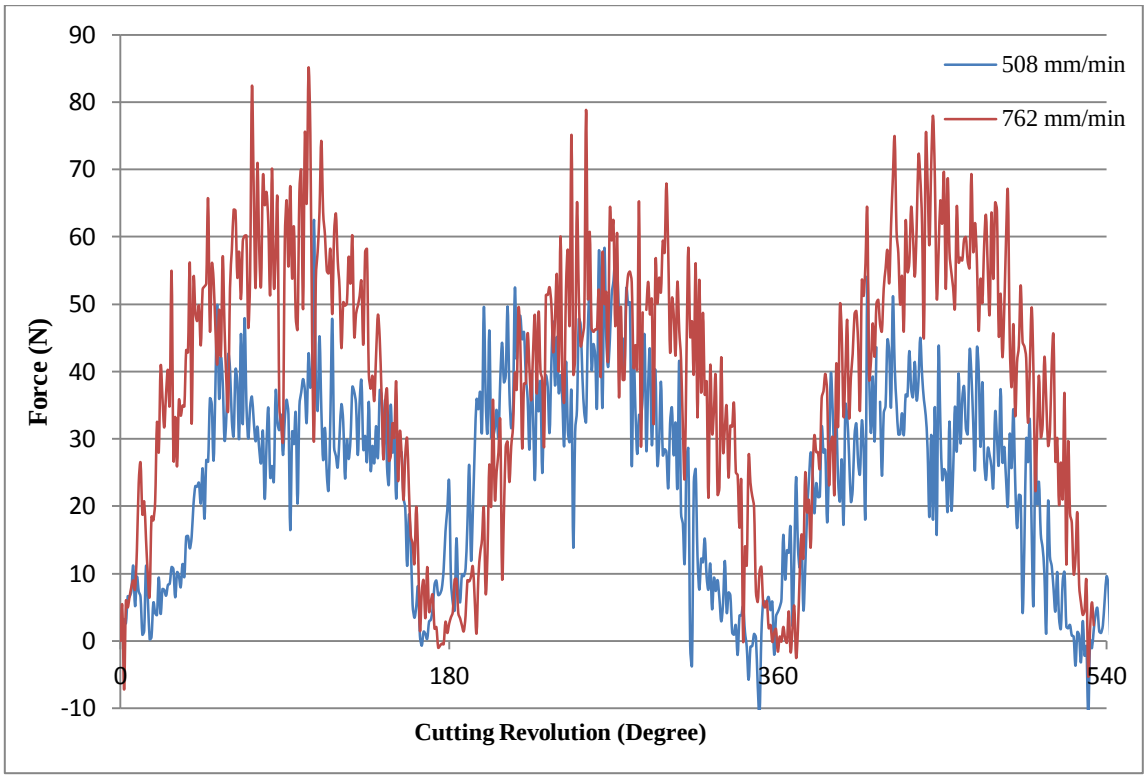


**Figure 53: Feed rate effect on FEA forces in the Z direction**

From Figures 51, 52, 53, it could be observed that as the feed rate increases, the cutting forces increase. A minor change in the increase of the cutting forces is observed from the simulated cutting forces in the X direction. These results are in perfect agreement with the findings from the parametric study done with the measured cutting forces. It should be also noted that the noise from the signal is due to FEA model technique as described above. The noises from the signal are created by element failure and deletion.

### *5.6.3 Effect of the spindle speed of the cutting forces*

To study the effect of the spindle speed, the simulated cutting forces will be compared at a constant speed of 508 mm/min and a depth of cut 2.54 mm. The simulated forces in the X, Y, and Z direction will be plotted respectively in Figures 54, 55, 56.

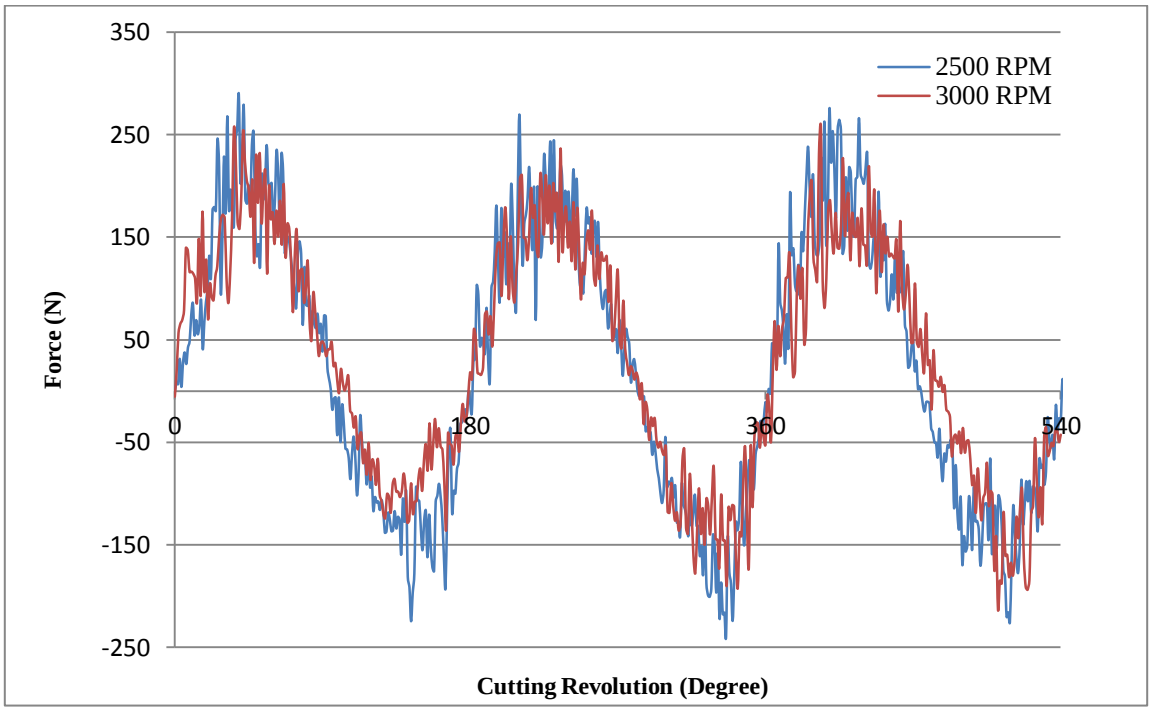


**Figure 54: Spindle speed effect on FEA forces in the X direction**

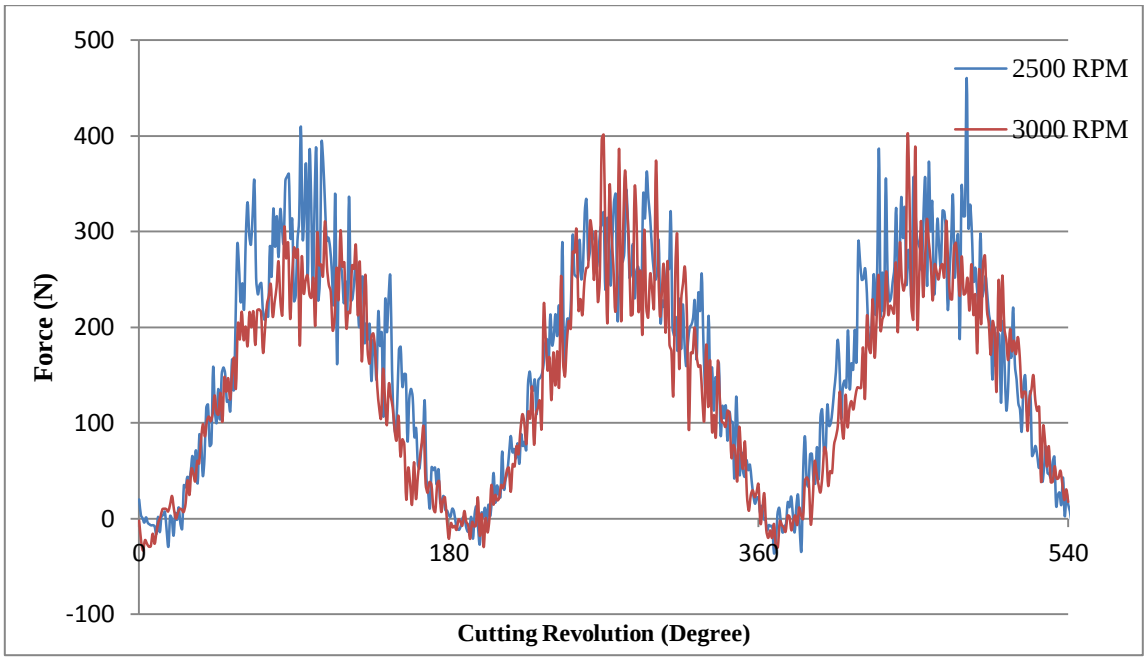


**Figure 55: Spindle speed effect on FEA forces in the Y direction**

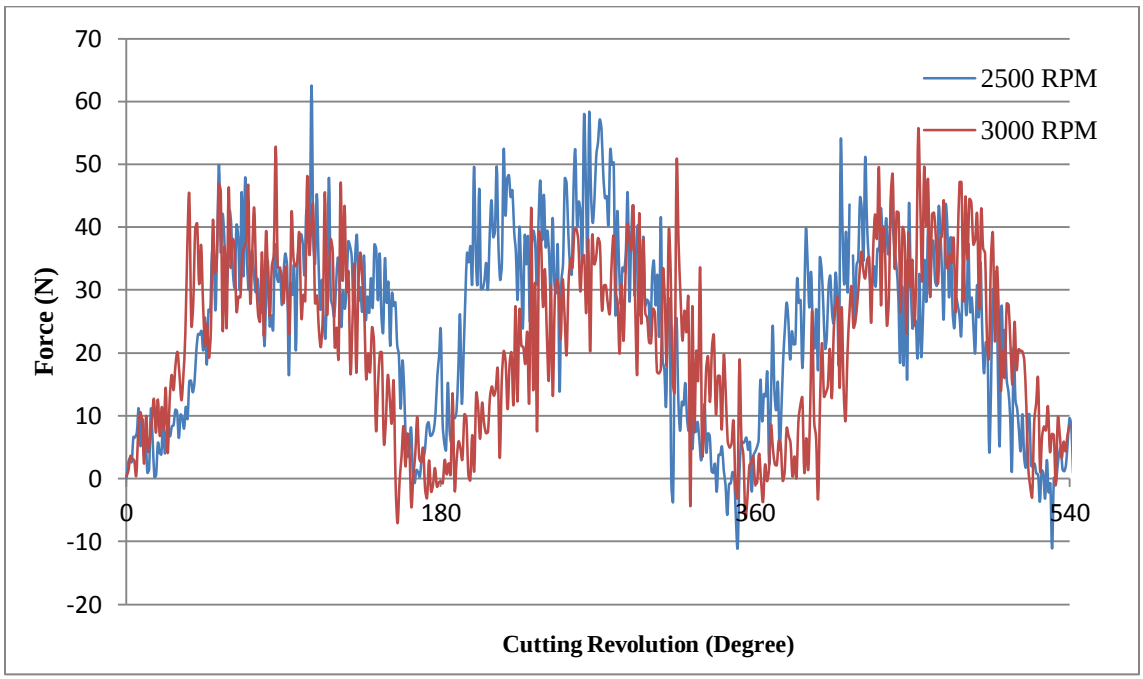


**Figure 56: Spindle speed effect on FEA forces in the Z direction**

The results from Figures 54, 55, 56 show a slight decrease on the cutting forces' magnitude. Based on the parametric study done with the measured cutting forces, the cutting forces should decrease as the spindle speed increase. The slight decrease might be due to effect of the tool run out and vibrations which are not included into the FEA model.

### *5.6.4 Measured and simulated cutting forces comparison*

To evaluate the accuracy of the FEA cutting forces model, the predicted cutting forces are compared to the measured cutting forces based on Experiment1. The cutting input parameters (2500 RPM the spindle speed, 508 mm/min the feed rate, 2.54 mm the depth of the cut) were used to simulate the cutting forces. The measured forces from Experiment 1 was used to do the comparison because a minimum forces' magnitudes of the peak deviation, which is mostly due to the tool run out, was observed compared to the measured forces from the others experiments. One should note that the predicted cutting forces are ideal. The predicted cutting forces do not include the effect of tool run out and overall machine vibrations which are present in the real cutting process. The comparison between the measured and predicted cutting forces in the X, Y, and Z direction is shown respectively in Figures 57, 58, 59.

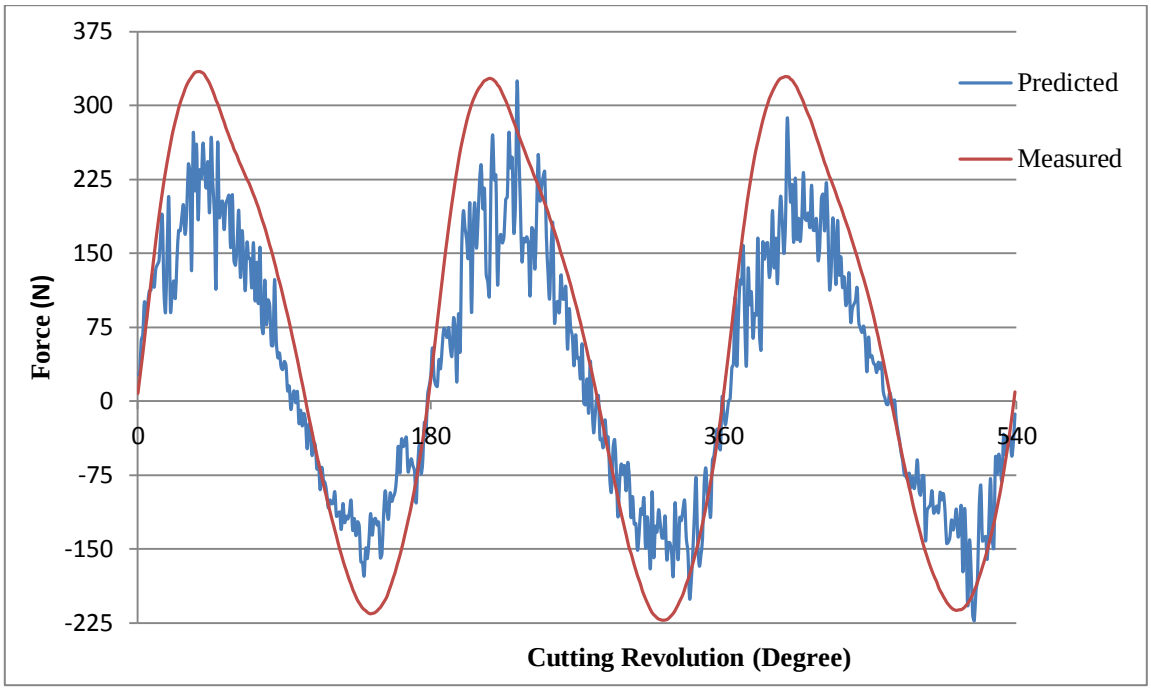


**Figure 57: Comparison of predicted and measured cutting forces in the X direction**

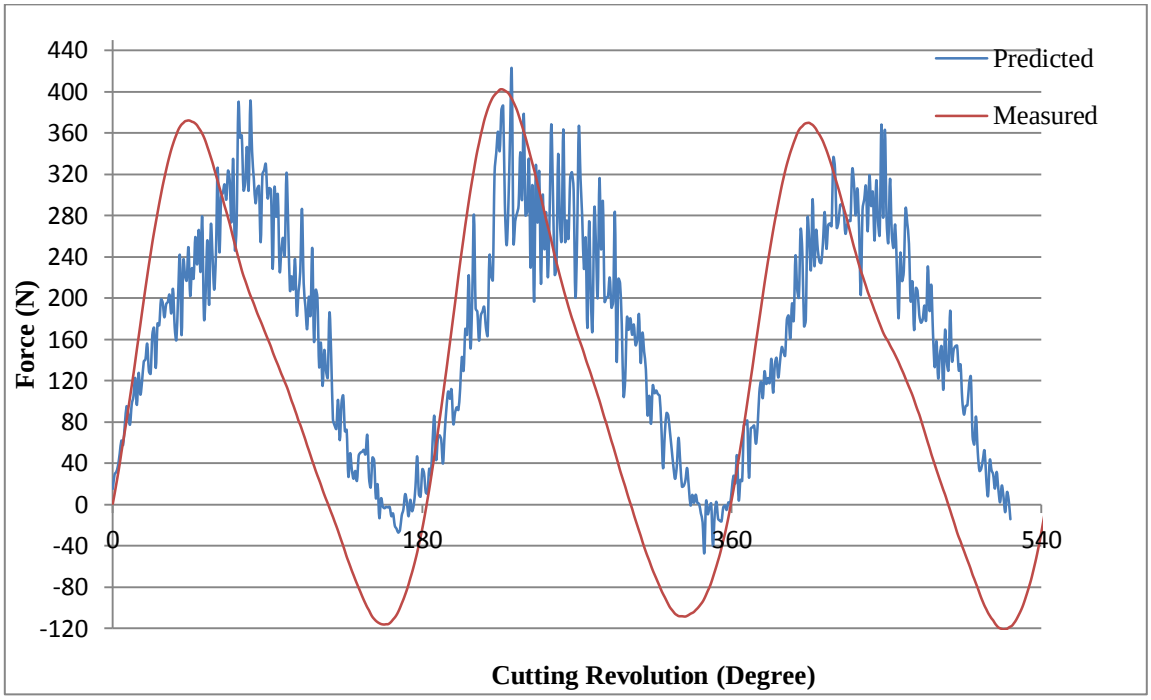


**Figure 58: Comparison of predicted and measured cutting forces in the Y direction**

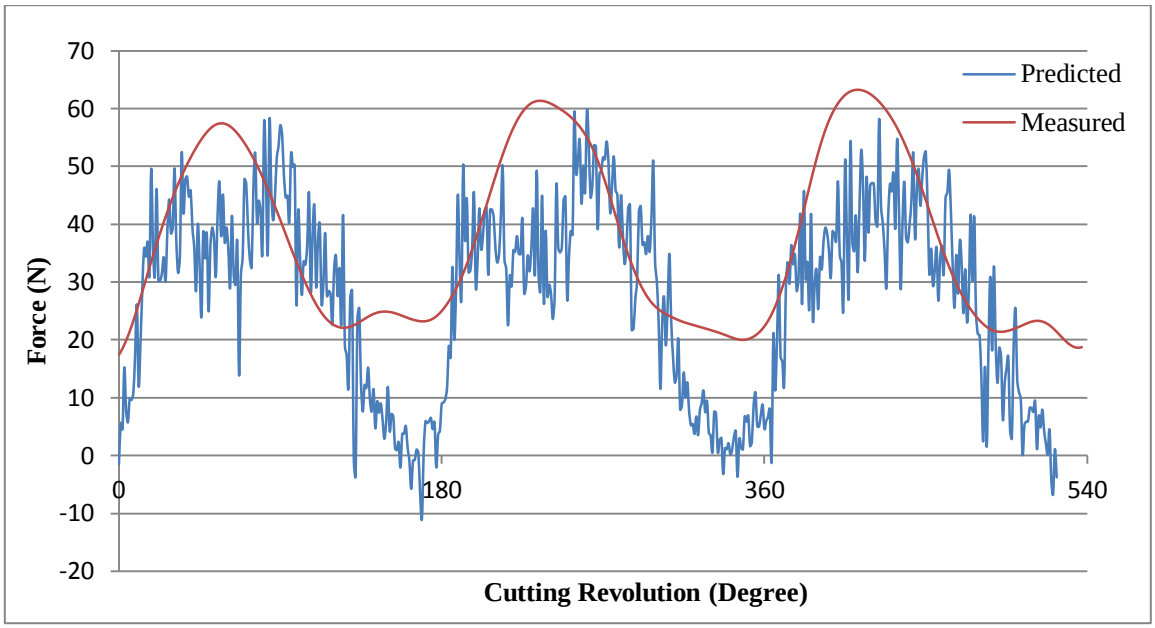


**Figure 59: Comparison of predicted and measured cutting forces in the Z direction**

Based on the plots in Figure 57, the patterns of the cutting forces in the X direction, for both predicted and measured, are identical. However, a difference in the peaks magnitudes of the cutting forces can be observed. For the case of the positive peaks magnitudes, an average of 330.44 N is calculated from the measured cutting forces and 293.43 N from the predicted cutting forces. These results lead to an error percentage of 11.2 % for the upper peaks values. For the case of the lower peaks magnitudes, an average of -216.69 N is calculated from the measured cutting forces and -199.87 N from the predicted cutting forces. These results lead to an error percentage of 7.76% for the lower peaks values.

For the case of the cutting forces in Y direction, a phase shift based on the cutting revolution is observed in Figure 58. This shift is due to the significant effect of the tool

run out observed from the measured cutting forces in the Y direction. A difference in the peak magnitudes for both measured and predicted cutting forces is also noticed. An average of the peak forces magnitudes of 381.29 N is calculated from the measured cutting forces whereas 393.17 N from the predicted cutting forces. The percentage of error is evaluated to 3.11 % for the upper peaks values of the cutting forces. For the lower peaks values, the average cutting forces value is -115.06 N for the measured cutting forces and -29.41 N for the predicted cutting forces. Thus, the error percentage is estimated to 74.4 %. The significant error percentage is mainly due to the tool run out which creates non circular motion as the tool teeth exit the work piece.

In the Z direction, only the upper peaks forces magnitudes will be compared as shown in Figure 59. The reason is because the FEA model does not includes the center cut effect. As result, the forces drop to zero magnitude every 180 degree. This behavior is not similar for the case of the measured cutting forces in the sense that the dynamometer still measuring voltages even when the tool teeth are not cutting as explained in section 4.2.1. The average peaks forces magnitudes of 60.69 N was calculated for the measured cutting forces and 58.69 N for the predicted cutting forces. An error percentage of 3.2 % is obtained from the peaks values comparison of the cutting forces.

### 5.7 Discussions of FEA model and forces prediction

Based on the results obtained from the FEA model, these conclusions can be made:

- The FEA simulation has a good agreement with the experimental milling process. Indeed, chip formation and effect of cutting input parameters can be observed from both FEA model and experiment cutting process.
- Comparing the percentage of error from the deviation of the average peaks values of the predicted and measured cutting forces, a low percentage is observed when not considering the tool run out which creates significant shift and deviation from the measured forces. These results show that the FEA model is valid and accurate for milling cutting simulation.
- However, the computation time is significant when low rated computer are used. To generate three cut using 8 CPUs, the simulation time is approximately 22 hours.

# 6. SURFACE FINISH AND CUTTING FORCES

In this section, the surface roughness of the machined specimen will be evaluated. Thus, a study will be conducted to evaluate the effect of the cutting input parameters on the surface finish and develop a relation between the surface roughness and the cutting forces.

## 6.1 Surface profile measurement

The surface finish of machined parts is a very important factor for part manufacturer. The surface finish characterizes the surface texture of the work piece.
To measure the surface texture of each specimen, a Zygo NewView 600 white light interferometer was used as shown in Figure 60.

**Figure 60: Zygo NewView 600**

The measurement process consists of capturing an image of the inner machined surface using an optical lens. The image is processed using Metro Pro imaging software as shown in Figure 61. Once the image is inputted inside the software, a three-dimensional surface characterization is done and different measured values of the surface profile are calculated.

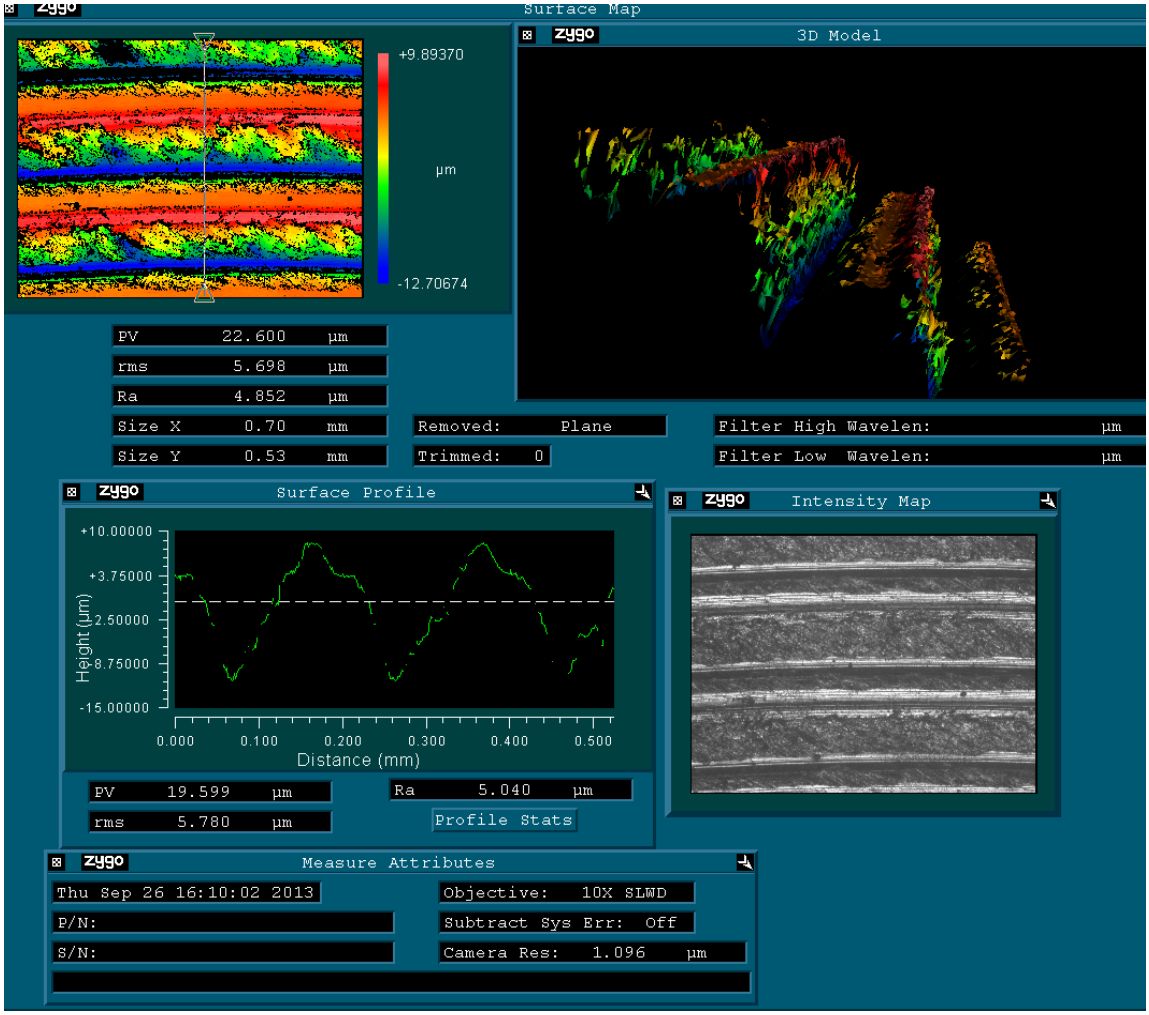


**Figure 61: Three-dimensional surface characterization**

In this study, the average surface roughness Ra of the captured images is measured and further study will be made based on the cutting input parameters, the CNC machine condition and the cutting force**.**

### 6.2 Effect of the feed rate and spindle speed on the surface roughness

As described in experimental design table, the surface roughness Ra of the specimens at three different feed rates (508, 635,762 mm/min) and spindle speeds (2500, 2750, 3000 RPM) with a constant depth of cut of 2.54 mm was measured. The obtained Ra value is then compared and plotted based of the cutting input parameters in Figure 62.

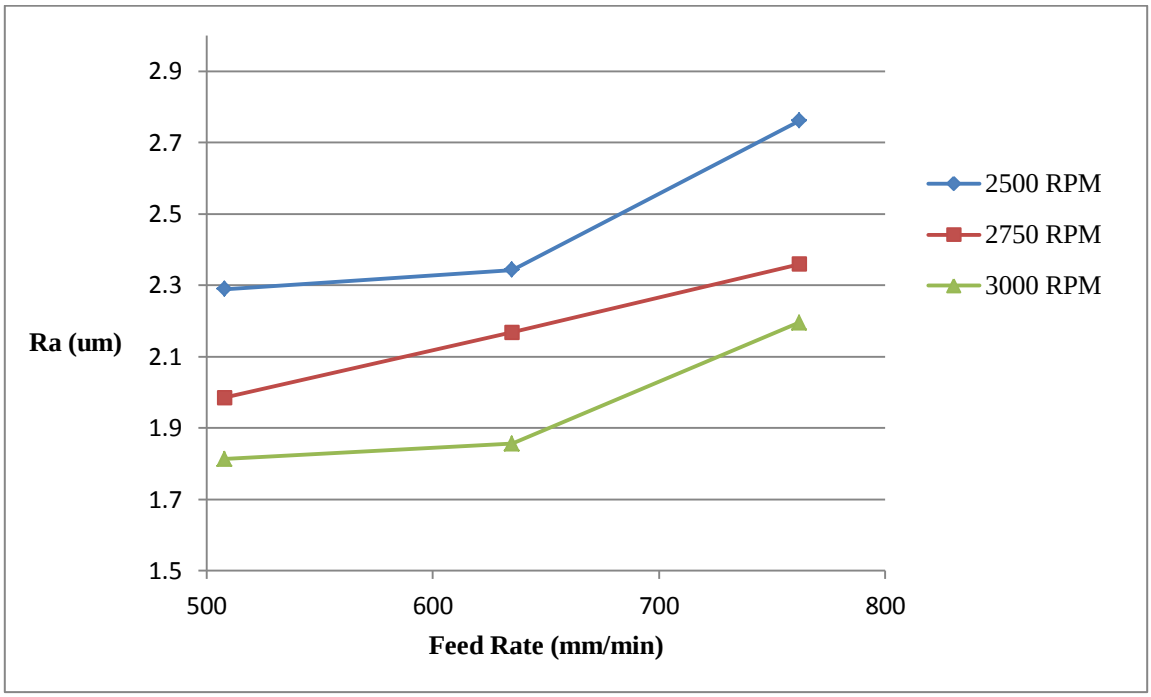


**Figure 62: Effect of the feed rate and spindle speed on the surface roughness**

The plots in Figure 62 show an increase of the surface roughness value as the feed rate increases. The surface roughness value also increases as the spindle speed decreases. The results found are in perfect agreement with data presented by Kuttolamadom, Hamzehlouia and Mears (2010) and other authors which agree that the surface roughness depend on the chip load. Thus the higher the chip load value is, the rougher the surfaces finish at a constant depth of cut.

### 6.3 Effect of the depth of cut on the surface roughness

To study the effect of the depth of cut, the surface roughness at three depth of cut (2.54, 3.175, 5.08 mm) was measured based on a spindle speed of 2500, 27500 RPM and a feed rate of 508, 762 mm/min. The measured values were plotted and compared in Figure 63.

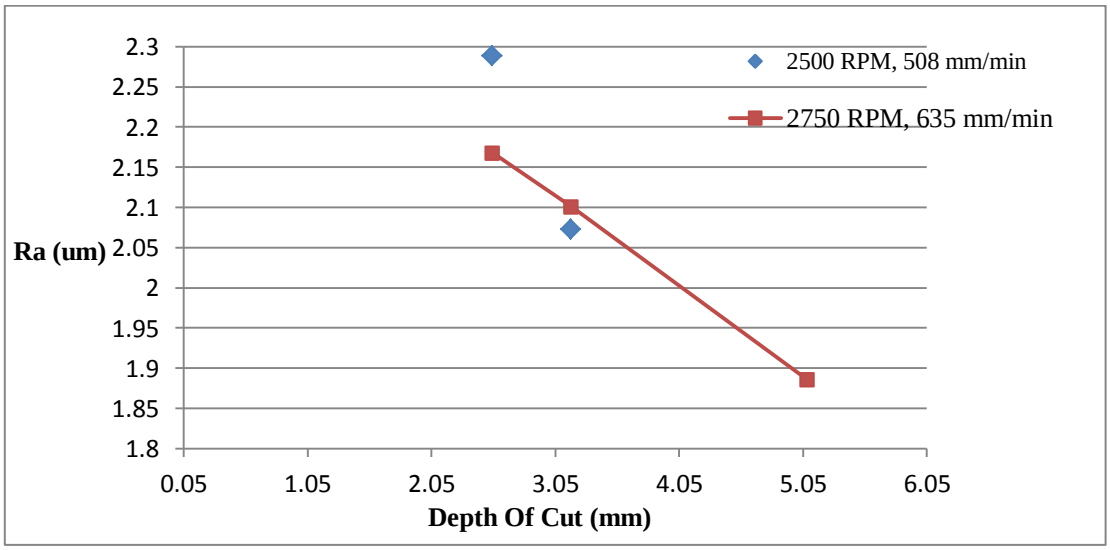


**Figure 63: Effect of the depth of cut on the surface roughness**

It could be observed that at a spindle speed and feed rate of 2750 RPM and 635 mm/min, the values of the surface roughness decrease at the depth of cut increase from 2.54 mm to5.08 mm. The same behavior is also observed at 2500 RPM and 508 mm/min

### 6.4 Effect of the CNC machine quality on the surface roughness

Two different parts made of the same material properties were machined with a HAAS and old CNC machine. The parts were machined as a constant spindle speed of 2500 RPM and depth of the cut of 2.54 mm. Three different feed rates (508, 635,762 mm/min) were used during the cutting process. The surface roughness Ra value was then measured and compared as shown in Figure 64.

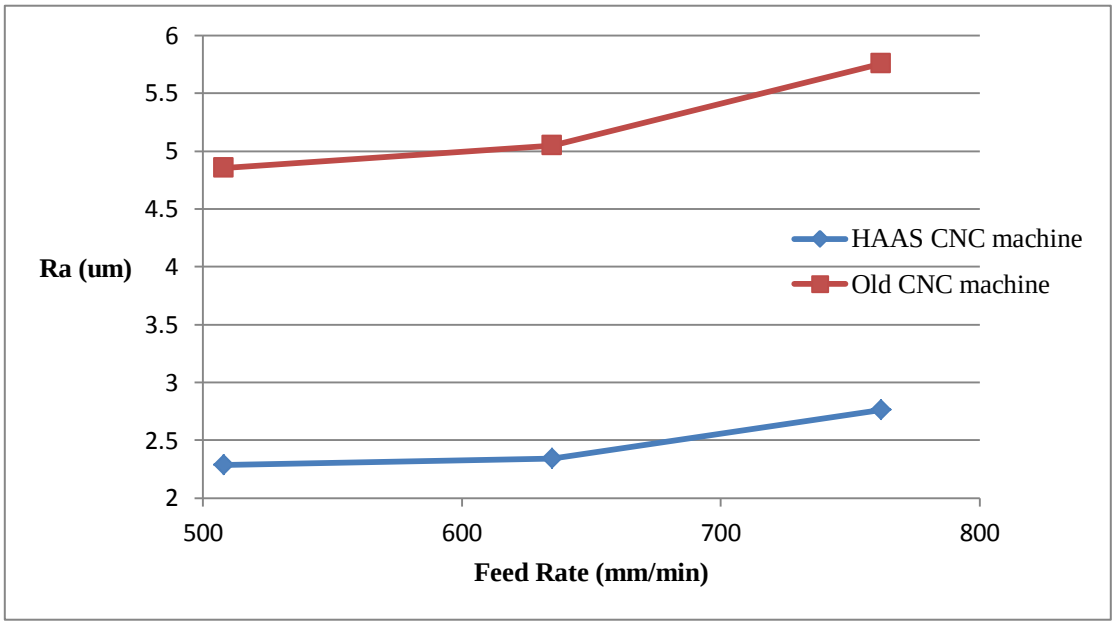


**Figure 64: Machine quality effect on the surface roughness**

The first observation that can be made is the surface roughness Ra was both CNC machine increases as the feed rates increase. This observation agrees with the effect of feed rates on the surface roughness Ra. The second observation is the high value of the Ra using the old CNC machine. Going back to the quality of the old CNC machine, it has been found that defective bearings inside the spindle create an excessive tool run out and were making the quill to vibrate. These defects were also found in the cutting forces' pattern measured during the cutting process using the old CNC machine. Thus, the vibration and excessive tool run out create a rougher surface. These facts are the main the reason why the Ra values using the old CNC machine are higher than the Ra values using the HAAS CNC machine.

### 6.5 Cutting forces and surface roughness

Based on the findings, the surface roughness Ra values increase when the feed rate increases and decreases when the spindle speed increases at a constant depth of the cut. The same observation is also made for the cutting forces. The cutting forces increase as the feed rate increases and decrease as the spindle speed increases at a constant depth of the cut.

Indeed, it can be conclude that both surface roughness and cutting forces behave based on the chip load. The higher the chip load is, the higher the cutting forces and the Ra value are. But the surface roughness Ra value also depends on the CNC machine that can be observed based on the cutting forces patterns.

# 7. CONCLUSIONS AND FUTURE WORK

Milling machining is one the most used cutting process nowadays. Understanding the cutting forces will give a significant improvement in part quality control. Indeed, machine anomaly and set up problems will be detected at the early stage of the production and limited the number of rejected parts due to the lack of geometry tolerance.

## 7.1 Conclusion

The work conducted during this research leads to the following conclusions:

- The cutting forces during the dry milling process were measured and the forces' signature agrees with the principle of the metal cutting mechanics. The cutting forces' signature describes the concept of up and down milling as well as the effect of the tool run out
- Results from the parametric study show that the magnitude of the cutting forces has a direct link with the cutting input parameters which are related to the chip load.
- The developed Finite Element Analysis model describes the cutting process and the results obtained are in a good agreement with the cutting forces measured experimentally. Also, the FEA model shows that the predicted cutting forces also depend on the cutting input parameters, moreover the chip load.

- The surface profile from different specimens was measured and the value of surface roughness obtained also depends on the chip load and the CNC machine quality. Therefore a correlation between the surface roughness Ra and the cutting forces' signature can be done.

## 7.2 Future work

The goal of this research was to study the effect of the cutting forces during a dry milling machine. But still, additional work can be done on the followings:

- The cutting process was done without using any coolant. In most industry, part manufacturers use different coolant during the cutting process. An investigation can be also done in this area to investigate the effect coolant on the cutting forces.
- Different materials and tool geometry could also create a different cutting forces' signature. A study can also be conducted to see the effect of the tool geometry and material on the cutting forces.
- The FEA model developed fit very well the experimental cutting process with some minimal deviation. But considerations such as effect of vibration and tool run out on the cutting forces were not included into the model which creates a deviation between the measured and predicted cutting forces.
- Since it has been found that there is a direct relation between the cutting forces and the surface roughness, empirical equations can be also developed to calculate the surface roughness directly from the cutting forces.

## REFERENCES


ABAQUS, 2012. ABAQUS documentation. Dassault Systèmes, RI, USA.

Adetoro, O.B., Wen, P.H., 2009. Prediction of mechanistic cutting force coefficients using ALE formulation. The International Journal of Advanced Manufacturing Technology 46, 79-90.

Benardos, P.G., Vosniakos, G.C., 2003. Predicting surface roughness in machining: a review. International Journal of Machine Tools and Manufacture 43, 833-844.

Budak, E., Altintas, Y., Armarego, E.J.A., 1996. Prediction of milling force coefficients from orthogonal cutting data. ASME 118, 216-224.

Devor, R.E., Kline, W.A., 1983. The effect of runout on cutting geometry and force in end milling. International Journal of Machine Tools and Manufacture 23, 123-140.

Grzesik, W., 1996. A revised model for predicting surface roughness in turning. Wear 194, 143-148.

Knight Marcel Dekker, W.A., Boothroyd, G., 1988. Fundamentals of metal machining and machine tools., New York, Second edtion.

Ko, J.H., Yun, W.-S., Cho, D.-W., Ehmann, K.F., 2002. Development of a virtual machining system, part 1: approximation of the size effect for cutting force prediction. International Journal of Machine Tools and Manufacture 42, 1595-1605.

Kuttolamadom, M.A., Hamzehlouia, S., Mears, M.L., 2010. Effect of machining feed on surface roughness in cutting 6061. SAE International Journal of Materials and Manufacturing 3, 108-119.

Lee, K.Y., Kang, M.C., Jeong, Y.H., Lee, D.W., Kim, J.S., 2001. Simulation of surface roughness and profile in high-speed end milling. Journal of Materials Processing Technology 113, 410-415.

Lesuer, D.R., Kay, G. J., and LeBlanc, M. M., 1999. Modeling large strain high rate deformation in metals. Proc., 3rd Biennial Tri-Laboratory Engineering Conf. Modeling and Simulation.

Liang, S.Y., Hecker, R.L., Landers, R.G., 2004. Machining process monitoring and control: The state-of-the-art. Journal of Manufacturing Science and Engineering 126, 297.

Lin, S.C., Chang, M.F., 1998. A study on the effects of vibrations on the surface finish using a surface topography simulation model for turning. International Journal of Machine Tools and Manufacture 38, 763-782.

Llanos, I., Villar, J.A., Urresti, I., Arrazola, P.J., 2009. Finite element modeling of oblique machining using an arbitrary lagrangian–eulerian formulation. Machining Science and Technology 13, 385-406.

Maurel-Pantel, A., Fontaine, M., Thibaud, S., Gelin, J.C., 2012. 3D FEM simulations of shoulder milling operations on a 304L stainless steel. Simulation Modelling Practice and Theory 22, 13-27.

Merchant, M.E., 1945. Mechanics of the metal cutting process. I: Orthogonal cutting and a type 2 Chip. Journal of Applied Physics 16, 267.

Özel, T., Altan, T., 2000. Process simulation using finite element method : prediction of cutting forces, tool stresses and temperatures in high-speed flat end milling. International Journal of Machine Tools and Manufacture 40, 713-738.

Rivière-Lorphèvre, E., Filippi, E., 2009. Mechanistic cutting force model parameters evaluation in milling taking cutter radial runout into account. The International Journal of Advanced Manufacturing Technology 45, 8-15.

Tao, Z., 2002. Friction analysis and modeling in metal cutting processes at elevated temperatures, Doctoral Dissertation. Department of Mechanical Engineering, University of Pittsburgh, Pittsburgh, p. 100.

Zhu, D., Mobasher, B., Rajan, S., Peralta, P., 2011. Characterization of dynamic tensile testing using aluminum alloy 6061-T6 at intermediate strain rates. Journal of Engineering Mechanics 137, 669-679.

## APPENDIX A

## EXPERIMENTS RESULTS

This section presented the measured cutting forces using the TiN coated tool during the cutting process. The cutting input parameters are specified according to the experiments number as presented in Table 2.

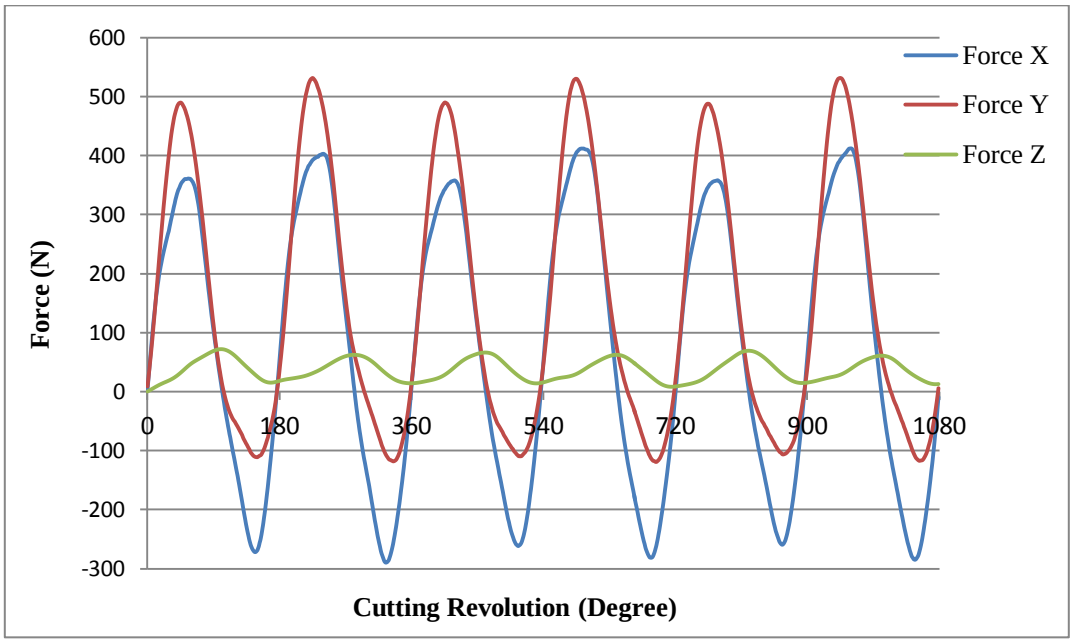


**Figure A1: Experiment 2**

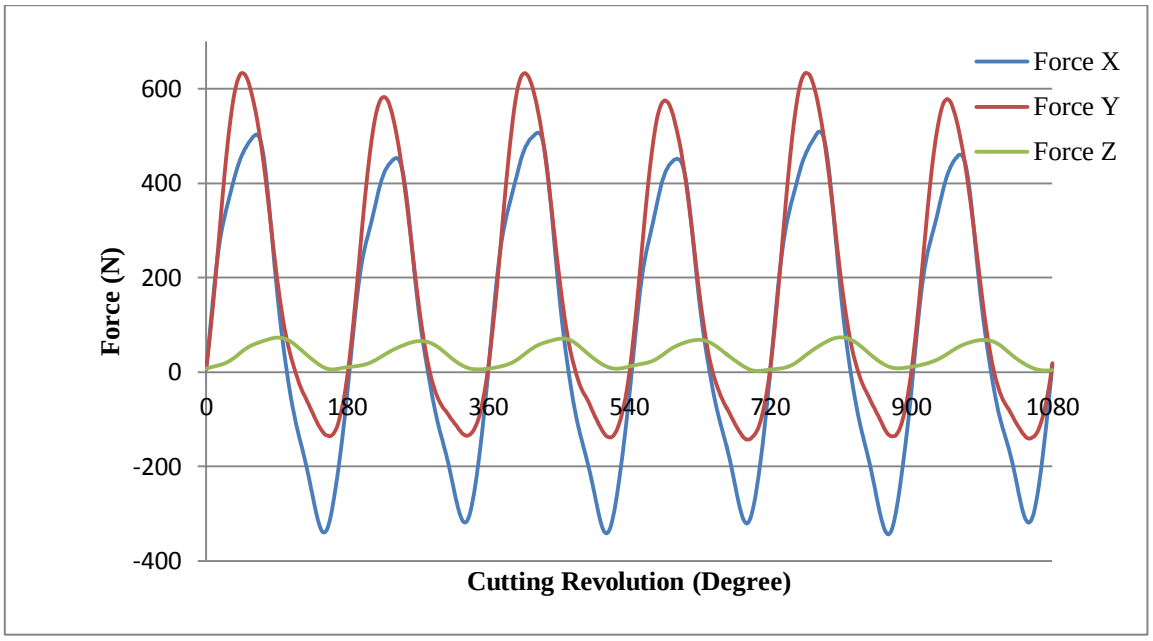


**Figure A2: Experiment 3**

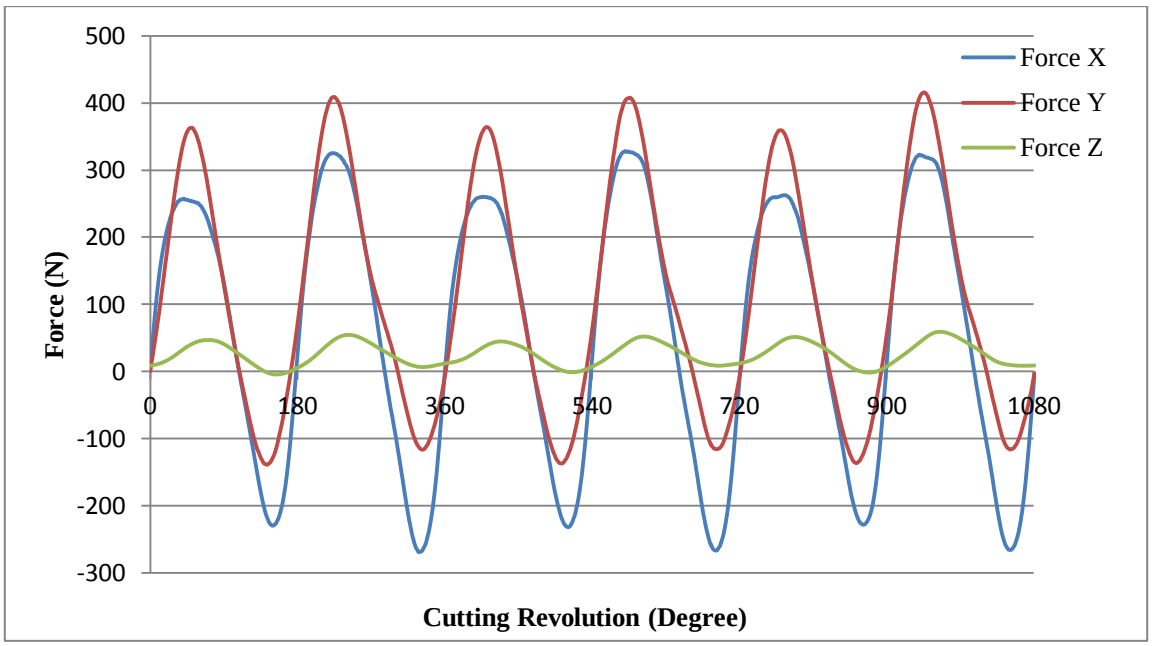


**Figure A3: Experiment 4**

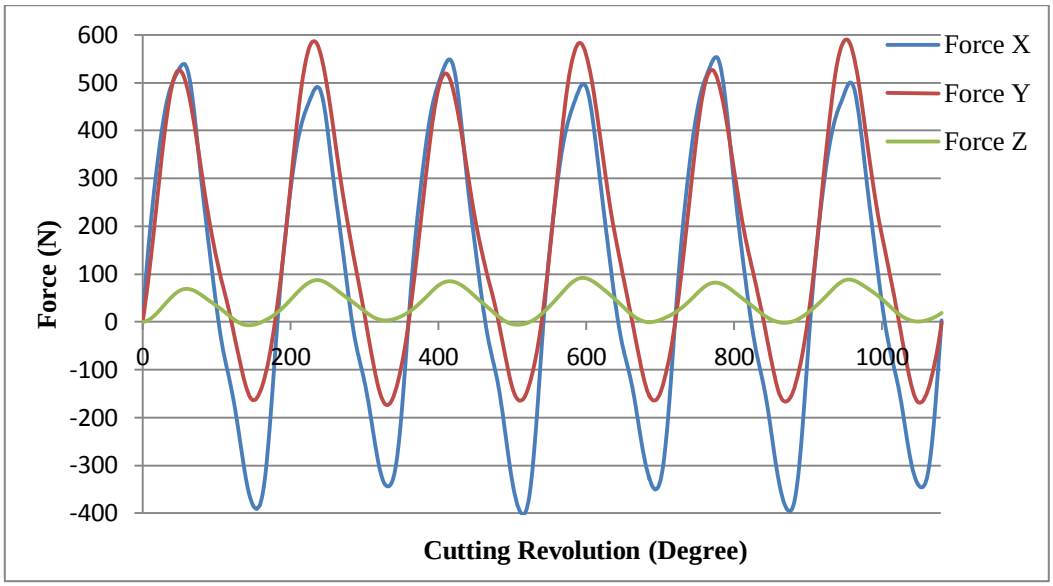


**Figure A4: Experiment 5**

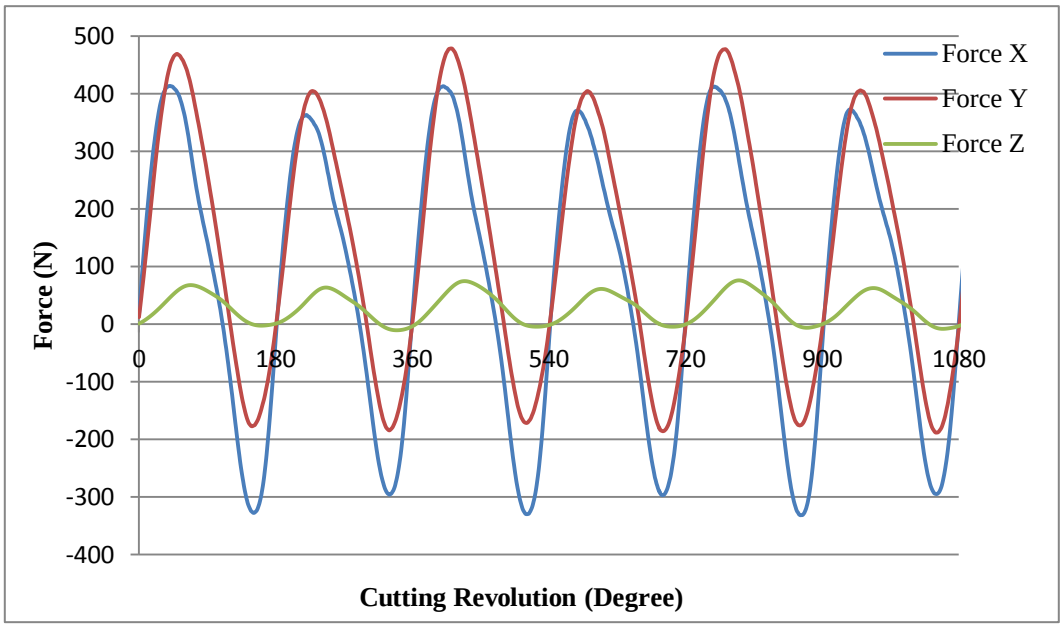


**Figure A5: Experiment 6**

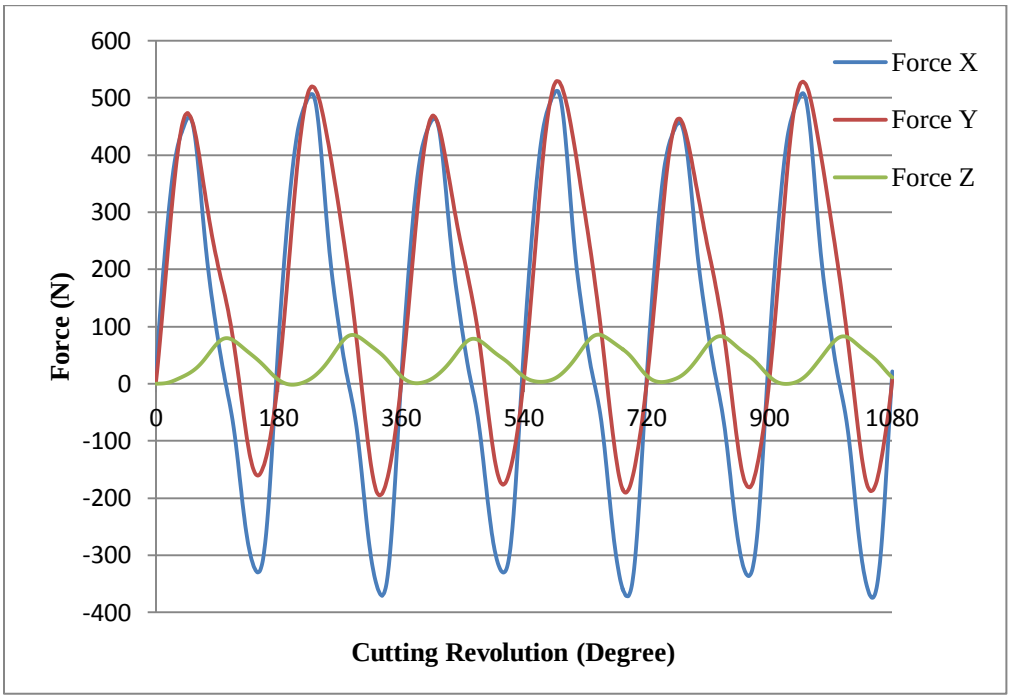


**Figure A6: Experiment 7**

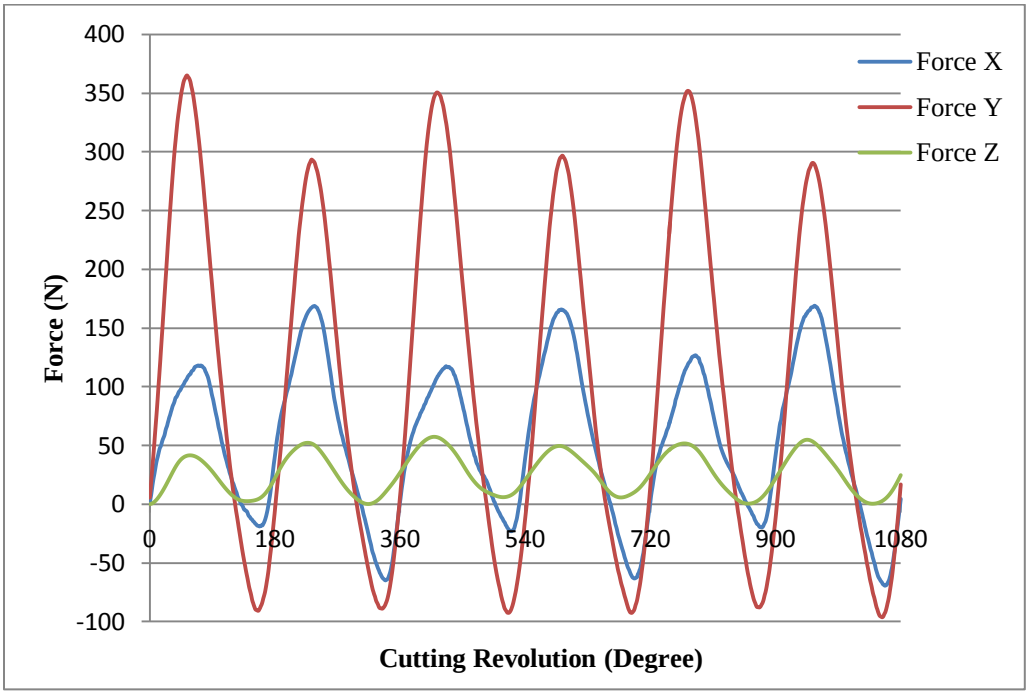


**Figure A7: Experiment 8**

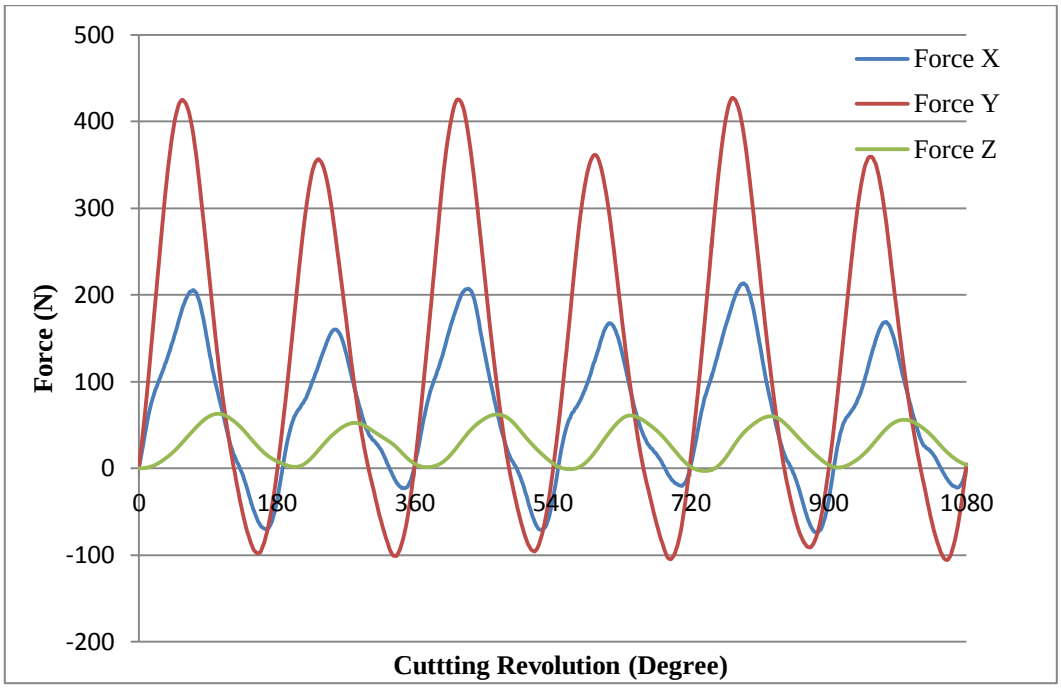


**Figure A8: Experiment 9**

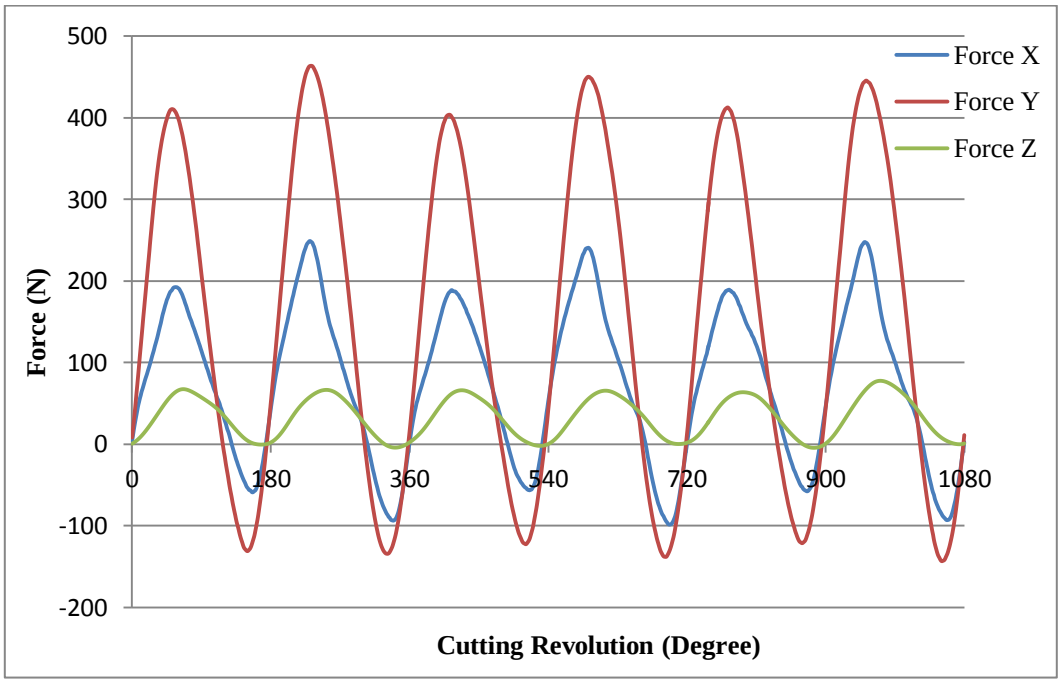


**Figure A9: Experiment 11**

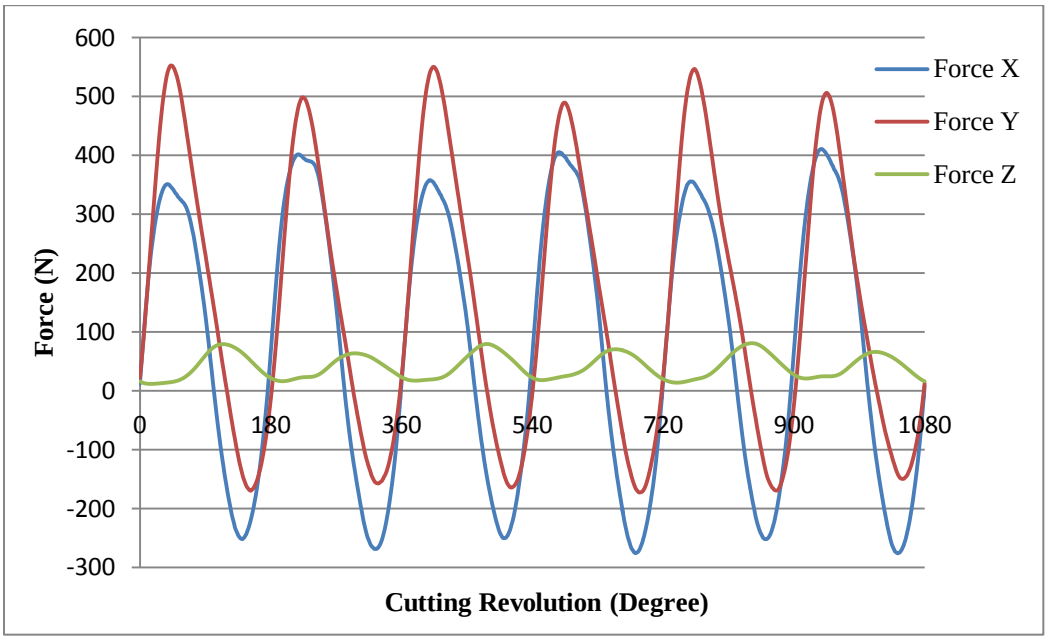


**Figure A10: Experiment 10**

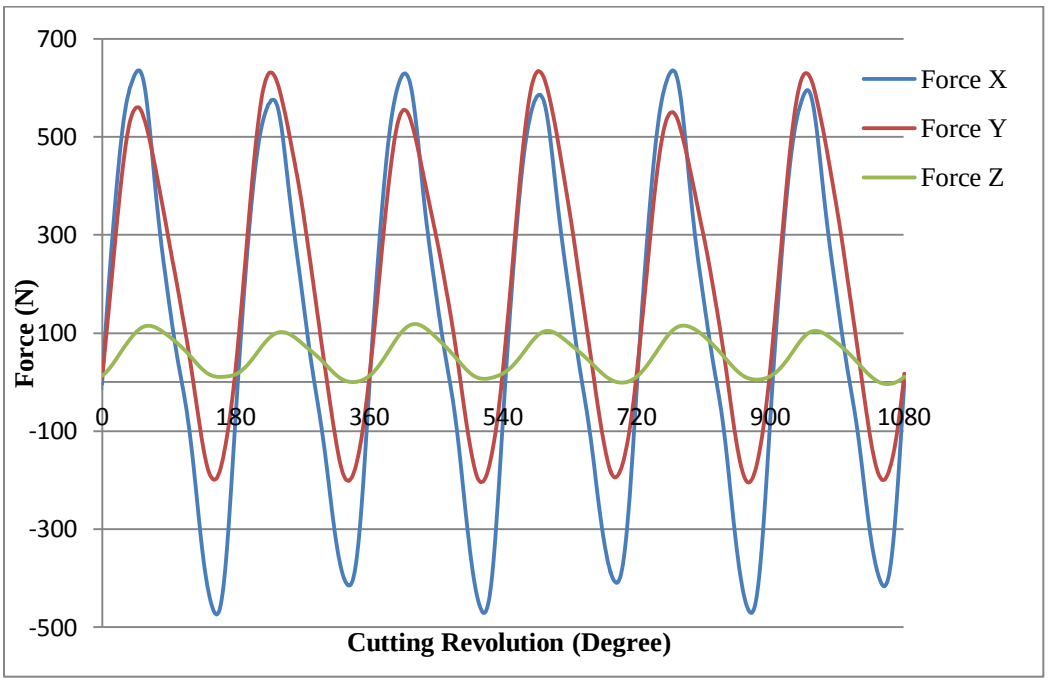


**Figure A11: Experiment 12**

## APPENDIX B

## FEA MODEL USE TO SIMULATE THE CUTTING PROCESS

The input file from ABAQUS used to run the milling cutting process is presented below. Part of the input file representing the tool and work piece mesh generation is not included because of its size.

** PARTS

**

*Part, name=cutter1

*End Part

**

*Part, name=w2

*End Part

*Surface, type=ELEMENT, name=Surf-2

,

chip, INTERIOR

** Constraint: Constraint-1

*Rigid Body, ref node=_PickedSet554, elset=rigid_Body, position=CENTER OF MASS

*End Assembly

**

** ELEMENT CONTROLS

**

```
*Section Controls, name=EC-1, ELEMENT DELETION=YES
1., 1., 1.
**
** MATERIALS
**
*Material, name=Workpiece_material
*Damage Initiation, criterion=JOHNSON COOK
 -0.77,  1.45,  0.47,    0.,    1.6,  925., 293.2,    1.
*Damage Evolution, type=ENERGY
0.,
*Density
2700.,
*Elastic
 6.9e+10, 0.33
*Plastic, hardening=JOHNSON COOK
 2.82e+08, 4.84e+08,    0.396,     1.34,     925.,    293.2
*Rate Dependent, type=JOHNSON COOK
 0.082,1.
*Specific Heat
896.,
**
** INTERACTION PROPERTIES
```

**

*Surface Interaction, name=CON

*Friction

0.9735,

*Surface Behavior, pressure-overclosure=HARD

**

** PREDEFINED FIELDS

**

** Name: Predefined Field-1  Type: Temperature

*Initial Conditions, type=TEMPERATURE

Set-375, 293.2

** ----------------------------------------------------------------

**

** STEP: Step-1

**

*Step, name=Step-1

*Dynamic, Explicit

,1.0

*Bulk Viscosity

0.06, 1.2

** Mass Scaling: Semi-Automatic

**  Whole Model

*Fixed Mass Scaling, factor=500.

**

** BOUNDARY CONDITIONS

**

** Name: BC-1 Type: Velocity/Angular velocity

*Boundary, type=VELOCITY

Set-374, 1, 1

Set-374, 2, 2

Set-374, 3, 3, -0.0084667

Set-374, 4, 4

Set-374, 5, 5

Set-374, 6, 6

** Name: BC-2 Type: Velocity/Angular velocity

*Boundary, type=VELOCITY

Set-365, 1, 1

Set-365, 2, 2

Set-365, 3, 3

Set-365, 4, 4

Set-365, 5, 5, -314.16

Set-365, 6, 6

**

** INTERACTIONS

**

** Interaction: Int-1

*Contact, op=NEW

*Contact Inclusions

tool_surf , Surf-2

*CONTACT CONTROLS ASSIGNMENT, NODAL EROSION=YES

*Contact Property Assignment

 ,  , CON

**

** OUTPUT REQUESTS

**

*Restart, write, number interval=1, time marks=NO

**

** FIELD OUTPUT: F-Output-1

**

*Output, field, number interval=18000

*Node Output

A, RF, RT, U, UR, UT, V, VR

*Element Output, directions=YES

E, MISES, S, STATUS

**

** HISTORY OUTPUT: H-Output-1

**

*Output, history, time interval=5.55556e-05

*Energy Output

ALLAE, ALLCD, ALLDMD, ALLFD, ALLIE, ALLKE, ALLPD, ALLSE, ALLVD,

ALLWK, ETOTAL

*Incrementation Output

DMASS, DT

*End Step

## APPENDIX C

## NUMERICAL CODE GENERATED WITH FEATURE CAM

The following presents the code generate with FEATURECAM to cut the slot feature during the milling process

```
%
(Bright - SLOT FEATURE)
( SETUP1 - 12/3/2013 - 14:22:23 )
( FEATURECAM - HAAS VF )
( MACHINE TIME = 1:27.4 )
N35 ( FINISH FACE FACE2 )
N40 G0 G17 G20 G40 G94
N45 T1 M6 ( WAXEATER  4.0 DIA. )
N50 G54 G90 X7.2 Y1.4 S1500 M3
N55 G43 H1 Z1.0
N60 Z0.1
N65 G1 Z-0.025 F20.0 (depth of facing cut)
N70 X-2.0
N75 G0 Z1.0
N80 G53 G49 Z0.
N85 M1
N90 (  SLOT GROOVE1 )
N95 G0 G17 G40 G94
```

N100 T7 M6 ( ENDMILL0625:REG--HSS  0.625 DIA. )

N105 G54 G90 X-0.5 Y0.75 S2500 M3

N110 G43 H7 Z1.0

N115 Z0.075

N120 G1 Z-0.125 F10.0 (depth of slot cut minus 0.025)

N125 X1.5 F20.0 (end coordinate and feed)

N130 G0 Z1.0

N135 G53 G49 Z0.

N140 M1

N145 (  SLOT GROOVE2 )

N150 G0 G17 G40 G94

N155 T8 M6 ( ENDMILL0625:REG--TINI  0.625 DIA. )

N160 G54 G90 X-0.5 Y2.25 S2500 M3

N165 G43 H8 Z1.0

N170 Z0.075

N175 G1 Z-0.125 F10.0 (depth of slot cut minus 0.025)

N180 X1.5 F20.0 (end coordinate and feed)

N185 G0 Z1.0

N190 G53 G49 Z0.

N195 G53 Y0.

N200 M30

%

## APPENDIX D

## SURFACE ROUGHNESS MEASUREMENT

The inner surface roughness of the machined specimens was measured using a MITUTOYO SURFTEST and the results are presented in the following plots.

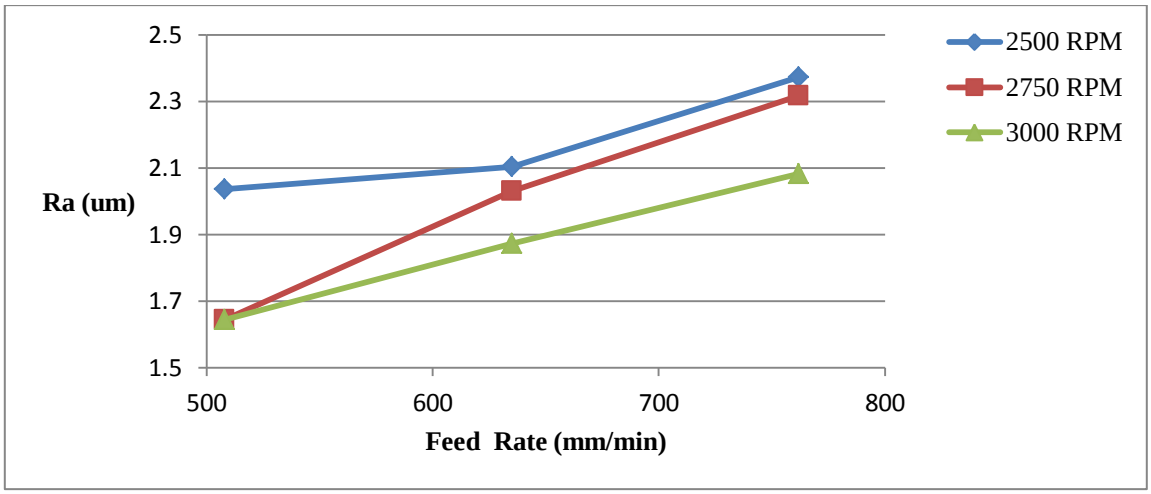


**Figure D1: Effect of the feed rate and spindle speed on the surface roughness**

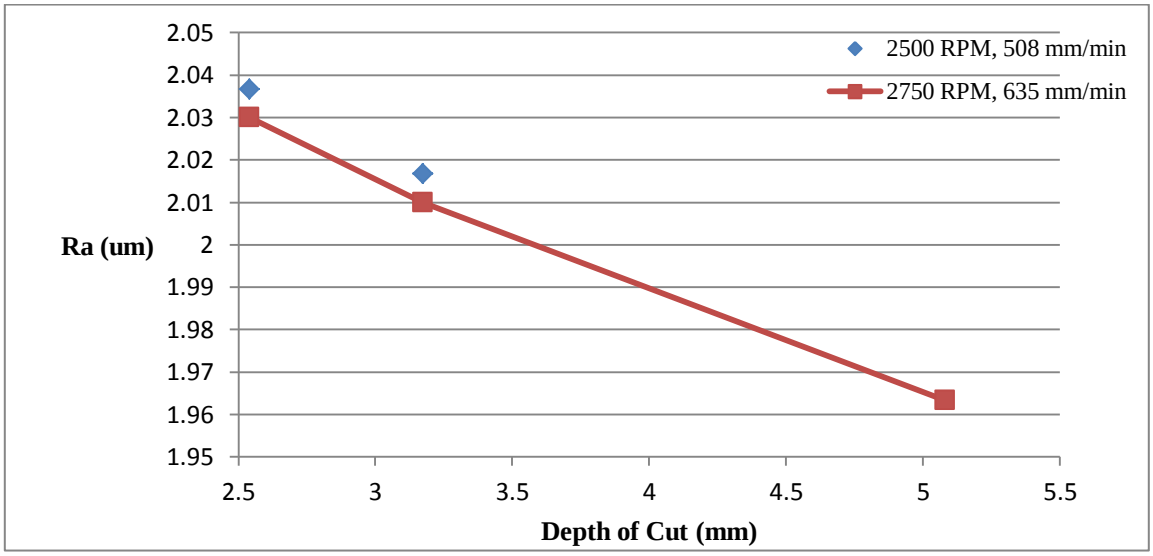


**Figure D2: Effect of the depth of cut on the surface roughness**